Master of Science Thesis

Structural Analysis of an Offshore Jack-up Installation Vessel

S. Wille

TU Delft Delft University of Technology

Structural Analysis of an Offshore Jack-up Installation Vessel

Master of Science Thesis

For obtaining the degree of Master of Science in Aerospace Engineering
at Delft University of Technology

S. Wille

6 July 2023

Faculty of Aerospace Engineering · Delft University of Technology

The work in this thesis was supported by Jan De Nul Group. Their cooperation is gratefully acknowledged.

Delft University of Technology
Faculty of Aerospace Engineering
Department of Aerospace Structures and Materials

GRADUATION COMMITTEE

Dated: 6 July 2023

Chair holder:

Prof. Dr. Chiara Bisagni

Committee members:

Dr. Saullo G.P. Castro

Dr. Carey L. Walters

Abstract

Offshore installation vessels are growing in size in order that they are capable of handling the next-generation 15 and 20MW wind turbines. At the same time, it is important to gain a better understanding of their structural behaviour using the finite element (FE) method. One approach that is often used is the full vessel FE analysis, which studies the vessel in its entirety. However, the drawbacks are that a coarse mesh must be adopted to have an acceptable simulation time and it takes months to create a 3D model of a vessel. Another approach is the partial vessel FE analysis, which considers only a section of the vessel. This research aims to develop a methodology for the partial vessel FE analysis of an offshore jack-up installation vessel.

The studied section of the vessel is between the four legs, which is where the highest bending moment is expected and the wind turbine towers are located on deck. The methodology was developed to analyse the vessel in still water and waves separately. The boundary conditions and hull girder load adjustments of the partial vessel model were described, which cause the vessel section to reflect the behaviour of the full vessel. The procedure to apply the loads on the model was also given. The finite element analyses were performed and the stress results compared to a simple analytical solution of the vessel based on Euler-Bernoulli beam theory.

The methodology of the partial vessel FE analysis was successfully applied to the offshore jack-up installation vessel. For the vessel in still water, the stress results were in agreement with the analytical solution. The results were accurate in the middle region for approximately 50% of the partial vessel model and thus it is advised to have a larger model for future use. The effect of torsion could not be fully justified as it is not captured in the analytical solution, but resulted in a significant improvement. For the vessel in waves, the stress results also showed a good agreement with the analytical solution. The accuracy depended on the equivalent design wave approach, which assumed a regular travelling wave. Lastly, it was proven that the presence of payload only leads to local changes in the stress field, but not in the global behaviour of the vessel.

Acknowledgments

Last year, I completed my internship at Jan De Nul Group, where I designed a seafastening grillage to secure a transition piece. I decided to stay there because of the fascinating and promising industry of offshore wind turbines and was given the opportunity to devote myself to research on offshore installation vessels for 9 months. My task was to analyse a section of an offshore jack-up installation vessel that reflects the structural behaviour of the full vessel.

First, I would like to thank my supervisor Prof. Bisagni from TU Delft. The reason I asked her to be my supervisor is because I genuinely enjoyed the two courses she taught me during my master. I would also like to thank the following people from Jan De Nul. Gemma and Wouter, the supervisors during my internship and thesis, for giving me this opportunity. Kris, an experienced structural design engineer who aided me with my numerous questions. He was involved in my internship and thesis and helped me the most. Ksenija, a skilled marine engineer with whom I closely collaborated throughout my thesis. And lastly, the entire team of the marine design & engineering department who were always available to provide me with insightful feedback on my work.

Furthermore, I would like to thank the following people. My uncle, to whom I always went for technical questions. My grandfather, who showed sincere interest in my studies. And Jade, for our countless shared adventures and as she is the person who understands me best.

Lastly and most importantly, I would like to thank my dad, a pilot who introduced me to the field of aerospace, and my mom for her endless support in my life.

Delft, University of Technology — S. Wille
6 July 2023

Table of Contents

List of Figures

List of Tables

List of Symbols

Latin symbol	Definition	Unit
A	Area	$[m^2]$
A	Wave amplitude	$[m]$
b	Buoyancy per unit length	$[kg/m]$
c	Wave speed	$[m/s]$
C	Concentrated weights	$[kg]$
d	Water depth	$[m]$
D	Mean draft	$[m]$
E	Young's modulus	$[Pa]$
f	Wave frequency	$[Hz]$
F_b	Buoyant force	$[N]$
F_s	Shear force	$[N]$
$F_{s,z}$	Vertical shear force	$[N]$
g	Gravitational acceleration	$[m/s^2]$
h	Height from free the water surface	$[m]$
H	Wave height	$[m]$
H_{max}	Expected maximum wave height	$[m]$
H_s	Significant wave height	$[m]$
I_y	Second moment of area	$[m^4]$
M	Bending moment	$[N \cdot m]$
M_{aft}	Aft bending moment for the shear force adjustment	$[N \cdot m]$
$M_{extremum}$	Maximum or minimum moment of the vessel section within its mid-hold from $M_{section}$ and the bending moment induced by the shear force adjustment	$[N \cdot m]$
M_{fore}	Fore bending moment for the shear force adjustment	$[N \cdot m]$
M_{full}	Full vessel bending moment	$[N \cdot m]$
$M_{section}$	Vessel section bending moment	$[N \cdot m]$
M_{target}	Maximum or minimum moment of the full vessel within the mid-hold of the vessel section	$[N \cdot m]$

M_y	Vertical bending moment	$[N \cdot m]$
p	Absolute pressure at a point in a fluid at rest	$[Pa]$
p_{atm}	Atmospheric pressure	$[Pa]$
p_{hydr}	Hydrostatic pressure	$[Pa]$
P	Pressure	$[Pa]$
R_{aft}	Reaction force at aft end	$[N]$
R_{fore}	Reaction force at fore end	$[N]$
S	Wave steepness parameter	$[-]$
t	Return period	$[s]$
T	Wave period	$[s]$
T_p	Peak wave period	$[s]$
T_z	Zero crossing wave period	$[s]$
v	Vessel speed	$[m/s]$
w	Weight per unit length	$[kg/m]$
W_{model}	Partial vessel model weight	$[kg]$
W_{vessel}	Vessel section weight	$[kg]$
x_{aft}	Aft end	$[m]$
x_{bow}	Fore end of the full vessel	$[m]$
x_{fore}	Fore end	$[m]$
x_{fr}	Frame spacing	$[m]$
$x_{mid-aft}$	Aft end of the vessel section's mid-hold	$[m]$
$x_{mid-fore}$	Fore end of the vessel section's mid-hold	$[m]$
x_{stern}	Aft end of the full vessel	$[m]$
$Z_{N.A.}$	Neutral axis location	$[m]$

Greek symbol	Definition	Unit
γ	Peak enhancement factor	$[-]$
Δ	Relative error	$[-]$
ΔF_s	Shear force adjustment	$[N]$
ΔM	Bending moment adjustment	$[N \cdot m]$
ΔM_{aft}	Bending moment adjustment at the aft end	$[N \cdot m]$
ΔM_{fore}	Bending moment adjustment at the fore end	$[N \cdot m]$
ΔT	Torsional moment adjustment	$[N \cdot m]$
ε	Strain	$[-]$
λ	Wavelength	$[m]$
μ	Shallow water parameter	$[-]$
ν	Poisson ratio	$[-]$
ρ	Density	$[kg/m^3]$
$\rho_{adjusted}$	Adjusted density	$[kg/m^3]$
ρ_{steel}	Structural steel density	$[kg/m^3]$
ρ_{water}	Water density	$[kg/m^3]$
σ	Normal stress	$[Pa]$
σ_{vm}	Von Mises stress	$[Pa]$
τ	Shear stress	$[Pa]$
φ	Phase angle	$[°]$
Ω	Wave direction	$[°]$

List of Abbreviations

Abbreviation	Definition
BM	Bending moment
BV	Bureau Veritas
CL	Centre line
COG	Centre of gravity
DNV	Det Norske Veritas
EDW	Equivalent design wave
FE	Finite element
FEA	Finite element analysis
GS	Graphical Supervisor
JONSWAP	Joint North Sea Wave Project
RAO	Response amplitude operator
SF	Shear force
TM	Torsional moment
WB	Water ballast

Chapter 1

Introduction

In recent decades, Europe has known a substantial growth of large-scale offshore wind farms as a result of advances made in wind turbines and foundation structures [1]. This is illustrated by the arrival of next-generation 15 and 20MW wind turbines, which are greater in size to generate more energy [2]. Due to this development, the need for larger offshore installation vessels is imminent, along with a better understanding of their structural behaviour.

The rules established by ship classification societies are used by engineers for the design and analysis of ships. These rules are derived from theory and are often adjusted by experimental data. Well established societies including Bureau Veritas and Det Norske Veritas, among others, publish their rules to this day. Although it remains deeply rooted in the shipbuilding industry, some challenges are also encountered with this approach. The rules introduce conservatism into the design and are not readily applicable to unconventional ship types. Accordingly, the finite element (FE) method has been increasingly used [3].

There are two approaches to analyse the global behaviour of a ship. The first one is the full vessel FE analysis which, as the name suggests, studies the vessel in its entirety. This approach is the most accurate as it captures the complete vessel response, but there are convincing reasons that it is not always preferred. A fine mesh must be used to acquire detailed results. However, a coarse mesh is often adopted due to the immense size of ships or else the simulation time would become too high. Moreover, it takes months to create a 3D model of a vessel.

The second approach to analyse the (global) behaviour of a ship is the partial vessel FE analysis, which considers only a section of the vessel. As a result, time is saved in modelling and a finer mesh can be adopted. However, there are additional challenges associated with this approach to guarantee that the vessel section reflects the behaviour of the full vessel. Literature often refers to this approach as the cargo hold FE analysis, which has to do with the fact that ships with cargo holds, such as container ships and bulk carriers, have been primarily investigated in the past. This research studies an offshore jack-up installation vessel with the noticeable differences that it has no cargo holds, a larger width to length ratio, legs to lift itself above the free water surface and high concentrated loads such as the

heavy lift crane and wind turbine towers. Consequently, the assumptions behind the cargo hold FE analysis may not be fully applicable.

This research aims to develop a methodology for the partial vessel FE analysis of an offshore jack-up installation vessel. The goal is to analyse a section of the vessel that reflects the structural behaviour of the full vessel. The research is performed in collaboration with Jan De Nul Group.

This thesis abides to the following structure. First, in chapter 2, a literature review is performed on hull girder loads and the state-of-the art in the field of research. Second, in chapter 3, the methodology of the partial vessel FE analysis is developed. This chapter also includes a section dedicated to the verification of the methodology. In chapter 4, the methodology is tested for the vessel in still water. It consists of a case study that analyses the vessel without water ballast and another that takes this into account. Then, in chapter 5, the methodology is tested for the vessel in waves, which comprises of a case study that maximises preselected hull girder loads. Lastly, in chapter 6, the partial vessel FE analysis of the offshore jack-up installation vessel with heavy payload on deck is performed. Finally, conclusions and recommendations about the methodology are made in chapter 7.

Chapter 2

Literature review

This chapter examines existing literature about the structural analysis of vessels. First, hull girder loads are discussed in section 2.1. Next, in section 2.2, currently used design and analysis approaches for vessels are investigated. Then, different verification and validation strategies are mentioned in section 2.3. Lastly, in section 2.4, conclusions of the literature review are drawn and the research objective and questions are established based on the remaining gaps in the state-of-the-art.

2.1 Hull girder loads

When dealing with the design (or analysis) of vessels, hull girder loads must be understood. They are induced by the loads that are listed below. The lightweight is the empty ship weight, and the deadweight is the summation of all components their weight. For instance, the payload and water ballast are part of the deadweight. Besides, the buoyancy and wave pressure are the loads that the water exerts on the hull. Five hull girder loads can be distinguished, which are shown in Figure 2.1. It is convenient to divide them into a (static) still water and (dynamic) wave component [4, 5].

- Lightweight
- Deadweight (includes payload and water ballast)
- Payload
- Water ballast
- Buoyancy (hydrostatic)
- Wave pressure (hydrodynamic)

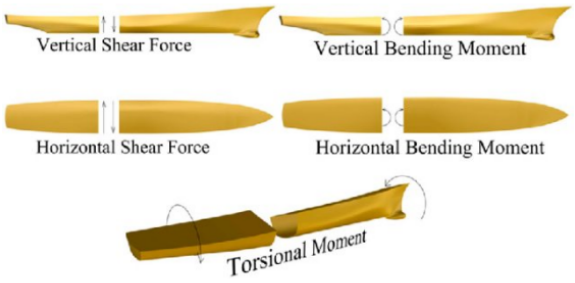

Figure 2.1: Hull girder loads: vertical shear force and bending moment, horizontal shear force and bending moment, and torsional moment [6].

2.1.1 Still water loads

Still water loads consider the vessel, as the name suggests, in still water at zero speed. It originates from the non-uniform distribution of the buoyancy and weight, where the latter is the summation of the lightweight and deadweight. As a consequence, the resultant load varies along the length of the vessel. This leads to still water vertical shear force and bending moment as illustrated in Figure 2.2. Even though the resultant load locally differs from zero, the net load equals zero, which indicates equilibrium [5, 7].

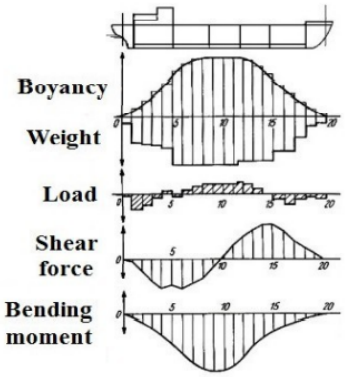

Figure 2.2: Still water vertical shear force and bending moment [4].

The still water vertical shear force F_s is obtained from the integration of the difference of the total weight w and buoyancy b per unit length over the vessel's length x. When integrated once more over the length, the vertical bending moment M_s is obtained [7, 8]. The mathematical formulation of the vertical shear force and bending moment are, respectively, given as

$$F_s = \int_0^x w\,dx - \int_0^x b\,dx \tag{2.1}$$

$$M_s = \int_0^x \int_0^x w\,dx\,dx - \int_0^x \int_0^x b\,dx\,dx \tag{2.2}$$

2.1.2 Wave loads

The still water loads were the result of the non-uniform distribution of the buoyancy and weight. On the other hand, wave loads stem from the dynamic wave pressure on the hull. Two components can be distinguished, namely wave-induced loads and ship-generated wave loads [4, 8]. First, the wave heading with regard to the vessel is shown in Figure 2.3.

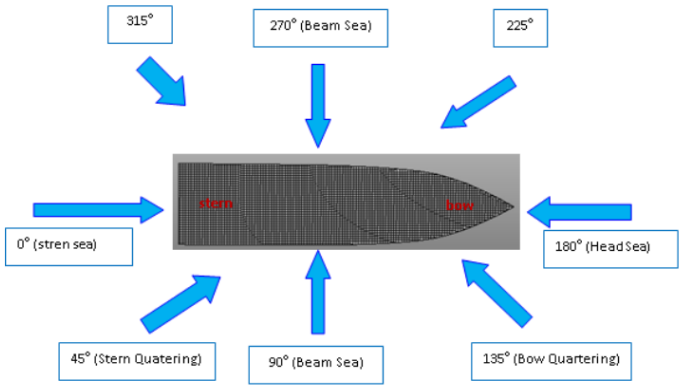

Figure 2.3: Wave heading with regard to the vessel [9].

Wave-induced loads occur for a vessel at zero speed in waves. Two extreme conditions can be distinguished when a vessel in a stern or head sea comes across a wave that has a wavelength equal to the ship's length, namely hogging and sagging as illustrated in Figure 2.4 [4, 10]. When the midship area finds itself in a wave crest, it causes the middle part of the vessel to bend upward. This behaviour is referred to as hogging and worsens when more payload is located at the fore and aft end. On the other hand, when the midship area is in a wave trough, the middle part of the vessel bend downwards. It is called sagging and is worsened with payload located at the middle part [5]. Following the same reasoning as with still water loads, it leads to vertical shear force and bending moment. Shama [4] summarises the variables that determine the magnitude of these loads: sea waves condition, draught, displacement, trim, vessel speed and heading to the waves.

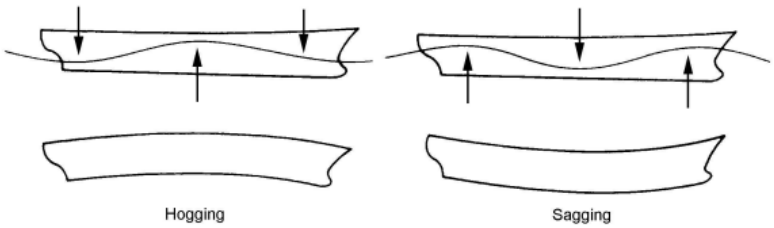

Figure 2.4: Hogging and sagging of a vessel [11].

Wave-induced loads additionally leads to horizontal shear force, horizontal bending moment and torsional moment. It occurs in case a vessel is sailing in oblique waves, as depicted in Figure 2.5. These loads will increase under oblique waves, while the vertical shear force and bending moment will decrease. For the torsional moment, it is clear there is a resultant

force at section A-A and C-C. Since they do not go through the shear centre, a torsional moment occurs at both ends that act in opposite direction [12]. Normally, the torsional rigidity is adequate to avoid excessive warping stresses in the vessel. Although, according to van Dokkum [5] and Eyres et al. [13], it can be significant with open deck ships.

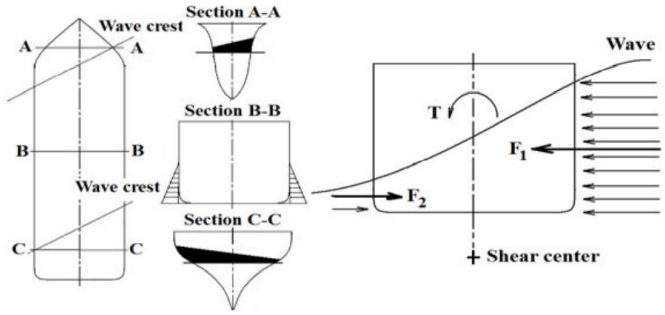

Figure 2.5: Hull girder torsional moment of a vessel sailing obliquely [4].

Ship-generated waves occur due to the motion of a vessel in still water, according to Bhattacharyya [8]. A wave pattern is created in function of the underwater hull form, which leads to an additional bending moment. Thus, the wave bending moment is a function of wave-induced and ship-generated wave loads. Finally, the still water and wave component, denoted with subscript 's' and 'w' respectively, should be added to obtain the total resultant [4, 8, 10]. The shear force F and bending moment M are, respectively, given as

$$F = F_s + F_w \tag{2.3}$$

$$M = M_s + M_w \tag{2.4}$$

The wave loads discussed up till now are slowly varying loads and can be considered as quasi-static. They are low frequency phenomena, which means their oscillating frequencies are significantly smaller than the natural frequency of the hull. Therefore, the dynamic response can be neglected [8]. There are, however, actual dynamic loads which must be analysed as such. For instance, the impact of the ship bow on the waves referred to as slamming, the vibration of an engine or propeller, green sea loads, etc. [4].

2.1.3 Concluding remarks

Hull girder loads, that originate from lightweight, deadweight, buoyancy and wave pressure, have been discussed. These induce vertical shear force and bending moment, horizontal shear force and bending moment, and torsional moment. A general description of the origin of hull girder loads is provided including some basic formulas, while an in-depth explanation remains out of the scope of this research. To compute the hull girder loads, a hydrodynamic analysis is performed using adequate software.

2.2 Design approaches for vessels

Ship classification societies date back to the 18th century. It was in 1760, when the first ship classification society, Lloyd's Register, was founded. In the past, their purpose was limited to classify the condition of a ship on an annual basis. As of today, ship classification societies form an indispensable part of the maritime industry and issue classification rules with the main purpose towards safety and pollution prevention [14]. Well known ship classification societies include Bureau Veritas (BV), Det Norske Veritas (DNV), American Bureau of Shipping (ABS), etc. [15].

In this section, four different design (or analysis) approaches for vessels are discussed. The first approach is about the guidelines of ship classification societies from knowledge and experience over the past two centuries, and consists of rules mainly of semi-empirical nature. The other three approaches that are considered include a full vessel finite element (FE) analysis, partial vessel FE analysis and fine mesh FE analysis. They are based on the finite element method and are related to one another. Nowadays, more interest is given to finite element analyses from ship classification societies and in literature [16–18]. There are many advantages to a finite element analysis: complex geometry can be modelled, a high degree of accuracy can be achieved, local details become apparent, etc. Additionally, its use is not restricted to marine engineering only. The theory behind the finite element method and its applications can be found in other engineering fields. The ship classification society BV [16] illustrates the approaches based on the finite element method in the flow diagram in Figure 2.6. Notice the partial vessel FE analysis is generally called a cargo hold FE analysis by ship classification societies or in literature. Their research focuses on ships with cargo holds, which explains the naming. A cargo hold is an enclosed space to store in payload and is separated from other holds by lateral bulkheads. Examples of ships with cargo holds include bulk carriers, container ships, etc. But the therm has little meaning with offshore installation vessels since all payload is secured on deck and no cargo holds exist, as such the naming partial vessel FE analysis is more appropriate. Together with the full vessel FE analysis, it is used to assess the stress and buckling behaviour. Besides, both comprise of fine mesh and very fine mesh FE analysis, for stress assessment and fatigue analysis respectively.

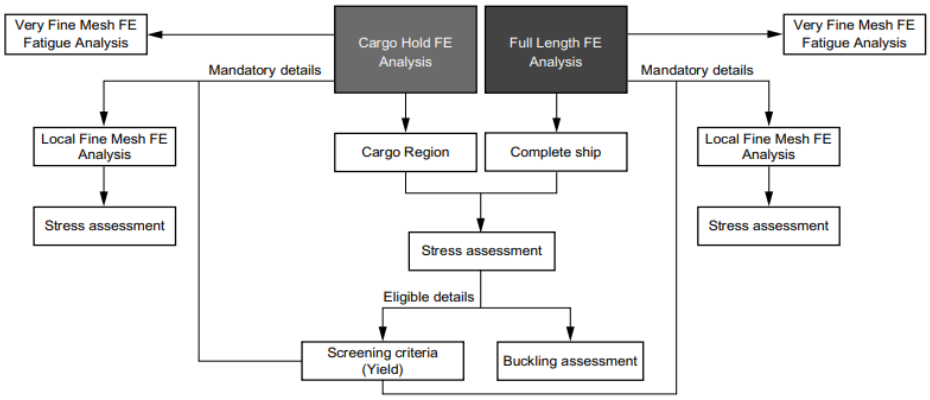

Figure 2.6: Flow diagram of a finite element analysis approach for the design (or analysis) of a vessel [16].

2.2.1 Semi-empirical rules

Formerly, it was common practise to design ships by rules, mainly of semi-empirical nature, set up by ship classification societies. Although this approach has served as a guideline in the early ship building and still does to standard vessel types, some deficiencies appear with it present-day. Bai et al. [3] mention that unconventional ship types and complex ship structures cannot rely on these rules, among which are large container ships, large LNG-carriers, drilling ships, etc.

Rörup et al. [19] conducted a study on the strength of ships with open decks (bulk carrier and container ship) which are subject to torsional loads. They state that simple beam theory cannot fully capture the structural response of the hull girder for ship types with large deck openings, for ships with a limited amount of transverse bulkheads over the length of the vessel and for ships with a partly effective superstructure and/or upper part of the hull girder. In the case of ships with large deck openings, warping takes place which is constrained from occurring. As a result, normal stresses will develop that must be considered in the analysis [20], for which they relied on a finite element analysis. It does not mean, however, semi-empirical rules are not useful. For instance, Shama [12] discusses a simplified approach for the torsional analysis of open deck ships, assuming thin-walled open sections. Although, it is explicitly mentioned it should be used in the preliminary design phase in case different designs are compared and the torsional loads are not yet accurately known.

In the case of offshore installation vessels, no large deck openings except for a few hatches at most are present. There are, however, other good reasons why semi-empirical rules would not always work. A key feature to offshore installation vessels is that all payload is stored on deck. Typically, seafastening grillages are placed on deck on which the payload is secured. It is simultaneously used to spread the load of the payload into deck. Both a grillage and payload can locally influence the stiffness of the deck. In case the vessel is analysed with its payload, there is no manner but to use a finite element analysis, to account for these local changes in stiffness. Thus, it would be relevant in this aspect to continue investigating the finite element method.

Although the relevance of a finite element analysis should be clear from the foregoing discussion, certainly in the later stages of a design, there are rules that always must be taken into account, among which is the following case. During the lifetime of a vessel, the (hull) structure will deteriorate due to corrosion by the rough sea environment. Therefore, corrosion allowances must be applied, apart from coating protection [10]. The guideline 'Allowable thickness diminution for hull structure' of DNV [21] determines a reduction in thickness based on the following variables: structural component, structural category (e.g. primary, secondary, etc.), vessel's years of service, protection system, etc.

2.2.2 Full vessel FE analysis

Scantling is referred to as determining the geometrical dimensions (e.g. wall thickness) for structural components or systems. In the case of scantling a hull girder, the calculations are based on classification rules. Over the past years, this process has been automated using appropriate software [10]. Many ship classification societies have developed their own dedicated software, used in-house and commercially available, which include, but are not limited to:

- **MARS 2000** - 2D ship structural assessment software by BV [22].
- **Nauticus Hull** - 2D/3D strength assessment of hull structures software by DNV [23].
- **POSEIDON** - 3D strength assessment of ship hull structures software by DNV [24].

Lately, however, more interest is shown in approaches using the finite element method, among them the full vessel FE analysis. This type of analysis is used to determine the overall hull girder stiffness and global stresses and deformations [3, 19]. An elaborate description of current practises is given. First, the three dimensional model is explained. Second, the boundary conditions are discussed. Lastly, the loading of the model is considered.

Three dimensional model Building the three dimensional full vessel model can be done in any appropriate software. When completed, the model must be discretized for the finite element analysis. This process, which includes the mesh density and type of elements, is discussed in the coming paragraphs. But first, for the purpose of consistent naming, the distinct structural parts in a vessel will be mentioned. A hull girder is mainly composed out of four structural components: bottom structure, side structure, deck structure and transverse & longitudinal bulkheads [25]. Each of these components are stiffened by other structural elements which have a naming of their own. In Figure 2.7, the most adequate naming is reported. Notice the bottom longitudinals are called stiffeners instead, while a longitudinal always indicates a bulkhead.

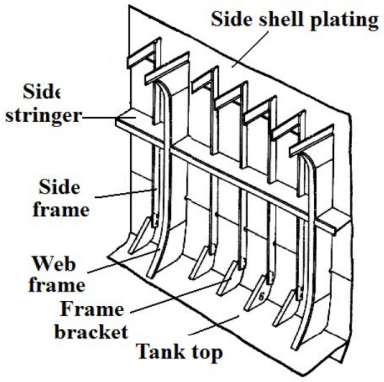

(a) Structural elements on the side structure [25].

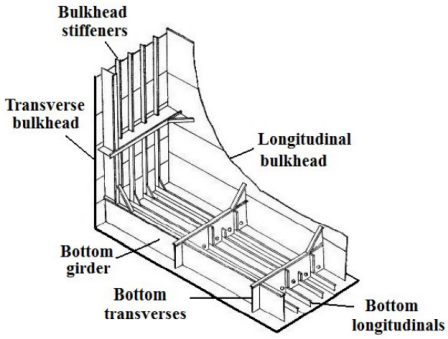

(b) Structural elements on the bottom structure and transverse and longitudinal bulkhead [26].

Figure 2.7: Naming convention of the structural elements of a vessel. Bottom longitudinal is called a stiffener instead.

For the mesh density, multiple independent sources state to use a coarse mesh [3, 17, 19, 27]. Else, the computational expense to run the model is too significant. As an initial observation, the number of elements should stay below one million but it depends on the available computational power. None of the aforementioned sources specify a rule of thumb in the creation of a coarse mesh. Another perspective on this matter comes from Rörup et al. [28, 29], who state to use one element between structural elements such as web frames, girders, stringers and deck of which an example is shown in Figure 2.8.

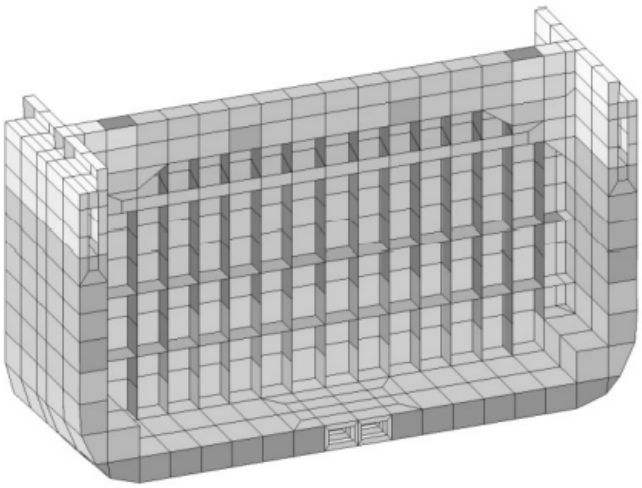

Figure 2.8: Coarse mesh with one element between web frames, girders, stringers and deck [28].

There exist a number of different element types in finite element software, among which are beam, shell and solid elements. Each structural part is assigned one of these elements, with the main requirement that it should be representative for the actual behaviour of the part under consideration. Ideally, a solid element should be chosen which will return the most accurate behaviour. But in general, solid elements are to be avoided to reduce the amount of degrees of freedom. Various sources specify their liking [16, 17, 19], among those are the guidelines from BV and DNV. Summarizing, shell elements (and sometimes membrane elements) can be used for plate areas. This includes the following structural parts: girders, stringers, web frames, deck structure, bottom structure and bulkheads. Other structural elements may be modelled as beam or rod element.

Boundary conditions The model should be properly constraint in order to prevent rigid body motion. But in addition, it should behave as expected and not introduce any abnormal stresses. In the BV rules [16], the boundary conditions for a full vessel model are discussed. It is suggested to use a three point boundary constraint, with the constraining of the degrees of freedom as defined in Table 2.1.

Table 2.1: Three point boundary constraint at the fore and aft end of the full vessel model according to BV rules (edition 2022) for the classification of steel ships [16].

Location	Translation			Rotation		
	x	y	z	x	y	z
Node on fore end of ship	-	fix	fix	-	-	-
Node on aft end ship at port side	fix	-	fix	-	-	-
Node on aft end ship at starboard side	-	fix	fix	-	-	-
Note 1: Nodes on aft end ship are symmetrical with respect to ship's longitudinal plane of symmetry. **Note 2:** [-] means no constraint is applied.						

Elhewy et al. [30] clearly depict the boundary conditions in Figure 2.9. They mention the boundary constraints should restrict the model from any translational or rotational motion. They, however, do not specify anything about the degrees of freedom of the three constraint points. DNV [17] mentions the boundary constraints should be simple supports to prevent any built-in stresses. Additionally, the reaction forces in the boundaries should tend towards zero, as also mentioned in [3]. In reality, the boundary conditions are not there, and the external forces and internal forces should balance. Furthermore, the boundaries should be far away from the area of interest, which indicates the results are not valid near the boundaries.

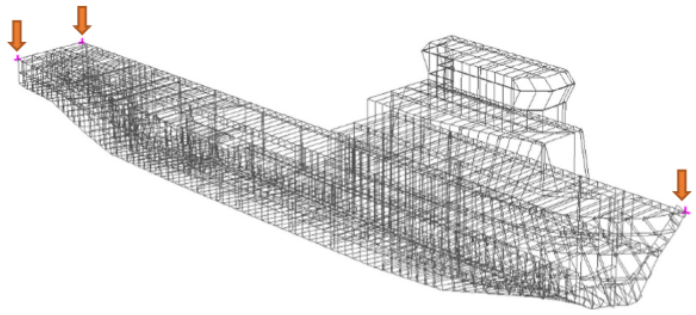

Figure 2.9: Three point boundary constraint of a full vessel model [30].

DNV proposes three different configurations to constrain the boundary conditions. Among them is the three point boundary constraint mentioned above, although the constraining of the degrees of freedom differ. They briefly mention this configuration may work for car carriers or Ro-Ro ships, not specifying any other ship types. Among the other two configurations, it is stated one can be applied in general. Again a three point boundary constraint is used, but with each point on the longitudinal plane of symmetry. Summarizing, different solutions exist and it remains difficult to tell which one suits best. In any case, it should not introduce additional stresses in the vessel and the boundaries should be far away from the area of interest.

Loading A vessel will encounter multiple load cases during sailing. Essential to each case at hand is the application of the loads to the finite element model. Firstly, a description of the guidelines of ship classification societies on this topic is made. Then, two promising software will be discussed, namely ShipLoad and Ansys.

The loads to consider for a full vessel FE analysis include the lightweight, deadweight, buoyancy and wave pressure. The first three loads can independently be applied on the finite element model [16, 17]. The wave pressure is retrieved from a hydrodynamic analysis, which it is not straightforward to transfer to a finite element model. In the BV guidelines [16], nothing is mentioned about the application of this load on the model, but only about which loads to consider. DNV [17] does specify there are two possibilities, namely pressure mapping and force mapping, with reference to one of their other guidelines [31].

Schellin et al. [32] explain that performing a structural analysis, with the loads available, is a complex and time consuming task. One of the main reasons is that multiple software will be used, which often is the expertise from different departments. For this reason, the software

ShipLoad was created by DNV, which can conveniently export the hydrodynamic loads to a finite element software such as POSEIDON or Ansys [28]. ShipLoad produces balanced quasi-static load cases, which are reduced to a handful of cases by applying the equivalent design wave approach. The loads are transferred to the finite element software as nodal forces. It is mentioned nodal loads are preferred over surface loads since it is accurate enough and is easy to integrate [32, 33].

Dementyev [34] explains the mapping of hydrodynamic loads from Ansys AQWA to Ansys Mechanical, of which the setup is shown in Figure 2.10. Two approaches are mentioned, the direct and interpolated method, with further explanation of the latter method. Additional information is reported by Ansys itself in [35].

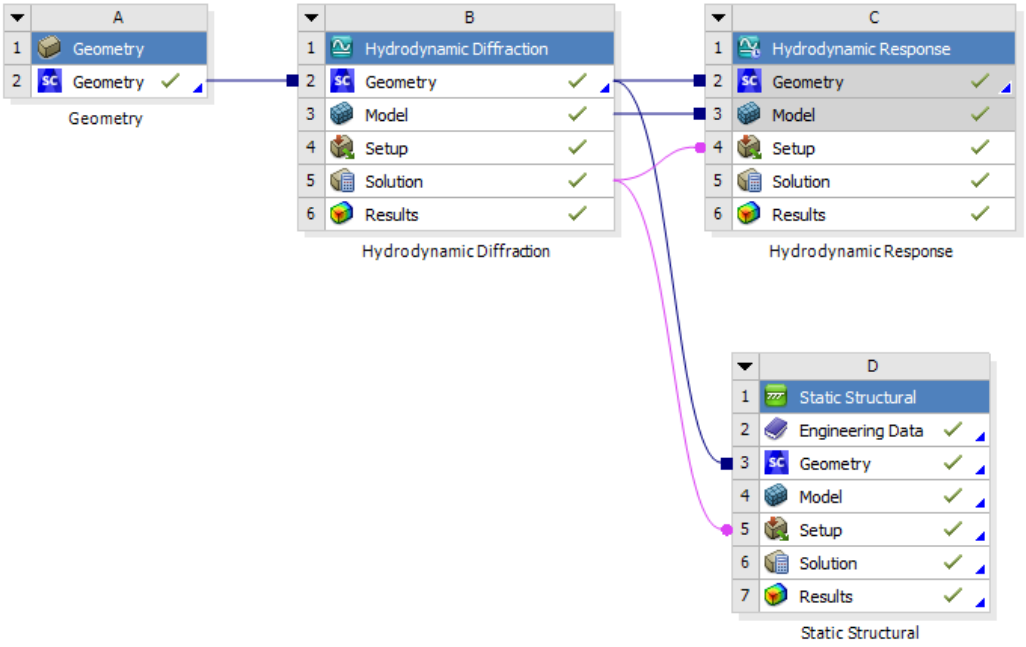

Figure 2.10: Hydrodynamic pressure mapping in Ansys from Hydrodynamic Diffraction (AQWA) to Static Structural (Mechanical).

2.2.3 Partial vessel FE analysis

In the previous section, the full vessel FE analysis is discussed. For the discretisation of the three dimensional model, it was advised to use a coarse mesh to avoid any computational difficulties [3, 27]. With the mesh size as coarse, this type of analysis could be used to determine the overall hull girder stiffness and global stresses and deformations as stated in subsection 2.2.2. While in case a more detailed view is desired, which can include local stresses, a standard mesh is required. For this reason, a partial vessel FE analysis is introduced, considering only a section of the vessel. It can accommodate the standard mesh since the size of the model has diminished. The same outline is followed as for the full vessel FE analysis in subsection 2.2.2, which includes the three dimensional model, the boundary conditions and the loading.

As stated earlier, this approach is called a cargo hold FE analysis by ship classification societies or in literature. Whereas the naming partial vessel FE analysis is deemed more appropriate for an offshore installation vessel. In fact, DNV [17] already makes the distinction between a partial ship (or vessel) and cargo hold analysis. But only provide documentation for the cargo hold FE analysis, and state it may be applied for ships without cargo hold arrangement, but with great care. In this research, only when the approach is explicitly called a cargo hold FE analysis by ship classification societies or in literature, it will be referred to as such, else the naming partial vessel FE analysis will be used.

Three dimensional model As was the case with a full vessel FE analysis, the model must be discretized. While the element types do not differ, the element size becomes more refined in order to capture local stresses. It is common practise to use a standard mesh, which has one element between each stiffening element and three elements over the height of web frames, girders and stringers [16, 28, 29]. An example is shown in Figure 2.11, which should be compared to Figure 2.8.

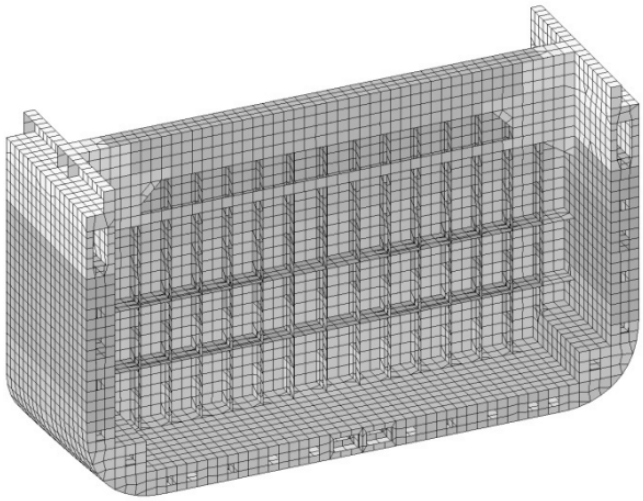

Figure 2.11: Standard mesh with one element between every stiffening element and three elements over the height of web frames, girders and stringers [28].

Additionally, the size of the vessel section must be decided upon such that the section ends are far enough to reduce the boundary conditions effect on the evaluation area (i.e. the analyzed area) [3]. In the DNV guidelines [17], they mention to use three cargo holds to create a vessel section, as does BV in their most recent rules [16]. Normally, the midship area is considered, but the analysis may be applied elsewhere (e.g. foremost or aftmost cargo hold region) with minor variations [29]. Both BV and DNV consider the mid-cargo hold as the evaluation area.

Until 2021, however, BV [36] specified to use one cargo hold for vessel lengths below 170 m, and at least three cargo holds for lengths above 170 m. In the case of one cargo hold, it should span half the hold length at each side with respect to the lateral bulkhead. Another viewpoint on this matter comes from Bai et al. [3], who note either two or three cargo holds are used among ship classification societies, depending on the vessel type. They however state by themselves to use one cargo hold which spans half the hold length at each end.

Boundary conditions The model is constrained at the vessel section ends to avoid rigid body motion, as well as to be representative for the actual behaviour and not introduce any abnormal stresses. In the BV rules [16], the boundary conditions for a cargo hold model (with three cargo holds) are discussed. The constraining of the degrees of freedom is given in Table 2.2, with reference to Figure 2.12, valid for any cargo hold model, except for the foremost cargo hold region. Rigid links, point constraints and end-beams are to be considered at both model ends. The rigid links establish the connection between the nodes of the longitudinal members and an independent point on the intersection of the centreline and neutral axis. An additional independent point is defined at the intersection of the centreline and inner bottom plate at the fore end, which is constrained in the x-direction. End-beams should only be applied to ships with large deck openings, which was independently verified by Rörup et al. [19] who studied this in depth. According to their findings, end-beams simulate that warping is constrained from occurring at the fore and aft end. Their out-of-plane stiffness acts as a constraint under torsional loading. Lastly, it is observed a hull girder torsional moment adjustment T_{end} is applied at the aft end, which will be later discussed in this section.

Table 2.2: Boundary conditions at the fore and aft end of the cargo hold model. Adopted from the rules of BV for the classification of steel ships (edition 2022) [16].

Location	Translation			Rotation		
	x	y	z	x	y	z
Independent point at aft end	-	fix	fix	T_{end}	-	-
Independent point at fore end	-	fix	fix	fix	-	-
Intersection centreline and inner bottom at fore end	fix	-	-	-	-	-
Cross section at both ends	-	rigid link	rigid link	rigid link	-	-
Note 1: Valid for any cargo hold model (with three cargo holds), except for the foremost cargo hold region. **Note 2:** [-] means no constraint is applied.						

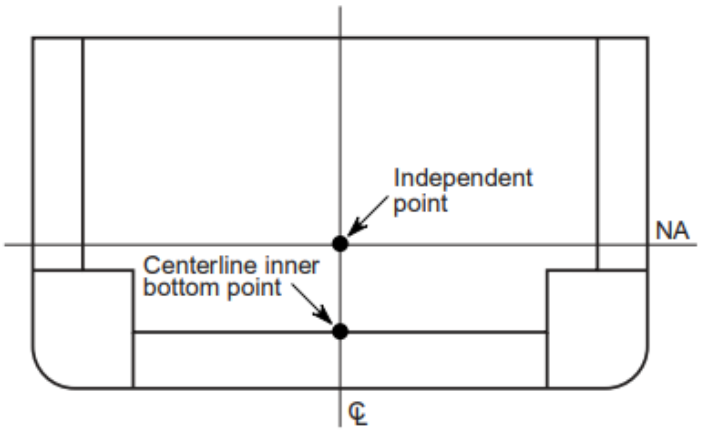

Figure 2.12: Cargo hold model section ends [16]. NA stands for neutral axis and CL stands for centreline.

Identical boundary conditions are reported in [19, 29] by Rörup et al. and in [17] by DNV. An opposing view comes from Salazar-Domínguez et al. [37], who conducted a study on the structural analysis of a barge midship section. It is mentioned the plane of the fore and aft end should remain flat under loading, but it must be able to rotate as a whole. Therefore, rigid links between all continuous longitudinal stiffeners and an independent point were created. The independent point is located on the centreline, close to the neutral axis. Although it was no requirement for the point to be exactly on the neutral axis. Furthermore, only rotation around the y-axis was allowed, which also differs from the boundary conditions in Table 2.2. But given their loading condition comprises only of a vertical bending moment (around the y-axis), the boundary conditions are very similar.

The earliest edition of the guideline from DNV which includes the boundary conditions as mentioned in Table 2.2 was published in October 2015 [38]. However, BV only had it incorporated in their rules as of 2022. Until 2021, the BV rules [36] reported apparent different boundary conditions. They made a distinction between one and at least three cargo holds used in the three dimensional model, for a vessel length below and above 170 m respectively. With at least three cargo holds, it was reported to fix one end, and apply the loading on the other end. Besides, rigid constraints are applied on the free end to the nodes of the longitudinal members, to ensure the section end remains plane after loading. For the cargo hold model with one hold, on the other hand, the constraining of the degrees of freedom is defined in Table 2.3.

Table 2.3: Boundary conditions at the fore and aft end of the cargo hold model with one hold according to BV rules (edition 2021) for the classification of steel ships [36].

Translation along axis			Rotation around axis		
x	y	z	x	y	z
fix	-	-	-	fix	fix

Tanny et al. [39] conducted a study on two design software to perform a finite element analysis of a container ship's cargo hold. First, they did an analysis using the software POSEIDON. Second, the same analysis was performed but in Ansys, with identical boundary conditions to those specified in Table 2.3, although BV is not explicitly mentioned in their paper. Besides, they analysed a cargo hold model with three holds.

Loading The loads to consider for a partial vessel FE analysis are identical to those for the full vessel FE analysis, which include the lightweight, deadweight, buoyancy and wave pressure. Again, the first three loads (i.e. the weight) can be independently applied to the finite element model [16, 17]. The wave pressure, on the other hand, comes from a hydrodynamic analysis and must be transferred to the finite element model. Different procedures for the mapping of hydrodynamic loads have already been discussed with the full vessel FE analysis. Additionally for the partial vessel FE analysis, the following must be considered. The above-mentioned loads induce hull girder loads which represent a semi-global effect since a section of the vessel is only treated [19, 29]. For this reason, hull girder load adjustments must be made to the model [16, 17].

The following is applicable to a cargo hold model with three holds in the midship area. First, hull girder targets are defined for each hull girder load. It is needed to adjust the hull girder

loads in order to reach these desired targets at required locations by applying additional forces and moments [16, 17]. In general, the procedure of applying the adjustments abides to the following steps below, which is clearly depicted by Rörup et al. in [19].

From a hydrodynamic analysis, the hull girder loads per frame can be retrieved to obtain a one-dimensional load distribution. Assuming the model is simply supported at both ends, the following adjustments can be made. First, vertical shear force adjustments are made to reach the required targets. Either vertical bending moments are applied at the model ends to reach the target at only one bulkhead, or vertical forces or applied at each frame to reach the target at both bulkheads of the mid-hold cargo. Second, the vertical and horizontal bending moment are adjusted by applying additional bending moments at the model ends to reach the target at the mid-hold cargo. Third, the torsional moment is adjusted by T_{end} at the aft end (see Table 2.2) to reach the target. And lastly, in case there are any longitudinal unbalanced forces, they must be adjusted so there is no reaction force at the model ends.

Only as of 2022, this procedure was incorporated in the BV rules [16] as well. Before, in 2021, BV [36] specified different boundary and loading conditions. The distinction was made between one and at least three cargo holds used in the three dimensional model. In case of the model with at least three cargo holds, hull girder loads are applied at the model free end. Already they mentioned adjustments to these loads, similar to the current rules. Interestingly, in the case of the model with one cargo hold, it is specified to add the hull girder loads to the stresses as obtained from the finite element analysis with the local loads (i.e. payload). Thus, they are not applied to the model as adjustments, but simply analytically added to the stresses obtained from the finite element analysis with the payload.

2.2.4 Fine mesh FE analysis

Previously, the full vessel and partial vessel FE analysis were discussed. The last approach, a fine mesh FE analysis, can be used simultaneously. Whereas nodal solutions (e.g. displacement and force reactions) are barely affected by the mesh density, elemental solutions (e.g. stress and strain) can vary [40]. Thus, in case a coarse or standard mesh does not suffice to capture local details of high stress regions, a fine mesh is used in the finite element analysis [16, 17]. It is reported by BV [16], for instance, to use a mesh size not greater than 50x50mm for shell elements and at least have ten elements in all directions. Since mesh refinement is possible in local areas of high stress, the entire mesh need not be refined. Still, it might be the case the amount of elements is too great for the available computational power, which is reasonable to think considering the size of a vessel.

To avoid excessive run-time, the sub-modelling technique is often used. The idea is to cut out a small region (i.e. sub-model) from the initial model (coarse/standard mesh) and apply the displacement results on the sub-model (fine mesh) as boundary condition. Since nodal solutions are not significantly affected by the mesh density, it should have a reasonable accuracy. The interpolation of the nodal displacements from the initial model can be retrieved and put as boundary conditions on the sub-model [41]. Sub-modelling is based on the Saint-Venant's principle, which says a load may be replaced by a statically equivalent load, as stress and strain will not change at sufficiently large distance from the load application [42]. For this reason, the cut in the initial model should be far enough from the evaluation area in the sub-model, otherwise the solution may not be representative [40].

2.2.5 Advancements in finite element analyses

Thus far, the focus has mainly been on the respective field of research. With finite element analyses, however, expertise can be found elsewhere. In this section, the progression in the field of aerospace engineering is investigated. Applications such as the fuselage of an airplane are studied, because to some extent, it is analogous to the partial vessel FE analysis.

A study conducted by Boni et al. [43] uses the finite element method to analyse a fuselage section of an airplane. They define an analysis zone between which the boundary effects due to the loads and constraints disappear. The model is divided into 36 bays, with only 7 attributed to the analysis zone. Shell elements are mainly used to represent the thin-walled parts in the structure, and beam elements are used to model stiffening members. On the other hand, the presence of stringers is accounted for by an equivalent thickness of the plates. Different to current practices in marine engineering, the analysis zone is characterised by more detail in the following manner. It is specified to adopt a structured and finer mesh there, while a coarser mesh near the boundaries satisfies. In between both regions, a transition region is present which has a free mesh. Furthermore, shell elements are used in the analysis zone, while frames and floor beams are modelled as a beam element in the boundary zones.

A later study by Boni et al. [44] discusses two different finite element analyses of a fuselage section, namely one where frames and floor beams are modelled as beam elements and the other which uses shells elements. It is stated that using beam elements is satisfactory to obtain the stress distribution at a sufficient distance from the frames. But in case stress results near the frames or of the frames themselves are desired, it is recommended to use shell elements. This is because it can account for the variation in cross-section along the perimeter, and it takes into account the presence of holes for the stringer crossings.

For the analysis of the fuselage section aft of the wing, the end near the rear spar of the wing is clamped, while the other end is free [43, 44]. The loads from the tail are applied at the free end via a multi-point constraint, which include a torsional moment, bending moment and vertical shear force. Other loads to consider are the upper and lower deck loads in the nominal case of 1-g acceleration, and the pressure load on the skin [44]. A graphical representation of the setup of the fuselage section is shown in Figure 2.13.

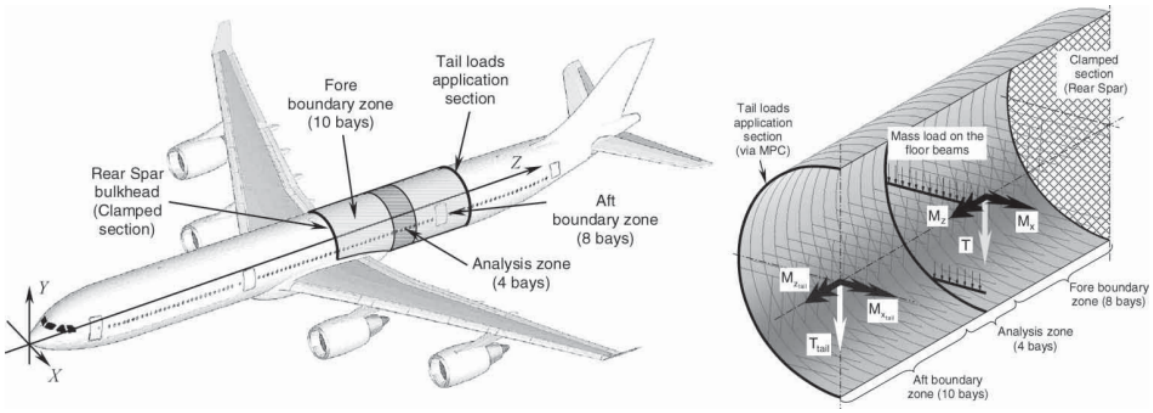

Figure 2.13: Fuselage section with boundary conditions and loads applied [44].

Adams et al. [45] performed a finite element analysis on the crashworthiness of an aircraft fuselage. The boundary conditions and forces are not discussed here because they are too distinct from the case in this research. Although it is worth mentioning that the water in the fuel tank is modelled as evenly distributed concentrated masses on its bottom. They repeatedly mentioned to reduce the complexity of the model, but at the same time it is stated this could result in an accumulation of errors to the extent that the model can no longer be representative to reality. The geometry, as well as the discretisation process, must reflect the actual model. It was decided to simplify windows to rectangular cutouts and fasteners and doublers were omitted from the model. Furthermore, every structural member should be reflected by an element that accurately describes its behaviour. For this reason, quad-shell elements were used to model the skin, frames, floor, etc. On the other hand, beams were used for stringers and the stiffening members at the cutouts. Lastly, different parts were enforced to share common nodes to provide a uniform load transformation.

Other than the fuselage of an airplane, its wing can be studied. Although it resembles to a lesser extent a vessel section, some features such as the element types are very similar. According to Shetty et al. [46], a general purpose eight-node shell element is appropriate, as one of its features is that it can be curved. Besides, the normal to the element surface is defined for each individual node, which facilitates pressure application normal to the element. Aabid et al. [47] conducted a study on the structural analysis of a three-dimensional wing. They mention a structured mesh will lead to more accurate results. Various mesh features exists, used for mesh manipulation. Among these features are capture curvature, capture proximity and mesh defeaturing [47, 48]. In particular, mesh defeaturing is interesting because it removes irrelevant details to obtain a high quality mesh.

Jang et al. [49] conducted a study about a finite element modelling methodology for the load analysis and preliminary sizing of a military aircraft wing structure. In their analysis, initially, a coarse grid mesh was adopted. It is generally used to define the load path, to calculate the internal load and free body load, and to acquire the stiffness and displacement of the structure. It is mentioned that accurately reflecting the stiffness is crucial since it has a direct impact on the internal load distribution. Furthermore, in the preliminary sizing design phase, it was decided to omit structural details from the analysis. Moreover the web, skin and longitudinals were modelled by shear, membrane and rod elements respectively. Only in later design phases, for instance to obtain accurate strain results to compare with test data, the model will have a finer mesh, the structure should be reflected in more detail, and shell and beam elements must be used.

The difference in usage between a coarse and finer mesh is explained in the previous paragraph. Although, the decision on the amount of elements used for the coarse mesh has not been emphasized. Previously, guidelines on the mesh size were provided for a full vessel FE analysis versus a partial vessel FE analysis. While it can certainly be used as a reference, it should not be followed blindly. The answer to this matter is a mesh discretisation study. Jackson et al. [50] conducted a study about a finite element simulation of vertical drop tests of two F-28 fuselage sections. For the first case study where a coarse mesh had been adopted, the results in the prediction of the soil crater depth showed discrepancies to the test data. With the second case study, on the other hand, a much finer mesh was used and the results closely agreed to the test data. A mesh discretisation study could have been used to avoid this issue in the first case study, but they reported it was not performed due to limited amount of time.

2.2.6 Concluding remarks

Four different design approaches for vessels have been discussed. The first one is based on rules, mainly of semi-empirical nature, established by ship classification societies. Its shortcomings have been highlighted for unconventional ship types, and it is argued why it would not suffice for an offshore installation vessel. While this approach lacks general applicability, rules such as corrosion allowances must always be considered.

Nowadays, more attention to finite element analyses is given, among which are the full vessel and partial vessel FE analysis. The full vessel FE analysis is used to retrieve the overall hull girder stiffness and global stresses and deformations. In case a more detailed view is desired, including local stresses, a standard mesh is necessary. To avoid any computational difficulties, a vessel section is made, leading to the partial vessel FE analysis. With the full vessel model, the analysis is similar across different ship types because the vessel is considered in its entirety. With the partial vessel model, on the other hand, the methodology as defined by ship classification societies or in literature is based on ships with cargo holds, referred to as a cargo hold FE analysis. For offshore installation vessels, no cargo holds are present, and thus the applicability of the cargo hold FE analysis to it remains unknown. For instance, the reported procedures of the load adjustments are based on a cargo hold model with three holds. Finite element analyses are extensively used in other fields too. For this reason, similar applications from aerospace engineering were investigated. The fuselage and wing of an airplane were studied, reporting any advancements in this field and analogies to the partial vessel FE analysis. Summarizing some of the important points: the consequence of simplifications in the three dimensional model on the accuracy must be examined, reasoning behind the hull girder load adjustments is desired, and the achievable accuracy in the evaluation area of the vessel section should be known.

An offshore installation vessel must also be analysed with its payload. Yet, no research on the modelling of offshore structures on an offshore installation vessel combined with the partial vessel FE analysis was found in literature. Likewise, it is not broadly discussed by ship classification societies. The effect of high local loads is, however, very relevant in the offshore industry. Offshore structures such as a monopile can weigh over a 1000 tonnes [51], which introduces high local stresses into deck. It is desired to know how to incorporate offshore structures and their seafastening grillages in the partial vessel FE analysis. On the one hand, the local change in stiffness at the deck should be represented. On the other hand, it must be known where it can be placed in the evaluation area.

2.3 Verification and validation strategies

The utility of a partial vessel model for the structural analysis of an offshore installation vessel was concluded upon in subsection 2.2.6. Its potential shortcomings have been pointed out and it should be clear it is not straightforward to perform a correct finite element analysis. To evaluate if the partial vessel FE analysis works as intended, it must be verified and validated. Two major aspects in the design of a vessel are hydrodynamics and structural mechanics. Both fields are therefore most often researched and are subject to verification and validation. For instance, Tupper [52] discusses the need of model testing for the motion analysis of unconventional ships, new theories and theories deemed not accurate enough. He mentions

that common strategies include theory, model testing (i.e. reduced scale testing) and full scale testing. Analogous to hydrodynamics, verification for structural analysis comprises of analytical models and numerical models, while validation consists of reduced scale testing and full scale testing.

Barrass et al. [53] mention three structural tests on full scale models. To load the hull of a vessel to destruction and record the ultimate load and failure mechanisms. To measure strains over a short time period at sea, at the same time recording the sea state conditions. Lastly, to measure strains over a long time period to understand the fatigue behaviour. For the scope of this research, full scale testing is not considered feasible because of limited time and resources. Reduced scale testing, on the other hand, is often reported in research, but a limited amount of studies exists for structural analyses. It is rather used to perform, among other things, a motion analysis in different sea conditions [54, 55], study sloshing effects [56], etc. In order to account for the scaling effect to relate the results back to full scale, an understanding of similitude theory is required as well [57, 58]. For this reason, reduced scale testing is deemed out of the scope of this research too, and thus validation is not treated.

With verification, the outcomes could be compared to a simple analytical model. This has the advantage to be easy to understand and to trace back any differences to the partial vessel FE analysis. Another strategy would be to compare the results to the original full vessel model. Since the full scale model is used, it must be more accurate. But the complexity also increases significantly, since a large, complex structure takes time and effort to model. In this section, an analytical stress calculation and a full vessel model are discussed.

2.3.1 Analytical stress calculation

Shama [59] discusses a straightforward analytical approach that can be used to obtain the von Mises stress at any position on the cross-sectional area along the vessel's length. Normally, all hull girder loads should be considered, but for illustration purposes, the vertical shear force and vertical bending moment are only included. The easy to understand calculation goes as follows. The flexure formula to obtain the normal stress σ_x is given as [42]

$$\sigma_x = \frac{M_v \cdot z}{I_y} \tag{2.5}$$

Where M_v is the vertical bending moment, I_y is the second moment of area about the y-axis, and z the distance from the neutral axis. It is convenient to define a geometrical parameter, the section modulus, as

$$Z = \frac{I_y}{z} \tag{2.6}$$

Shear stress τ_{xz} can be obtained from the vertical shear force F_s, the first moment of area Q_y, the second moment of area I_y and the thickness t [42].

$$\tau_{xz} = \frac{F_s \cdot Q_y}{I_y \cdot t} \tag{2.7}$$

Notice the shear flow q is defined as the shear stress times the thickness. Since the first moment of area is highest at the neutral axis, so is the shear flow there. Then, the von Mises stress σ_{vm} predicts an equivalent tensile stress for ductile materials under a 3D stress state, which can be compared to the stress results from the partial vessel FE analysis.

$$\sigma_{vm} = \frac{1}{\sqrt{2}}\sqrt{(\sigma_x - \sigma_y)^2 + (\sigma_x - \sigma_z)^2 + (\sigma_y - \sigma_z)^2 + 6(\tau_{xy}^2 + \tau_{xz}^2 + \tau_{yz}^2)} \tag{2.8}$$

In the end, this is one example of an analytical stress calculation which includes vertical shear force and vertical bending moment. Other book chapters that can be used as reference include, but are not limited to:

- **Ship Construction** - Stresses to which a ship is subject [13].
- **Introduction to Naval Architecture** - Structures [7].
- **Design Principles of Ships and Marine Structures** - Structural Design [60].

2.3.2 Full vessel model

A full vessel FE analysis is commonly used to determine the overall hull girder stiffness and global stresses and deformations as described in subsection 2.2.2. Although, it was argued in subsection 2.2.3 that a partial vessel FE analysis should be used in case a detailed view of the local stresses is required. In order to prove the structural analysis of a partial vessel model is correctly performed, its full vessel model can be used as a verification tool. It is stated by Rörup et al. [19, 29] that traditionally a global strength analysis was dealt with in a separate finite element model. But they emphasize that by using the same mesh and load cases, it should return identical results as for the cargo hold model. As an example, the von Mises stress at the main deck for the cargo model versus the full vessel model of a bulk carrier is shown in Figure 2.14. It can be seen the stress is very similar in the evaluation area. However, the same comparison was done for a container ship, which showed more discrepancies.

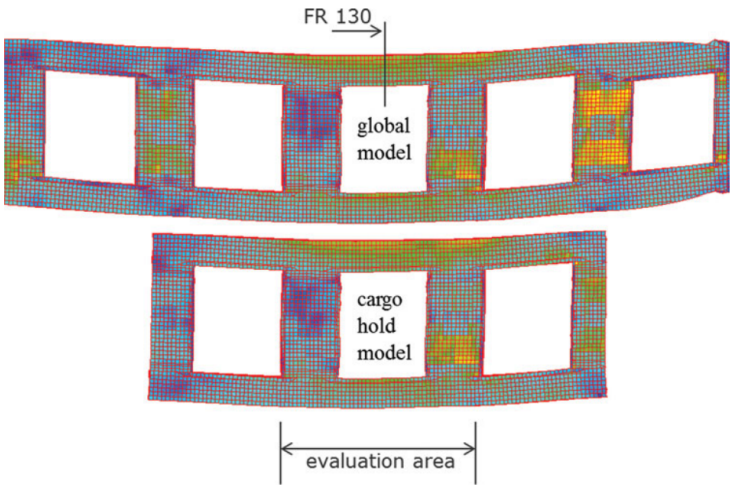

Figure 2.14: Comparison of a cargo hold vs full vessel FE analysis, von Mises stress at main deck of a bulk carrier [19].

2.3.3 Concluding remarks

In this section, verification and validation strategies relevant to the structural analysis of an offshore installation vessel were discussed. Experimental testing as part of validation was considered out of the scope of this research, while verification on the other hand is feasible. The analytical stress calculation is by no doubt the most straightforward manner, whereas the full vessel is most accurate since it forms a better representation of reality. It should be noted, however, that both manners can serve as a good verification tool, where one is not better than the other. In fact, it is only important to be able to explain why differences, if any, to the partial vessel FE analysis occur. For this reason, a critical review is made on both verification strategies.

With the analytical stress calculation, the maximum shear stress and bending moment may be used simultaneously to calculate the von Mises stress. However, as they do not occur at the same location on the cross-sectional area, it would overpredict the stress. At the same time, the average shear stress could be taken instead of the maximum, and thus the stress would be underpredicted. Furthermore, simplifications made to estimate the second moment of area of a cross-section would lead to higher stresses since not every structural detail is taken into account. One must be aware of the implications of these actions on the stress results. Moreover, an offshore installation vessel has a (double) deck which is very stiff, as opposed to the structure underneath. Any seafastening grillage and payload on deck may further increase the deck stiffness. As a consequence of this sudden change in stiffness, high stress concentrations will occur right underneath the deck. This local effect cannot be captured with simple analytical equations. According to the flexure formula, the highest stress due to the bending moment would occur at the most outward location (e.g. hull or main deck). When comparing the maximum stress results, it would be done at two different locations, which is not correct. On the other hand, the full vessel FE analysis could be used. The modelling has already been discussed in subsection 2.2.2. While a global vessel returns the most accurate results since it is the best representation of reality, it can also be prone to errors due to its complexity.

2.4 Conclusions, research objective and questions

Rules in the guidelines issued by ship classification societies are used for the design of vessels. However, this approach lacks general applicability and does not always provide enough detail. For instance, in the case of an offshore installation vessel, it does not take into account the change in stiffness on deck where the seafastening grillages and payload are positioned. For this reason, approaches based on the finite element method are investigated.

The full vessel and partial vessel FE analysis are both approaches to analyse the global behaviour of a ship. There are two reasons the full vessel FE analysis is not always preferred. First, a coarse mesh must be adopted and second, it takes months to model an entire vessel. This research will investigate the partial vessel FE analysis of an offshore jack-up installation vessel. The cargo hold FE analysis described by ship classification societies and in literature can serve as reference. Furthermore, an offshore jack-up installation vessel is loaded by heavy payload on deck. The modelling of the payload will be incorporated in the partial vessel FE analysis to gain a better understanding of high local loads on deck.

Concluding, the first aim of this research is to develop a methodology for the partial vessel FE analysis of an offshore jack-up installation vessel. The goal is to analyse a section of the vessel that reflects the structural behaviour of the full vessel. The second aim is to perform the partial vessel FE analysis including offshore structures. The research objective goes as follows:

> *To develop a methodology for the structural analysis of an offshore jack-up installation vessel by means of a partial vessel finite element analysis.*

Two research questions are formulated to be able to answer the research objective, which are further decomposed into a few sub-questions.

1. How to perform a partial vessel FE analysis of an offshore jack-up installation vessel?
   (a) How does the mesh size in the model affect the accuracy of the stress results?
   (b) What are the required hull girder load adjustments?
   (c) What accuracy can be achieved and how large is the evaluation area?
2. How should loads from offshore structures on deck be accounted for in the partial vessel FE analysis?
   (a) How to model offshore structures and their seafastening grillages?
   (b) Can the same mesh size be used as for the vessel without payload?

Chapter 3

Partial vessel FE analysis methodology

This chapter describes the methodology for the partial vessel (linear elastic) FE analysis of an offshore jack-up installation vessel. The general outline of this methodology is visualised by the flow chart in Figure 3.1. First, the three dimensional model is considered in section 3.1. Second, the boundary conditions of the model are mentioned in section 3.2. The different constraints will be examined and their effects anticipated. Third, the loads are covered from section 3.3 until section 3.5. It will be extensively discussed and includes the load adjustments, which is an essential part of this research. Fourth and lastly, in section 3.6, the verification of the methodology is explained.

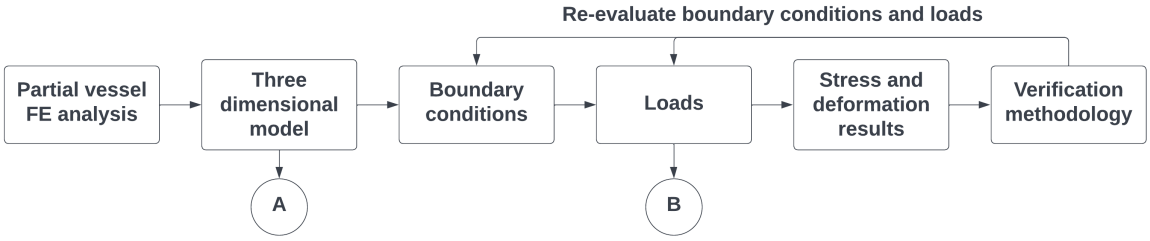

Figure 3.1: Flow chart showing the methodology for the partial vessel FE analysis of an offshore jack-up installation vessel.

3.1 Three dimensional model

This section discusses the three dimensional model following the flow chart in Figure 3.2. First, the detailed model of the offshore installation vessel that will be analysed is defined in subsection 3.1.1. Next, in subsection 3.1.2, the choice of element types and mesh size is reasoned. Then, subsection 3.1.3 describes the steps to acquire the simplified model. Lastly, different approaches to define contacts between individual parts of the model are compared in subsection 3.1.4. When the foregoing is completed, the quality of the mesh must be checked using available mesh metrics in the finite element software.

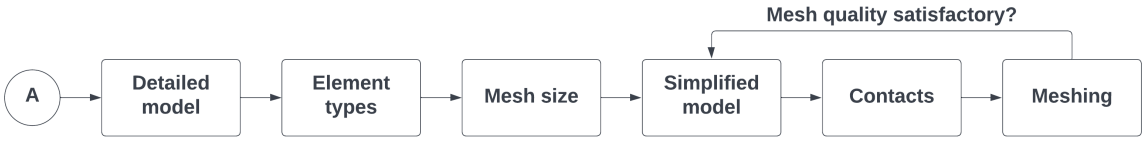

Figure 3.2: Flow chart showing the process of how to prepare the detailed model for the finite element analysis.

3.1.1 Detailed model

This research studies an offshore jack-up installation vessel, which is used for the installation of wind turbines at sea. The main feature of this vessel is that it is has legs to lift itself above the free water surface. In Figure 3.3, an offshore jack-up installation vessel is shown with wind turbine towers. The region between the four legs will be studied for two main reasons. It is where the highest bending moment is expected and the towers are located on deck.

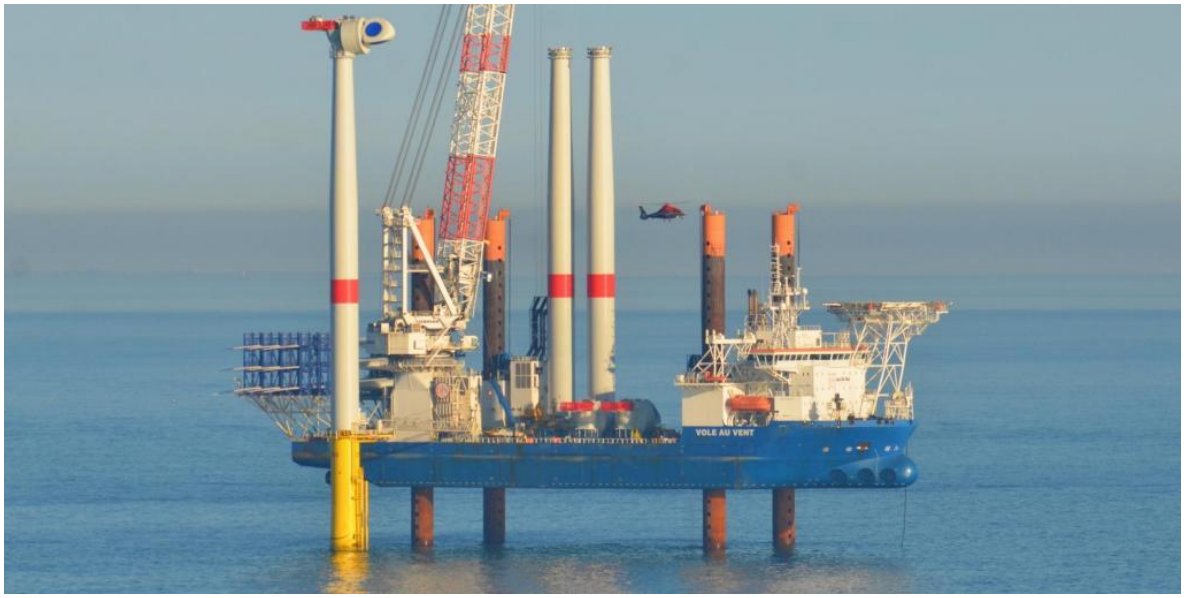

Figure 3.3: Offshore jack-up installation vessel with wind turbine towers between the four legs.

In Figure 3.4, the detailed model of the analysed region between the four legs of the offshore jack-up installation vessel is shown. A right-handed coordinate system is adopted with the x-axis pointing to the bow and the y-axis to port side. The origin is located at the bottom hull, centre line and frame zero. Besides, the wave directions with respect to the vessel used in this research are given in Figure 3.5, which are the same as defined in Ansys. In order to be consistent in naming, the following conventions are employed. When the vessel in its entirety is meant, it is called the 'full vessel'. The analysed region is called the 'vessel section' when referred to this region in the full vessel. On the other hand, the analysed region is called the 'partial vessel model' when referred to in the finite element analysis (FEA).

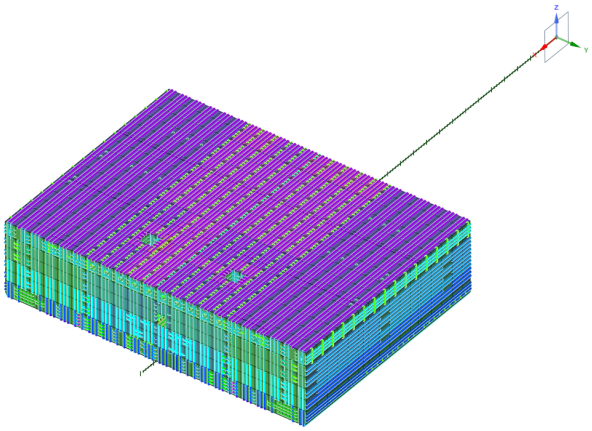

Figure 3.4: Detailed model of the analysed region between the four legs of the offshore jack-up installation vessel.

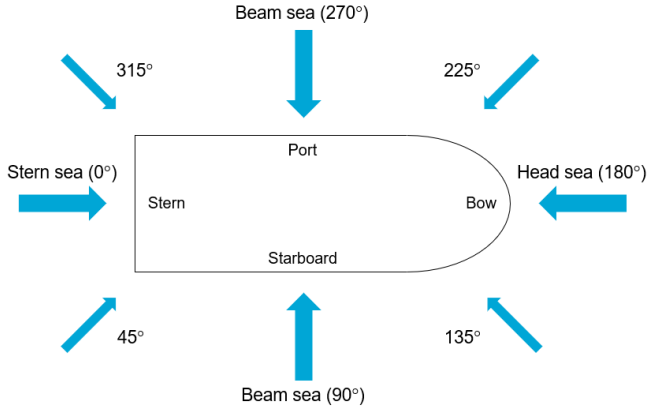

Figure 3.5: Wave directions with respect to the vessel as defined in Ansys.

The relevant parameters of the vessel section are given in Table 3.1. Besides, the material properties of structural steel can be found in Table 3.2. The yield strength is necessary to check that plasticity does not occur (i.e. linear elastic FEA). The detailed model consists of plate areas and stiffener profiles, which were modelled as shell element (2D). There are two type of profiles, namely flat bars and Holland profiles. Due to the complex shape of the latter, it was also modelled as a flat bar with equivalent thickness. The original profile specifications were retained, though.

Table 3.1: Relevant parameters of the vessel section.

Parameter	Value
Frame spacing	$700mm$
Aft end	$x = 63.7m$
Fore end	$x = 107.8m$

Table 3.2: Material properties of structural steel.

Property	Value
Density	$7850kg/m^3$
Poisson's ratio	0.3
Young's modulus	$200GPa$
Yield strength	$355MPa$

3.1.2 Element types and mesh size

The mesh of the partial vessel model is elaborated upon here. The fact that different load cases must be analysed, highlights the importance of carefully selecting the element types and mesh size.

First, the choice on the element types is explained. While the vessel itself is a complex structure, the individual parts consist of plate areas and stiffener profiles. It is decided to use shell elements (2D) for plate areas since it takes into account the in-plane and out-of-plane stiffness. For stiffener profiles, comprising of flat bars and Holland profiles, it is decided to use beam elements (1D) as it considers the bending stiffness. The element order can be linear or quadratic, which means without or with a mid-side node respectively. Eventually, first order elements were adopted due to the use of batch connections. The latter is a contact tool in Ansys, discussed further in subsection 3.1.4, which does not allow second order elements. In Spaceclaim, 1D elements are made by assigning a beam profile to a line body. For 2D elements, a surface is created to which a thickness is specified. In Ansys, the element type of the beam is BEAM188 and that of the shell is SHELL181.

Second, the mesh size is discussed. It is initially set equal to the frame spacing, which is in accordance with the rules of BV and DNV that state to have one element between each stiffener [16, 28, 29]. It should be avoided to use a fine mesh when not needed to, as it leads to a high element count and so increases the simulation time. In order to determine what mesh size is fine enough, a mesh convergence study is performed. The mesh size is further refined and taken as a factor of the frame spacing, i.e. 350mm, 233.33mm, etc. Subsequently, the stress results of the different mesh sizes are compared.

3.1.3 Simplified model

The current partial vessel model is too detailed. It would need a very fine mesh size and this significantly increases the simulation time. Therefore, the detailed model must be simplified with the aim of creating a structured mesh. The steps leading to this simplified model are discussed below, which have in common that they are based on the frame spacing to attain a possible (maximum) mesh size of $700mm$. Ultimately, from the mesh convergence study, the required mesh size should be determined.

- Plate areas are extended or retracted to a multiple of the frame spacing. The thicker of two adjacent plates is always shortened. Web frames, girders and stringers are not altered.
- Stiffener profiles are extended to a multiple of the frame spacing (see Figure 3.6). In reality, they are slightly smaller since plate areas have a thickness or two profiles intersect.
- Stiffener profiles are shifted to their closest location that is a multiple of the frame spacing.

- (Man)holes are represented by rectangular cutouts (see Figure 3.7). They are are shifted to their closest location that is a multiple of the frame spacing. The exception on this rule is found between the cofferdam and main deck and between the bottom hull and tank top, where the holes are retained at their initial position. That is because high stress is expected there and additional or fewer plate area would lead to an over- or under-estimation of the stiffness respectively.
- Brackets bounded by two stiffener profiles are deleted (see Figure 3.8). They are small enough and the profiles were already extended.
- The portion of the stiffener profile that touches girders and stringers is deleted and the latter is extended to the adjacent part (see Figure 3.9).
- Holes at a bulkhead or water ballast tank are filled because they are in reality reinforced and a pipe goes through.

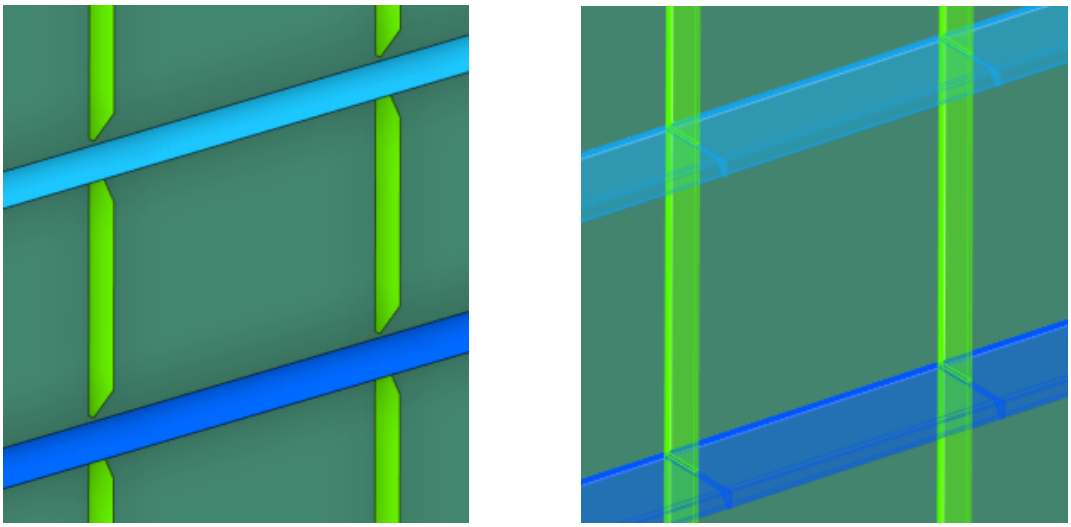

(a) Before simplification. **(b)** After simplification.

Figure 3.6: Simplification: extension of stiffener profiles.

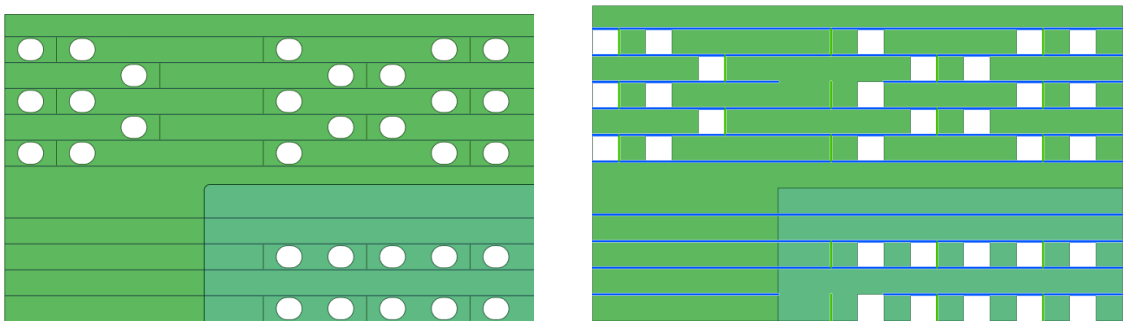

(a) Before simplification. **(b)** After simplification.

Figure 3.7: Simplification: (man)holes represented by rectangular cutouts.

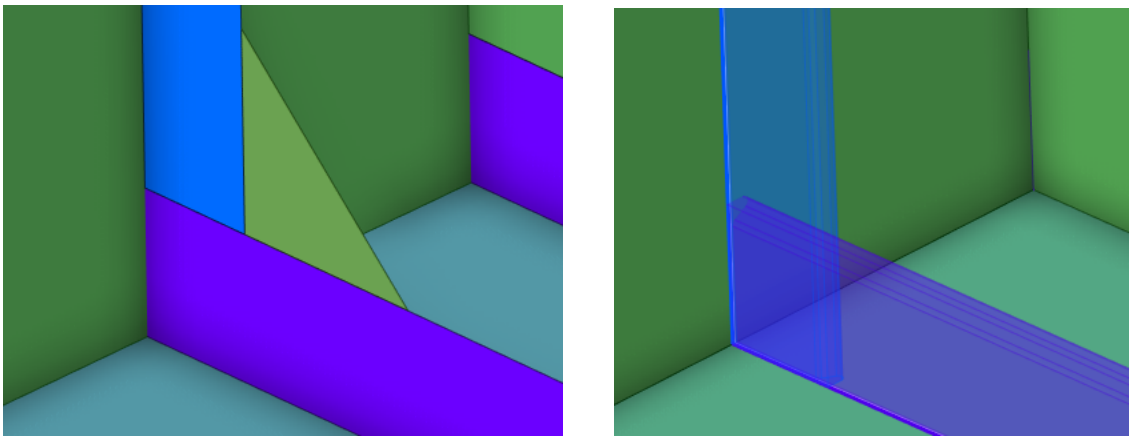

(a) Before simplification. **(b)** After simplification.

Figure 3.8: Simplification: deletion of brackets bounded by two stiffener profiles.

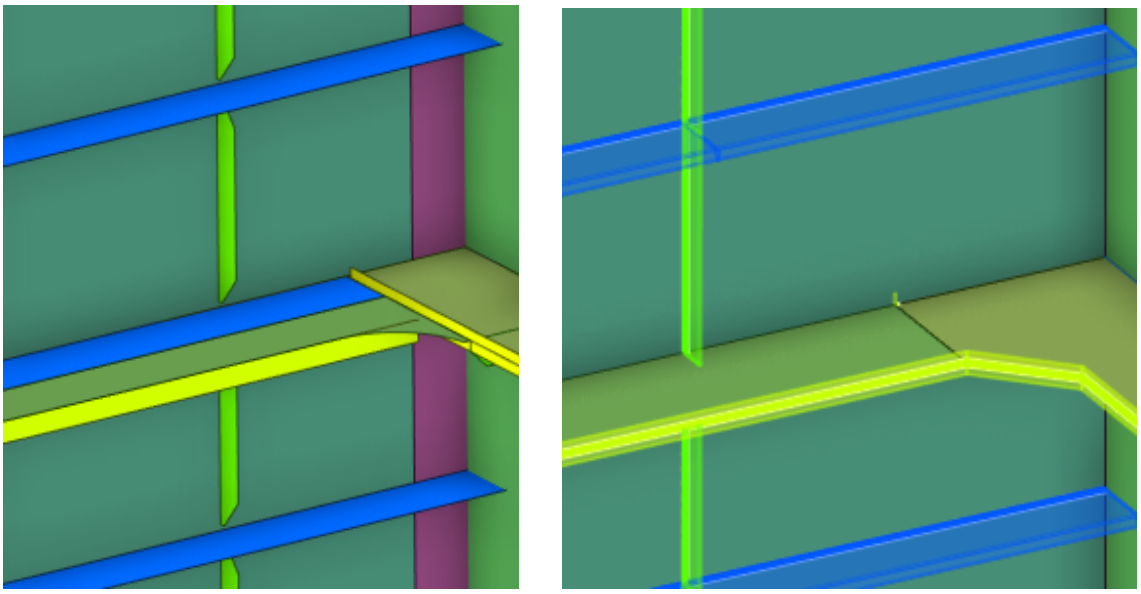

(a) Before simplification. **(b)** After simplification.

Figure 3.9: Simplification: extension of girders or stringers at a stiffener profile.

3.1.4 Contacts

The adjacent parts of the partial vessel model must be connected to each other for which two methods can be used. The advantages and disadvantages are stated per method for the software Spaceclaim and Ansys. From the discussion below, it is reasoned that batch connections are the best choice.

Shared topology is the first possibility that is examined. It is similar to a mesh connection from the point of view that a continuous mesh is created. However, the difference is that the contact is defined in Spaceclaim. The connections can be found automatically and different

colours indicate the amount of adjacent parts. Even in case the software fails to see some connections, they can be added manually. The main drawback to this method is that it is a lengthy process. But once completed, the mesh can be immediately generated without defining any additional contacts in Ansys.

The new feature of Ansys called batch connections is also considered, which is applicable to beams and shells and should replace shared topology for this matter.[1] It is able to automatically detect any connection based on the tolerance value specified by the user and generates the mesh at the same time. The main advantage is that it is quick and removes the tedious work that comes with shared topology. The only disadvantage is that this is a new feature and can yet be prone to bugs.

3.2 Boundary conditions

The partial vessel model in the FEA should reflect the actual behavior of the full vessel as accurately as possible and therefore must be constrained appropriately. The boundary conditions in the rules of BV for the classification of steel ships are followed, which are repeated for reference from the literature study in Table 3.3. This section explains the reasoning behind these conditions and discusses them with regard to Ansys. But first, the following matter is addressed. It is assumed that the presence of the legs does not affect the rigidity of the surrounding structure. The legs are fully enclosed and the surrounding structure is reinforced. Therefore, the boundary conditions at the fore end of the partial vessel model, which is close to the front two legs, remain unchanged.

The translation in y and z are fixed at both ends to prevent rigid body motion. It is valid to assume that each model end is at the same position along y and z. The translation in x, on the other hand, is only constrained at the fore end. This allows for the partial vessel model to freely expand or retract, which would otherwise cause axial stress. Furthermore, the rotation about y and z is free at both ends. Lastly, the rotation about x is fixed at the fore end to avoid rigid body motion, but not at the aft end to allow for torsion. In summary, the boundary conditions closely resemble a simply supported constraint in 3D.

Table 3.3: Boundary conditions at the aft and fore end of the partial vessel model. Adopted from the rules of BV for the classification of steel ships (edition 2022) [16].

Location	Translation			Rotation		
	x	y	z	x	y	z
Independent point at aft end	-	fix	fix	-	-	-
Independent point at fore end	-	fix	fix	fix	-	-
Intersection centre line and inner bottom at fore end	fix	-	-	-	-	-
Cross-section at both ends	-	rigid link	rigid link	rigid link	-	-
Note 1: [-] means no constraint is applied.						

[1] https://www.finiteelementanalysis.com.au/featured/batch-connections-in-ansys-never-use-share-topology-for-beam-and-shell-models/, Accessed [15-01-2023]

Interpreting these boundary conditions is not too difficult, but applying them to the partial vessel model in the FEA is not straightforward, which is emphasized as follows. It would be incorrect to constrain the cross-section of both ends in y and z because this would create a clamped constraint. For example, taking two nodes constrained on opposite side of the neutral axis, a moment about this axis would result in a counter reaction moment caused by opposite oriented reaction forces at each node. A solution to this matter is to connect all longitudinal members of each end to their respective independent point via rigid links. This point is located on the centre line at the neutral axis. The two independent points are constrained in y and z, and also about x at only the fore end. Nonetheless, all nodes of both ends are free to deform in such way that they allow rotation about y and z, and additionally about x at the aft end.

In Ansys, a remote displacement constraint can be defined that scopes a selected geometry (i.e. the longitudinal members) to an independent point. The behaviour of the links can be specified as rigid, deformable, coupled or beam. The rigid behaviour is selected for the reason that the vessel extends at the ends. The deformable behaviour, on the other hand, would allow for excessive deformation.

3.3 Load cases and case studies

In the following sections up to and including section 3.5, the loads are discussed following the flow chart in Figure 3.10. This section starts with a description of the load cases and leads to three distinct case studies that will be analysed. Then, in section 3.4, the hull girder load adjustments are covered. Lastly, in section 3.5, the application of the loads on the partial vessel model in the FEA is explained. When the aforementioned is completed, reaction forces and moments are retrieved from the FEA for verification.

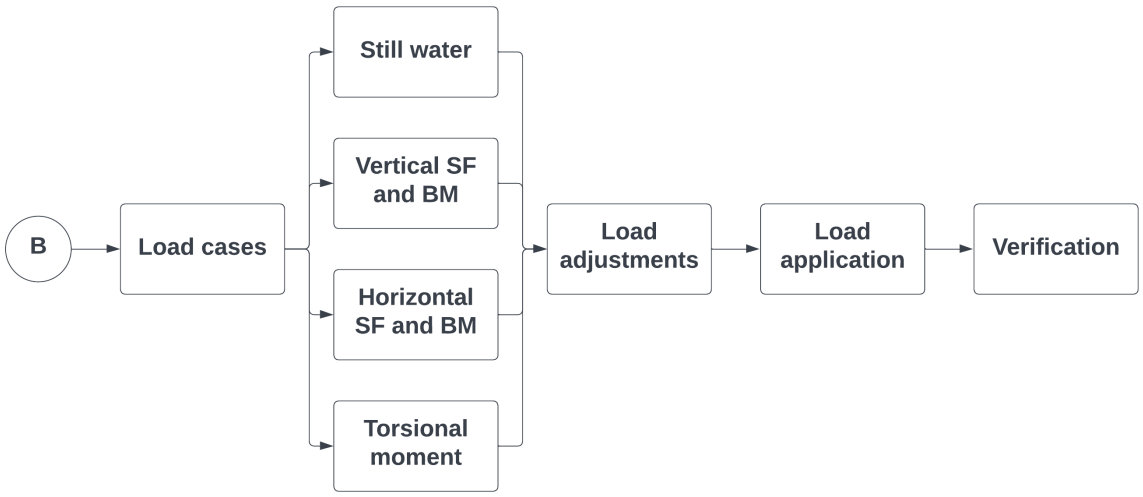

Figure 3.10: Flow chart showing the process to be followed for the loads in the finite element analysis. SF and BM stand for shear force and bending moment respectively.

A load case is defined by the following set of loads: weight, buoyancy, water ballast, wave pressure and payload. Strictly speaking, the water ballast is included in the weight, but its data is also provided since it is separately applied on the partial vessel model. The loads, on their turn, depend on the following variables: water depth d, vessel speed v, mean draft D, the significant wave height H_s, wave direction Ω, wave period T and wave spectrum. In Table 3.4, the values of most of these variables are given. The vessel speed is set equal to zero for simplicity and two mean drafts are specified for which the reason is mentioned in the next paragraph. Data that has not been provided will be mentioned in the corresponding chapter.

Table 3.4: General variables of the vessel and sea state.

Variable	**Value**
Water depth d	$100m$
Vessel speed v	$0m/s$
Mean draft D (without water ballast)	$4.75m$
Mean draft D (with water ballast)	$6.01m$

The methodology of the partial vessel FE analysis can be tested with a limited amount of load cases, which are referred to as case studies. It is convenient to separate the still water and wave component, although recall they occur simultaneously in reality. The first two case studies analyse the vessel in still water, which uses the weight, buoyancy and water ballast. The first case study (1a) is a fictive case that excludes the water ballast. The vessel would be unstable this way, unless any weight at port or starboard side is assumed to be on the centre line. The hull girder loads will in this case only comprise of the vertical shear force and bending moment. On the other hand, the second case study (1b) takes into account the water ballast and transversal position of weights and as a result will also include torsion. For both case studies, the hull girder loads are summarised in Table 3.5. The reason for two drafts should now also be clear.

Table 3.5: Case study 1 to test the methodology of the partial vessel FE analysis in still water. SF, BM and TM stand for shear force, bending moment and torsional moment respectively.

Hull girder load (still water component)	**Case study 1a**	**Case study 1b**
Vertical SF	↗	↗
Vertical BM	↗	↗
Horizontal SF	0	0
Horizontal BM	0	0
TM	0	↗

The last case study (2) analyses the vessel in waves and uses the wave pressure. By selecting the wave conditions carefully, one is able to decouple the hull girder loads. This research is limited in maximising the vertical shear force and bending moment, which is summarised in Table 3.6.

Table 3.6: Case study 2 to test the methodology of the partial vessel FE analysis in waves. SF, BM and TM stand for shear force, bending moment and torsional moment respectively.

Hull girder load (wave component)	**Case study 2**
Vertical SF	↗
Vertical BM	↗
Horizontal SF	≈ 0
Horizontal BM	≈ 0
TM	≈ 0

3.4 Hull girder load adjustments

Thus far, a partial vessel model is created and constrained appropriately at its ends. Different load cases are defined and subsequently, the loads should be applied on the model in the FEA. Although, first, it is necessary to determine the hull girder load adjustments. This is for the reason that a significant part of the vessel is neglected on which these loads act that are not seen by the partial vessel model. As a result, its behaviour does not reflect the full vessel behaviour. This section covers the load adjustment that must be applied on the model in the FEA. First, the adjustments for the vessel in still water are discussed and second, for the vessel in waves.

3.4.1 Vessel in still water

Vertical shear force and bending moment diagrams

In order to reason the load adjustments, the effect of the loads that act on the vessel section and full vessel must be compared in some way. For the vessel in still water, the weight and buoyancy are important. The water ballast will later also be needed, but recall it is already incorporated in the weight. It is assumed that the weight and buoyancy are uniformly distributed across the width of the vessel. By modelling the vessel section and full vessel as a beam, their vertical shear force and bending moment diagram can be constructed. Although the fundamental property of a beam is that two dimensions are much smaller than the third, with all three dimensions of the vessel being considerable, this choice is convenient for comparing both instances.

Since it is the full vessel behaviour that must be captured of which the bending moment measures zero at the free ends (i.e. the bow and stern), a simply supported beam is adopted as shown in Figure 3.11. A frame is denoted by the variable i, N is the total number of frames and x_{fr} is the frame spacing. The aft end x_{aft} and fore end x_{fore} are at $i = 1$ and $i = N$ respectively. Furthermore, a right-handed coordinate system is used, which means a positive moment goes counter-clockwise when viewed from the top of either axis. This also means that a positive vertical bending moment indicates the vessel experiences hogging, while a negative moment indicates sagging.

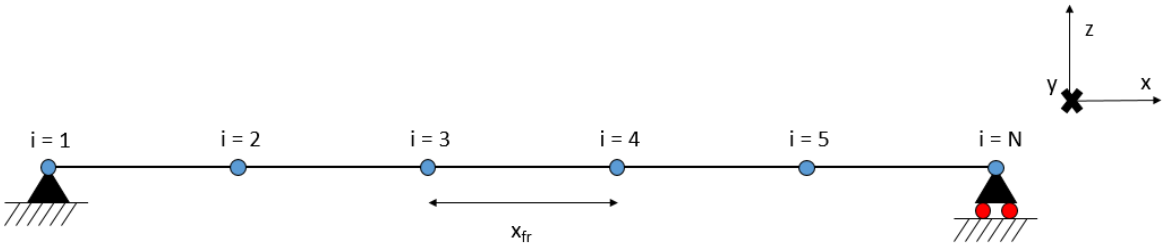

Figure 3.11: Vessel section and full vessel modelled as simply supported beam. A frame is denoted by the variable i, N is the total number of frames and x_{fr} is the frame spacing.

The weight w and buoyancy b per unit length should be known at each frame. The free body diagram of the beam is drawn in Figure 3.12, which shows these loads and the reaction forces R_{aft} and R_{fore} defined in positive z.

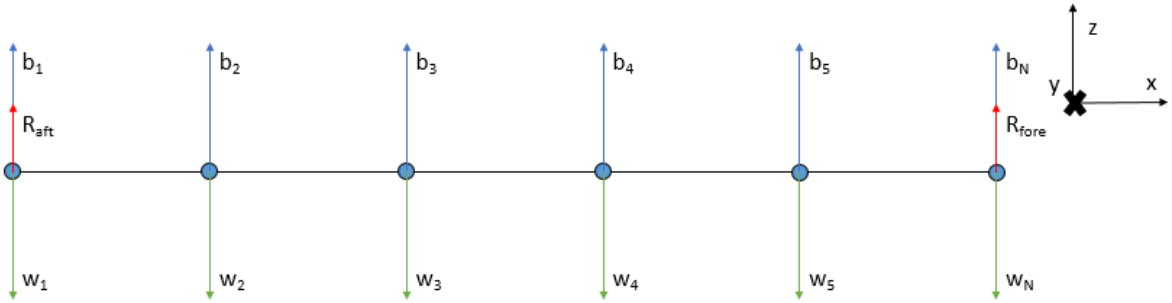

Figure 3.12: Free body diagram of the beam showing the weight w and buoyancy b per unit length at each frame and the reaction forces R_{aft} and R_{fore}.

The following intermediate calculation computes the average of the difference of weight and buoyancy per unit length between two consecutive frames, which is denoted by $(w-b)_{i,i+1}$.

$$(w-b)_{i,i+1} = \frac{(w-b)_i + (w-b)_{i+1}}{2} \tag{3.1}$$

Next, the reaction forces R_{aft} and R_{fore} are calculated. From moment equilibrium about the aft end, where the moment equals zero, the reaction force at the fore end is obtained. The reaction force at the aft end is calculated from force equilibrium along z.

$$R_{fore} = \frac{\sum_{i=1}^{N-1}(w-b)_{i,i+1} \cdot x_{fr} \cdot (x_i + 0.5x_{fr} - x_{aft})}{x_{fore} - x_{aft}} \tag{3.2}$$

$$R_{aft} = -R_{fore} + \sum_{i=1}^{N-1}(w-b)_{i,i+1} \cdot x_{fr} \tag{3.3}$$

Then, the shear force F_s is computed at each frame. Notice the subscript j is introduced, which follows the same numbering as subscript i.

$$F_{s,j} = -R_{aft} + \sum_{i=1}^{j-1} (w - b)_{i,i+1} \cdot x_{fr} \tag{3.4}$$

Lastly, the bending moment M is computed at each frame. While it possible to calculate this from the loads and reaction forces, the relation between the shear force and bending moment is directly utilised. The derivative of the bending moment with respect to x is equal to the shear force. Hence, the bending moment at a frame can be approximated by the area under the shear force diagram up till that frame.

$$M_j = \sum_{i=1}^{j-1} \frac{F_{s,i} + F_{s,i+1}}{2} \cdot x_{fr} \tag{3.5}$$

The foregoing calculation is applied to the vessel section and full vessel to obtain their shear force and bending moment diagram for comparison. In both instances, the bending moment equals zero at the ends. Although this holds true for the full vessel as it are free ends, it is incorrect to presume for the vessel section. Similarly, the shear force of the vessel section will not be entirely accurate. For this reason, the shear force and bending moment diagram of the vessel section will be adjusted to match those of the full vessel. Since the beam is simply supported and the partial vessel model as well (see section 3.2), the load adjustments can be directly applied on the model in the FEA. In what follows, the reasoning behind these adjustments is discussed.

Shear force adjustment

The shear force diagram of the vessel section will have the same shape as that of the full vessel, but with a constant offset. This is the case because a force does not depend on the distance (i.e. the moment arm). Therefore, the shear force adjustment should result in a constant shear force. For any point or distributed force, the shear force will always reverse sign at some point along the beam. The only configuration that would work is shown in Figure 3.13, which has two equal oriented moments, M_{aft} and M_{fore}, applied on each end.

Figure 3.13: Shear force adjustment of the vessel section. Free body diagram with two equal oriented moments, M_{aft} and M_{fore}, applied on each end and the reaction forces, R_{aft} and R_{fore}, defined in positive z.

Moment equilibrium about the aft end, which is equal to zero, is as follows.

$$\sum M(x_{aft}) : M_{aft} + M_{fore} - R_{fore} \cdot (x_{fore} - x_{aft}) = 0 \tag{3.6}$$

While the moments M_{aft} and M_{fore} can take on any value, it is decided to make them equal. This is not strictly required to obtain a constant shear force, but is done for good reason as will soon become apparent.

$$M_{aft} = M_{fore} = \frac{R_{fore} \cdot (x_{fore} - x_{aft})}{2} \tag{3.7}$$

The reactions forces at the ends are equal to

$$R_{fore} = -R_{aft} = \frac{2M_{aft}}{x_{fore} - x_{aft}} \tag{3.8}$$

The shear force diagram is shown in Figure 3.14. The shear force adjustment ΔF_s is defined in positive z, which then equals -R_{aft} = R_{fore}.

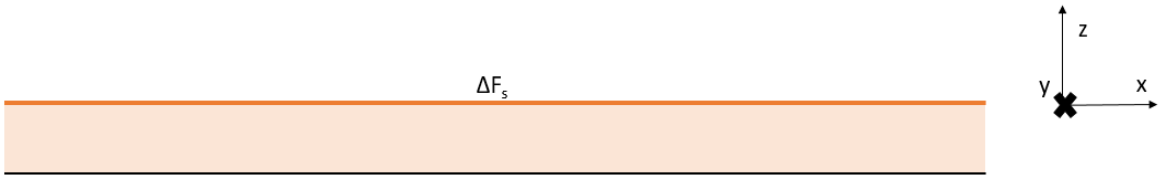

Figure 3.14: Shear force diagram from the shear force adjustment of the vessel section.

When the shear force adjustment ΔF_s is inserted in Equation 3.7, the expression in the box below is obtained. The moments M_{aft} and M_{fore} are applied on the ends of the partial vessel model in the FEA. In case the shear force adjustment needs to be positive in z, the moments should be positive about y as well. The opposite holds true when the shear force adjustment must be negative.

$$\boxed{M_{aft} = M_{fore} = \frac{\Delta F_s \cdot (x_{fore} - x_{aft})}{2}}$$

The shear force adjustment also results in a linearly varying bending moment. Figure 3.15 shows the bending moment diagram, which is equal to $-M_{aft}$ at the aft end and M_{fore} at the fore end. Recall the decision to have equal moments, which means the zero bending moment will occur exactly at the centre of the beam.

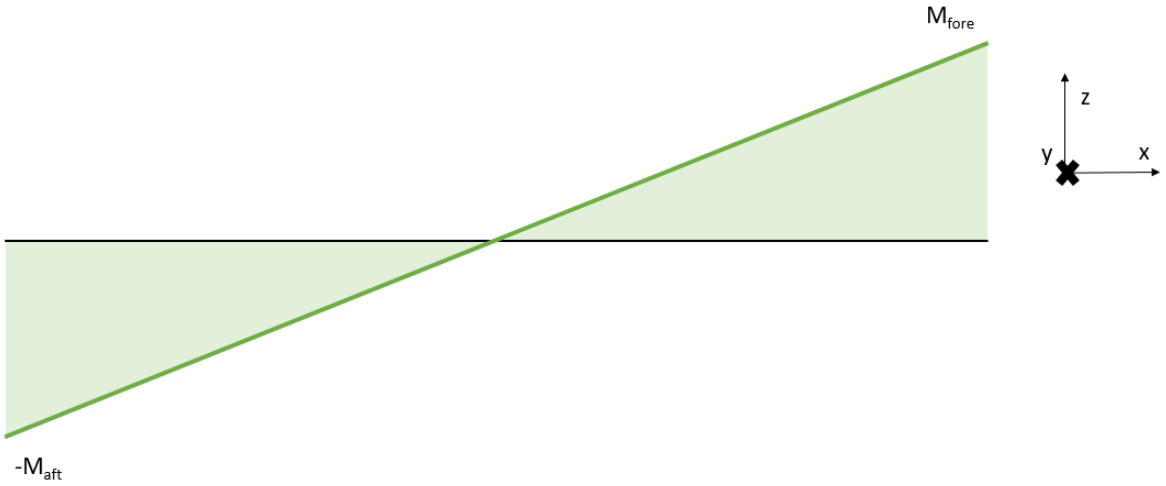

Figure 3.15: Bending moment diagram from the shear force adjustment of the vessel section.

Bending moment adjustment

The following is partly based on the rules of BV for the classification of steel ships (edition 2022) [16]. The bending moment of the vessel section is significantly under-estimated as it equals zero at its ends. While for the full vessel, the moment there is far from zero. Therefore, the bending moment adjustment is made, which additionally corrects the bending moment induced by the shear force adjustment. First, the moment M_{target} is retrieved, which is the maximum (hogging) or minimum (sagging) bending moment M_{full} of the full vessel within the mid-hold of the vessel section from $x_{mid-aft}$ until $x_{mid-fore}$.

$$M_{target} = |\max(M_{full}(x))|, |\min(M_{full}(x))| \quad \text{for } x \in [x_{mid-aft}; x_{mid-fore}] \tag{3.9}$$

Next, the moment $M_{extremum}$ is calculated, which is the maximum or minimum bending moment of the vessel section within its mid-hold. Two contributions can be distinguished, namely the bending moment $M_{section}$ of the vessel section, and the bending moment induced by the shear force adjustment.

$$M(x) = M_{section}(x) - M_{aft} - R_{aft} \cdot (x - x_{aft}) \quad \text{for } x \in [x_{mid-aft}; x_{mid-fore}] \tag{3.10}$$

The equation above is rewritten to express the last two terms related to the shear force adjustment only as function of the moment M_{aft}.

$$M(x) = M_{section}(x) + M_{aft} \cdot \left(2\frac{x - x_{aft}}{x_{fore} - x_{aft}} - 1\right) \quad \text{for } x \in [x_{mid-aft}; x_{mid-fore}] \tag{3.11}$$

Finally, the moment $M_{extremum}$ is equal to

$$M_{extremum} = |\max(M(x))|, |\min(M(x))| \quad \text{for } x \in [x_{mid-aft}; x_{mid-fore}] \tag{3.12}$$

The bending moment adjustment ΔM is equal to the difference of M_{target} and $M_{extremum}$ as shown in the box below. Two equal and opposite oriented moments ΔM are applied on the ends of the partial vessel model in the FEA. In case the vessel experiences hogging, the moments are applied as drawn in Figure 3.16. The direction reverses if the vessel experiences sagging.

$$\boxed{\Delta M = M_{target} - M_{extremum}}$$

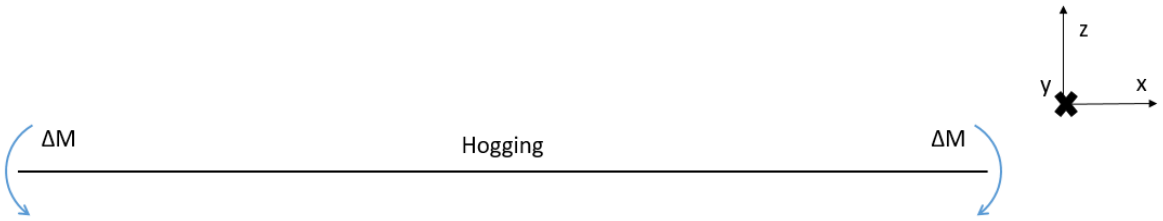

Figure 3.16: Bending moment adjustment of the vessel section for when the vessel experiences hogging. Free body diagram with two equal and opposite oriented moments, ΔM, applied on each end.

Torsional moment adjustment

The assumption was previously made that the weight and buoyancy are uniformly distributed across the width of the vessel. While this is valid to assume for the buoyancy, it is not true for the weight. For instance, the heavy lift crane is positioned at starboard side, but requires water ballast on port side for the vessel to be stable. Since these weights are at different longitudinal locations, a torsional moment distribution will exist. Therefore, the torsional moment adjustment is required.

The lightweight and every component of the deadweight, which are denoted by the load f_z, should be known. Moreover, their respective longitudinal location x and transversal location y must be known. The fore end of the partial vessel model in the FEA is fixed about x (see section 3.2), and thus every load that comes before this end is considered. However, the loads that fall within the vessel section must be included in the FEA, but not taken into account in the adjustment. The torsional moment adjustment ΔT is the summation of every torsional moment component induced by the loads that come before the aft end of the vessel section as shown in the box below. Notice the terminology x_{stern} is used here to indicate the aft end of the full vessel, which is done to distinct from the aft end x_{aft} of the vessel section. The moment ΔT is applied on the aft end of the partial vessel model in the FEA.

$$\boxed{\Delta T = \sum_{x_{stern}}^{x_{aft}} f_z(x) \cdot y(x)}$$

Application load adjustments

The load adjustments are applied at the ends of the partial vessel model on the corresponding independent point, as shown in Figure 3.17. Notice that the case shown is specific to the studied offshore jack-up installation vessel, which experiences hogging and has a positive torsional moment due to the presence of the heavy lift crane over the aft leg at starboard side. Moreover, the yellow arrow indicates the Standard Earth Gravity (i.e. the weight) and the red surface represents the hydrostatic pressure. In summary, at the aft end, the moment about y is equal to

$$M = M_{aft} - \Delta M \tag{3.13}$$

On the other hand, the moment about y at the fore end is equal to

$$M = M_{fore} + \Delta M \tag{3.14}$$

Lastly, at the aft end, the torsional moment is simply equal to ΔT.

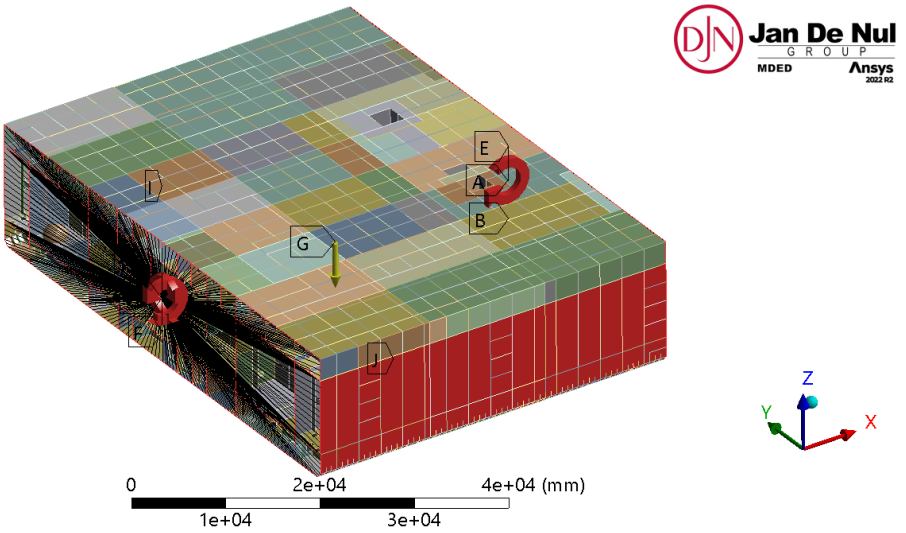

Figure 3.17: Load adjustments applied at the ends of the partial vessel model on the corresponding independent point.

3.4.2 Vessel in waves

Shear force and bending moment diagrams

Similar to the vessel in still water, load adjustments are applied on the partial vessel model for the vessel in waves. The only load to be taken into account is the wave pressure. Shear force and bending moment diagrams are again constructed. But first, the wave spectrum is briefly explained and second, the response amplitude operator (RAO) is discussed.

Sea waves originate from wind and are irregular. The non-periodic nature of the irregular wave can be decomposed into a sum of regular waves of different frequency. The sea state is mathematically described by a wave spectrum as shown in Figure 3.18, which gives the energy distribution of the waves as function of the frequency. There are several spectra to model the sea state, which are based on historical measurements.

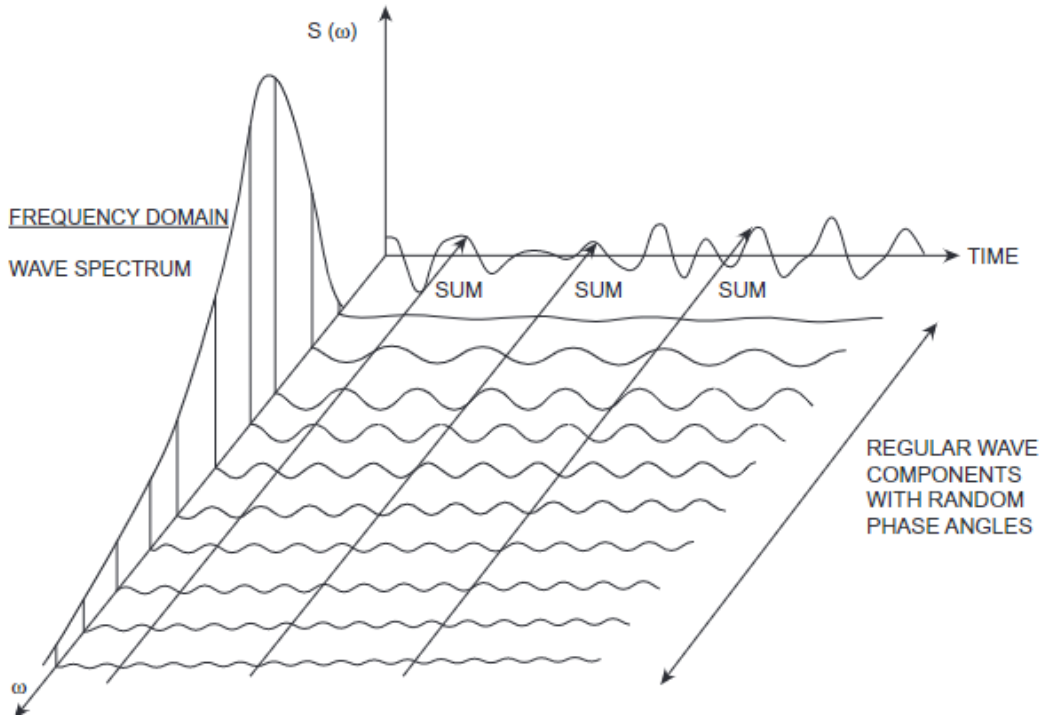

Figure 3.18: Wave spectrum: irregular wave decomposed into a sum of regular waves of different frequency [61].

This research uses the Joint North Sea Wave Project (JONSWAP) spectrum. It is similar to the Pierson-Moskowitz spectrum, but can additionally be used for regions with geographical boundaries such as the North Sea where various wind farms are located. It can be defined with the following variables: the significant wave height H_s, the peak wave period T_p and the peak enhancement factor γ.[2] The peak wave period corresponds to the period with the highest energy. The peak enhancement factor is a parameter that describes the ratio of the maximum wave energy (at the peak period) to the corresponding value in the Pierson-Moskowitz spectrum. A higher value indicates that there is more energy at the peak period, which then also has a narrower distribution. Typical values are in the range of 1-7. Notice that for $\gamma = 1$, the JONSWAP spectrum reduces to the Pierson-Moskowitz spectrum. Any other variable that defines the JONSWAP spectrum is taken as default or derived from the aforementioned variables [62].

[2] https://www.orcina.com/webhelp/OrcaFlex/Content/html/Waves,Wavespectra.htm#JONSWAP, Accessed [05-06-2023]

RAOs are used to determine the behaviour of the vessel in response to waves. The displacement RAO describes the vessel motions, which include heave, pitch, roll, etc. On the other hand, the load RAO describes the shear forces and bending moments experienced by the vessel, which is relevant for the load adjustments. This RAO shows the magnitude of the load per unit wave amplitude and is expressed as function of the wave direction, wave frequency and position along the vessel. It can be obtained from a diffraction analysis, which requires the following main inputs:

- Geometry: hull of the full vessel
- Vessel properties: mass, inertia, etc.
- Wave properties: range of wave directions and frequencies

In reasoning the load adjustments, the shear force and bending moment diagrams are needed, but not per unit wave amplitude as for the RAOs. The software AQWA Graphical Supervisor (GS) is used to determine the shear force and bending moment in absolute terms, which uses the RAOs in combination with the wave spectrum. The option 'Significant Amplitude' gives the shear force and bending moment for the significant wave amplitude as function of the position along the vessel. It can be retrieved for multiple wave directions and peak wave frequencies. Recall this research is limited in maximising the vertical shear force and bending moment. This is denoted by 'Z/R_y', which returns the shear force in z and bending moment about y.

Load adjustments

Thus far, the shear force and bending moment diagrams of the full vessel can be computed. For the vessel in still water, this was also the case for the vessel section. The shear force and bending moment diagram were based on the weight and buoyancy per unit length. Besides, these loads will also be applied on the partial vessel model (see subsection 3.5.1 - subsection 3.5.3). For the vessel in waves, on the other hand, it would mean that the vessel section must be analysed in AQWA GS as well, if that were possible at all. Moreover, a regular travelling wave using the equivalent design wave approach will be applied on the partial vessel model (see subsection 3.5.4). These are two different approaches and thus it would not make much sense to construct the shear force and bending moment diagrams of the vessel section.

The following solution is proposed for this. First, the shear force adjustment is unnecessary, which is proven in chapter 4. The bending moment adjustment, on the other hand, is simply based on the bending moment of the full vessel at the aft and fore end of the vessel section. It is known that the bending moment of the partial vessel model is zero at its ends since it is simply supported (see section 3.2). This makes it possible to directly apply the bending moment of the full vessel there. It only remains unknown which bending moment diagram to consider. This should depend on the waves being analysed as it must correspond to the wave pressure applied on the partial vessel model (see subsection 3.5.4). Although, it is conservative to take the value of the bending moment envelope, which combines all frequencies. The bending moment adjustment at the aft and fore end are denoted as ΔM_{aft} and ΔM_{fore} respectively.

3.5 Finite element analysis load application

This section discusses how the loads, which include the weight, buoyancy, water ballast and wave pressure, are applied on the partial vessel model in the FEA. All but the last one are required for the vessel in still water. The wave pressure, on the other hand, is needed for the vessel in waves. Previously, in section 3.4, the hull girder load adjustments were developed. The application of these load adjustments at the ends of the partial vessel model was already mentioned there. Besides, the payload will not be discussed here, but in chapter 6.

3.5.1 Weight

The weight of the partial vessel model will inevitably be smaller than the actual weight of the vessel section. This is because simplifications were made, among which are rectangular cutouts, the removal of brackets, etc. In addition, the components of the deadweight such as piping, wires, etc. are not modelled. Therefore, the weight of the partial vessel model must be adjusted so that it equals that of the vessel section. First, from the weight w per unit length, the vessel section weight W_{vessel} is calculated. The summation of the average value of weight between two consecutive frames for all intervals of the vessel section is computed.

$$W_{vessel} = \sum_{i=1}^{N-1} \frac{w_i + w_{i+1}}{2} \cdot x_{fr} \tag{3.15}$$

From the vessel section weight, (high) concentrated weights are subtracted, which can include engines, water ballast, payload, etc. The resultant comprises of the lightweight and all components of the deadweight that can be assumed to be uniformly distributed. The weight of the partial vessel model should be equal to this. Accordingly, in Equation 3.16, an adjusted density $\rho_{adjusted}$ is defined from the density of structural steel ρ_{steel} and the ratio of the vessel section weight W_{vessel} minus the concentrated weights (denoted as C) and the partial vessel model weight W_{model}.

$$\rho_{adjusted} = \frac{W_{vessel} - C}{W_{model}} \cdot \rho_{steel} \tag{3.16}$$

The adjusted density is updated in the material properties and the weight is applied as Standard Earth Gravity in Ansys. Lastly, the subtracted concentrated weights must be separately applied on the partial vessel model in the FEA. For the studied vessel section in this research, it is limited to the water ballast (see subsection 3.5.3) and payload (see chapter 6).

3.5.2 Buoyancy

According to Archimedes' principle, the upward buoyant force on a (partially) immersed body in a fluid is equal to the weight of the displaced fluid. From the buoyancy b per unit length, the buoyant force F_b that acts on the vessel section is calculated. The summation of the average value of the buoyancy between two consecutive frames for all intervals of the vessel section is computed.

$$F_b = \sum_{i=1}^{N-1} \frac{b_i + b_{i+1}}{2} \cdot x_{fr} \tag{3.17}$$

The buoyant force can be directly applied on the bottom hull area. On the other hand, one could decide to apply the pressure P that the buoyant force exerts on this area. However, it would be more accurate to regard the fluid as a pressure distribution over the entire immersed body, rather than only on the bottom hull. The absolute pressure p at a point in a fluid at rest, regardless of direction, is equal to

$$p = \rho \cdot g \cdot h + p_{atm} \tag{3.18}$$

The first term includes the fluid density ρ (water density: $\rho_{water} = 1025\ kg/m^3$), the gravitational acceleration g and the height h from the free water surface (i.e. the depth). The second term p_{atm} is the atmospheric pressure, which acts on each side of the hull and thus should not be modelled as it cancels out. Therefore, Equation 3.18 reduces to the first term only, which is referred to as the hydrostatic pressure p_{hydr}.

$$p_{hydr} = \rho \cdot g \cdot h \tag{3.19}$$

This pressure acts on the immersed hull, both in vertical and horizontal direction, and varies linearly with height. It is convenient to use a hydrostatic pressure load in Ansys instead of defining this manually. It requires as input the fluid density, gravitational acceleration, free surface location and all surfaces on which the fluid acts. Notice the normal direction of each surface must be correctly oriented in the FEA. Lastly, since the bottom hull is almost horizontal, the draft can be approximated by the height using Equation 3.19, the buoyant force and the bottom hull area. It is also often the case that the draft is specified together with the buoyancy data.

3.5.3 Water ballast

The water ballast (WB) is there to ensure the stability of the vessel. It serves as a counterweight so that the resultant mass is close to the centre line. If the vessel were to roll to either direction, the centre of buoyancy would shift laterally past the centre of gravity to create a moment that counteracts this rolling motion. Two ways to model the water ballast are discussed.

It is possible to model the water ballast in the same way as the buoyancy (see subsection 3.5.2), although this is arguably not the best choice. The hydrostatic pressure must be applied on all walls of the WB tank, which means it requires the correct orientation of each surface normal. But, there are many shared walls since these tanks lie next to each other and the hull can be part of it. Furthermore, a rectangular and L-shaped WB tank can be distinguished as shown in Figure 3.19. In case both tanks have the same base area and are filled to the same height, the hydrostatic pressure at the bottom is equal and then it appears to have the same weight. Gravity indicates the force of the rectangular tank must be higher, though. The discrepancy occurs because the pressure on the shorter horizontal plate of the L-shaped tank was not

considered, which is incorrect. In order to achieve vertical (and horizontal) equilibrium, it is important to apply the pressure on all surfaces [63].

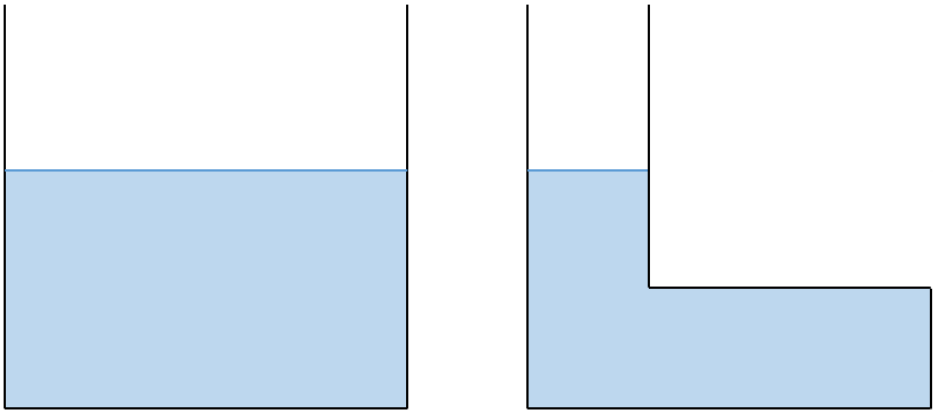

Figure 3.19: Rectangular and L-shaped water ballast tank with the same base area and filled to the same height.

While the hydrostatic pressure is the most accurate, it is also tedious and prone to errors to model in the FEA. The intended use of water ballast is to guarantee the stability of the vessel by adding mass away from the centre line so that the resultant mass is close to it. Therefore, it is decided to model the water ballast as point mass at its centre of gravity, which is scoped to the bottom of the WB tank. The only disadvantage is that it becomes impossible to detect stress concentrations in the vicinity of the tanks, but it is not relevant in this research.

3.5.4 Wave pressure

The wave pressure is the result of waves hitting the vessel. First, a hydrodynamic diffraction analysis is performed in the software Ansys AQWA. This analysis uses as geometry the hull of the full vessel, which is split at the free water surface into two parts. Besides, the mass of the full vessel should be given as point mass and the depth d of the water must be specified. It is further required to define a range of wave directions and frequencies.

Among other things, the hydrodynamic diffraction analysis is able to calculate the hydrodynamic pressure for a regular travelling wave. The pressure components include the incident, diffracted, radiated and hydrostatic varying pressure. The regular wave is described by a periodic sinusoidal function as shown in Figure 3.20. The wave speed c is equal to the wavelength λ divided by the wave period T. The period can also be replaced by the wave frequency f, which is the inverse. The other parameters to be specified are the wave amplitude A or the wave height H, which is twice the amplitude. In addition, the phase angle φ, which describes the wave position and covers 360°. In Ansys AQWA, a zero degree phase means the wave crest passes through the centre of gravity of the structure (i.e. the hull of the full vessel).

$$c = \frac{\lambda}{T} = \lambda \cdot f \tag{3.20}$$

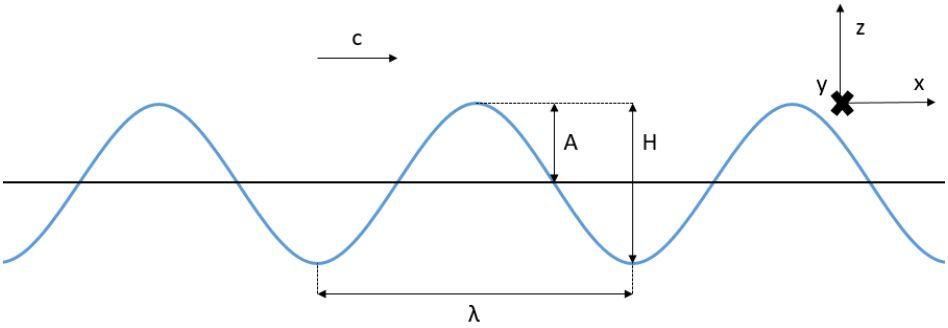

Figure 3.20: Regular travelling wave described by a periodic sinusoidal function.

The only parameter that remains unknown is the wavelength. There exist different regular wave theories, which uniquely depend on the shallow water parameter μ and wave steepness parameter S [64].

$$\mu = 2\pi \frac{d}{g \cdot T^2} \tag{3.21}$$

$$S = 2\pi \frac{H}{g \cdot T^2} \tag{3.22}$$

For instance, linear wave theory uses the relation below to calculate the wavelength when $d > \lambda/2$ is satisfied [64]. Note that while it is briefly explained how this can be calculated, Ansys AQWA does this calculation internally.

$$\lambda = \frac{g \cdot T^2}{2\pi} \tag{3.23}$$

The results of the Hydrodynamic Diffraction analysis can be sent to the (FE) Static Structural analysis in Ansys, as shown in the Workbench setup in Figure 3.21. Note that the geometry of the hydrodynamic diffraction analysis is the hull of the full vessel, whereas the FEA uses the partial vessel model.

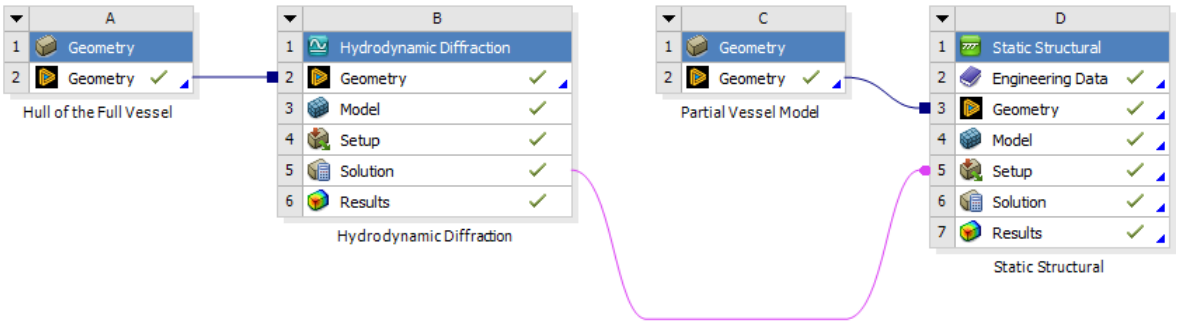

Figure 3.21: Workbench setup to send the results of the Hydrodynamic Diffraction analysis to the (FE) Static Structural analysis.

A hydrodynamic pressure load can then be defined in the FEA. But first, the geometries should be matched. In Ansys AQWA, the hull is divided into two parts with the interface at the free water surface and thus the origin is often defined there as well. In the FEA, on the other hand, the partial vessel model has the origin usually defined at the bottom hull. Therefore, a translation along z is necessary. Finally, a single wave case can be selected, choosing a wave direction and frequency. In addition, an (incident) wave amplitude and phase angle(s) must be specified.

In summary, it has been explained how to define the wave pressure. However, it has not yet been discussed which wave direction and frequency to use. It relates to subsection 3.4.2 and will further be elaborated upon in chapter 5.

3.6 Verification methodology

The partial vessel FE analysis is verified against a simple analytical solution of the vessel based on Euler-Bernoulli beam theory. It is particularly convenient to use because the shear force and bending moment diagram of the full vessel were already previously constructed in section 3.4 to reason the load adjustments. Moreover, the neutral axis location $Z_{N.A.}$, cross-sectional area A and second moment of area I_y should be known at each frame.

The normal stress σ_x is known by the flexural formula. The vertical bending moment M_y, the second moment of area I_y and the distance from the neutral axis $(z - Z_{N.A.})$ are needed.

$$\sigma_x = \frac{M_y \cdot (z - Z_{N.A})}{I_y} \tag{3.24}$$

The average shear stress is also calculated. It is decided to neglect the actual shear stress distribution, which means the maximum value will be under-estimated. The shear stress τ_{xz} is equal to the vertical shear force $F_{s,z}$ divided by the cross-sectional area A.

$$\tau_{xz} = \frac{F_{s,z}}{A} \tag{3.25}$$

In addition to these individual stress components, the von Mises stress σ_{vm} is calculated. It is assumed that the normal and shear stress occur at the same location. This means the von Mises stress will be over-estimated as the normal stress is maximum at the outer surface and zero at the neutral axis, while the opposite holds true for the shear stress. However, it is a good approximation given the fact that the average shear stress is considered.

$$\sigma_{vm} = \sqrt{\sigma_x^2 + 3\tau_{xz}^2} \tag{3.26}$$

Chapter 4

Offshore installation vessel in still water

This chapter covers the partial vessel FE analysis of the offshore jack-up installation vessel in still water. Afterwards, in chapter 5, the vessel is analysed in waves. Excluding the wave component allows to identify any discrepancies between the FEA results and analytical solution that can be accounted to the still water component. While the still water loads may sound negligible, they will be larger than the wave loads due to the intrinsic high variation in weight of an offshore jack-up installation vessel. In section 4.1, the first case study (1a) that was without any water ballast is analysed. Then, in section 4.2, the second case study (1b) that includes the water ballast and takes into account the transversal position of the weights is analysed. This is done to gradually build up the complexity of the analysis.

4.1 Case study 1a

For the offshore jack-up installation vessel, different heavy weights can be distinguished. Some major contributions are the heavy lift crane, crane boom rest, legs, helicopter platform, water ballast, engines, etc. Case study 1a is a fictive case that does not consider the water ballast. It would be incorrect to presume the vessel is stable this way since, for instance, the heavy lift crane is positioned at starboard side and will induce a rolling motion. Although, by assuming the heavy lift crane and any other weight is positioned along the centre line, the vessel is no longer unstable without water ballast. However, it does imply that torsion is ignored in this case study.

4.1.1 Shear force and bending moment diagrams

Two reasons to construct shear force and bending moment diagrams can be found in chapter 3. First, it is used in reasoning the load adjustments that are required to reflect the full vessel behaviour in the partial vessel model. Second, it is needed to determine the normal and shear

stress for the analytical solution based on Euler-Bernoulli beam theory in order to verify the methodology. The weight w and buoyancy b per unit length at each frame, required in constructing these diagrams, are obtained from the software SARC and are respectively given in Figure 4.1a and Figure 4.1b. The position of the legs and heavy lift crane should be clear from the left graph. Besides, a near constant buoyancy is observed in the right graph, which rapidly drops at the stern and bow.

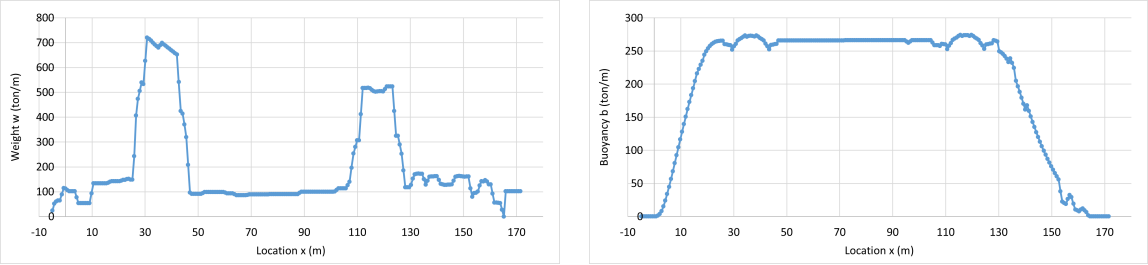

(a) Weight w per unit length. **(b)** Buoyancy b per unit length.

Figure 4.1: Case study 1a: Loads per unit length at each frame.

The difference in weight and buoyancy $w-b$ per unit length at each frame is given in Figure 4.2. A positive value means the accumulated weight is greater than the accumulated buoyancy. Despite a variation in load, vertical equilibrium still exists. This is confirmed from the reaction forces at the aft and fore end of the full vessel (i.e. stern and bow). Their summation approximately equals zero, indicating no resultant force. Additionally, their absolute value is negligible compared to the range of magnitude. The latter is expected since the stern and bow are both free ends.

$$R_{aft} = -152.39kN$$

$$R_{fore} = 100.86kN$$

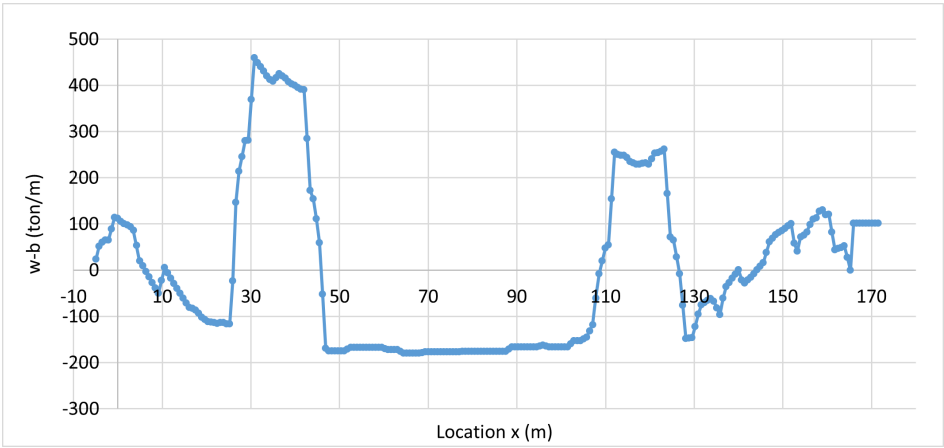

Figure 4.2: Case study 1a: Difference in weight and buoyancy $w - b$ per unit length at each frame.

The procedure for the calculation of the shear force and bending moment as explained in subsection 3.4.1 is followed. The shear force and bending moment diagram of the full vessel are given in Figure 4.3 and Figure 4.4 respectively. For the shear force, a positive value means the accumulated weight is greater than the accumulated buoyancy. Besides, the bending moment is positive as the accumulated weight rises earlier than the accumulated buoyancy. This indicates the vessel experiences hogging in still water, which is expected since most heavy weights such as the heavy lift crane, crane boom rest, legs, etc. are located outwards near the stern and bow. In other cases, where more weight is located in the midship area, sagging occurs in still water.

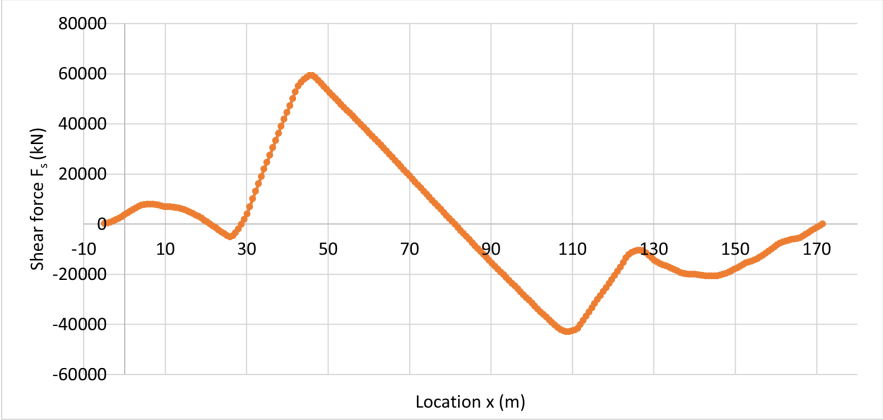

Figure 4.3: Case study 1a: Shear force diagram of the full vessel.

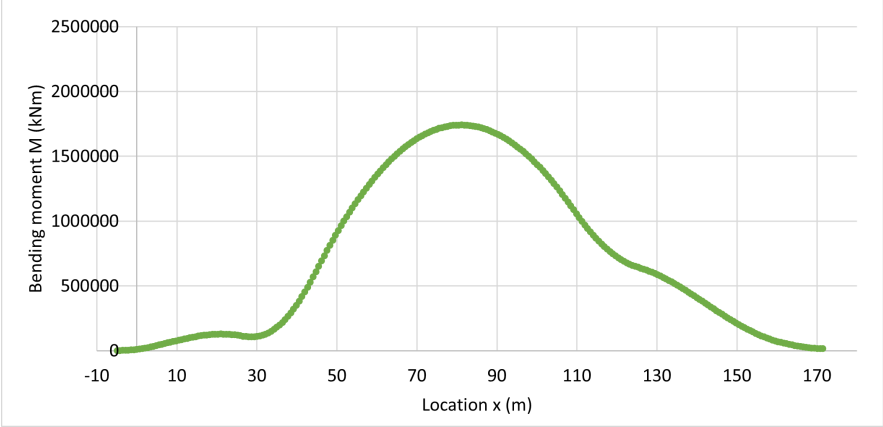

Figure 4.4: Case study 1a: Bending moment diagram of the full vessel.

Thus far, the shear force and bending moment diagram of the full vessel have been computed. The same calculation is now repeated, but for the vessel section. Its reaction forces are both negative, which indicates the accumulated buoyancy is greater than the accumulated weight.

$$R_{aft} = -37828.9kN$$

$$R_{fore} = -35168.87kN$$

The shear force and bending moment diagram of the vessel section, together with those of the full vessel, are given in Figure 4.5 and Figure 4.6 respectively. The shear force shows a constant, small offset as expected given the fact it does not depend on the distance. The bending moment, on the other hand, is off by a large amount. This can be attributed to the fact that the moment equals zero at the ends of a simply supported beam. In case the weight and buoyancy would now be applied on the partial vessel model as is, it would closely follow the bending moment diagram of the vessel section and severely under-estimate the actual bending moment that occurs in the full vessel. Therefore, in what follows, the hull girder load adjustments will be calculated.

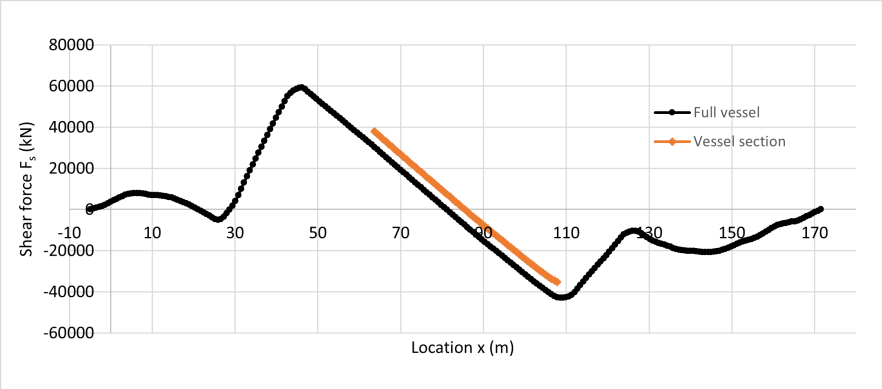

Figure 4.5: Case study 1a: Shear force diagram of the vessel section versus the full vessel.

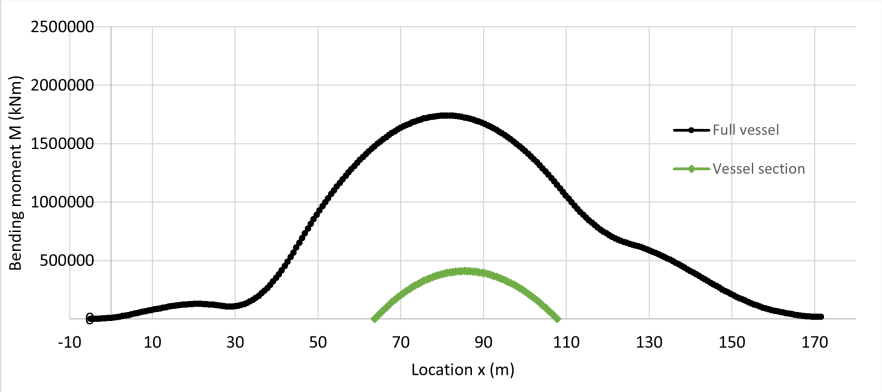

Figure 4.6: Case study 1a: Bending moment diagram of the vessel section versus the full vessel.

4.1.2 Hull girder load adjustments

The hull girder load adjustments are required so that the partial vessel model reflects the full vessel behaviour. First, as it was observed that the shear force of the vessel section had only a small offset that may be negligible, the partial vessel FE analysis is performed with solely the bending moment adjustment. Then, the analysis is repeated with both the shear force and bending moment adjustment. The load adjustments, which are given in Table 4.1, are calculated following the procedure in subsection 3.4.1.

Table 4.1: CS1a: Hull girder load adjustments. SF and BM stand for shear force and bending moment respectively.

Parameter	BM adjustment	SF and BM adjustment
ΔF_s	$0kN$	-7511.76kN
M_{aft} $(=M_{fore})$	$0kNm$	-165634.32kNm
ΔM	1330125.93kNm	1311504.48kNm

4.1.3 Results and discussion

This section discusses the results of the partial vessel FE analysis of case study 1a. The partial vessel model is constrained according to the boundary conditions given in section 3.2. Besides, the weight and buoyancy are applied to the model as described in section 3.5. The adjusted density $\rho_{adj} = 9397.61kg/m^3$, the buoyant force $F_b = 126418.76kN$ and the height $h = 4.75m$. With solely the bending moment adjustment, the directional deformation along z and the normal stress σ_x are given in Figure 4.7 and Figure 4.8 respectively.

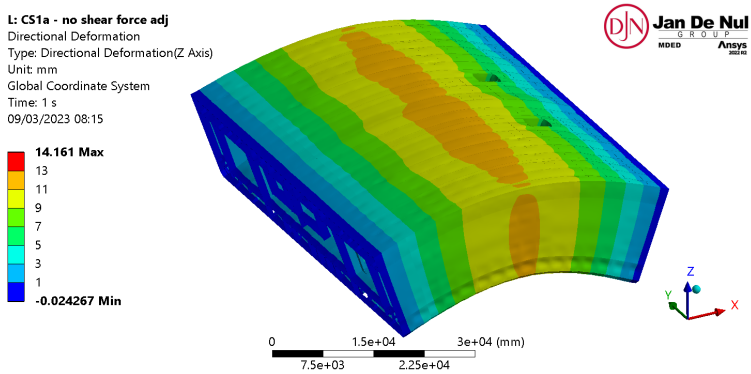

Figure 4.7: CS1a: Directional deformation along z of the partial vessel model with solely the bending moment adjustment. Mesh size = 350mm and deformation scale factor = 500.

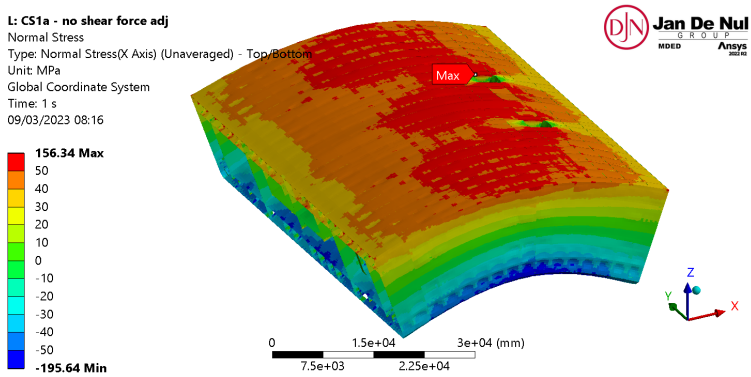

Figure 4.8: CS1a: Normal stress σ_x of the partial vessel model with solely the bending moment adjustment. Mesh size = 350mm and deformation scale factor = 500.

The partial vessel FE analysis is verified against the analytical solution as explained in section 3.6. It is decided to individually examine the normal and von Mises stress, but not the shear stress. The latter is generally much smaller for vessels, which is indeed observed in Figure 4.3 where the shear force is close to zero in the midship area. The highest stress of the partial vessel model is expected to occur at main deck. Therefore, the stress results are retrieved there along the centre line. The stress of the plate area from its top is used and not of stiffener profiles, although they follow a very similar stress pattern. The stress is evidently also evaluated at main deck for the analytical solution.

Figure 4.9 shows the normal stress σ_x of the partial vessel model and analytical solution. A mesh size of $700mm$ equal to the frame spacing is initially adopted. Additionally, a mesh size of $350mm$ is used that proves the larger mesh size is adequate. The FEA shows a good agreement with the analytical solution for the middle region as expected since the normal stress is an individual stress component. However, this region is limited from about 76 to $96m$, which means approximately 50% of the current model yields inaccurate results. Moreover, the stress is under-estimated at the aft and fore end. To conclude, in case the region that returns trustworthy results needs to be increased, the partial vessel model should be extended. In this research, the full vessel model was not available to run further analyses using a larger model.

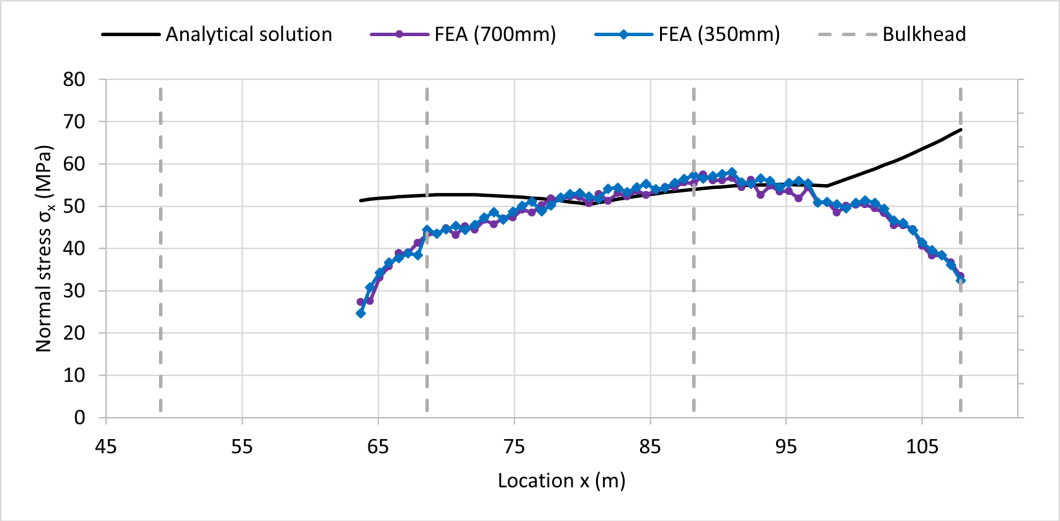

Figure 4.9: CS1a: Comparison of normal stress σ_x between the partial vessel model and analytical solution with solely the bending moment adjustment.

The von Mises stress σ_{vm} of the partial vessel model and analytical solution is shown in Figure 4.10. In both instances, the von Mises stress follows a similar trend to the normal stress σ_x, which is expected as it is the largest stress component. For the analytical solution, the von Mises stress is slightly larger than the normal stress due to presence of shear stress. For the FEA, on the other hand, it is observed that the von Mises stress is below the normal stress and so the von Mises stress of the FEA is also smaller than its analytical solution. This can be attributed to the fact that the analytical solution only considers the normal stress σ_x and shear stress τ_{xz} and computes the von Mises stress as such (see Equation 3.26). On the other hand, the FEA encompasses all six stress components and uses the von Mises stress in

its full form given by Equation 4.1. Because the normal stress σ_y of the FEA is in range of 10-15MPa, the von Mises stress becomes smaller.

$$\sigma_{vm} = \frac{1}{\sqrt{2}}\sqrt{(\sigma_x - \sigma_y)^2 + (\sigma_y - \sigma_z)^2 + (\sigma_x - \sigma_z)^2 + 6\tau_{xy}^2 + 6\tau_{yz}^2 + 6\tau_{xz}^2} \tag{4.1}$$

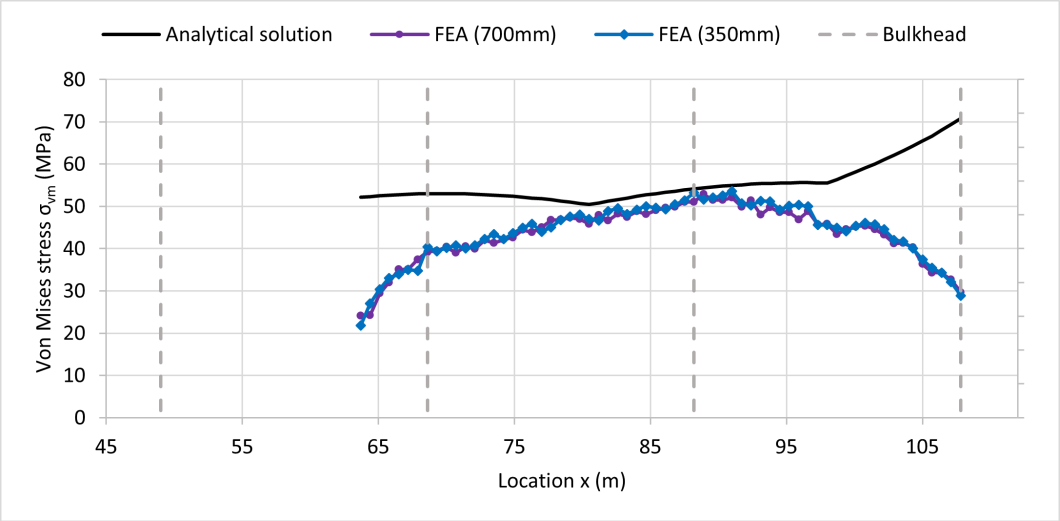

Figure 4.10: CS1a: Comparison of von Mises stress σ_{vm} between the partial vessel model and analytical solution with solely the bending moment adjustment.

The existence of the normal stress σ_y can be reasoned as follows. In case a material specimen is stretched in one direction, it will shrink in the other two directions. This holds true for a simple specimen, as it does for the vessel. Because the partial vessel model experiences hogging, the main deck will elongate in x, but at the same time contract in y and z. This is seen from the strain results of the FEA where ε_y and ε_z are both negative. Below, the relation between stress and strain is described by Hooke's law for isotropic materials in 3D. Using this relation, it was manually verified that the strain results at main deck (along centre line) lead to a normal stress σ_y in range of 10-15Mpa and σ_z near $0Mpa$. The latter indicates plane stress at main deck.

$$\begin{bmatrix} \sigma_x \\ \sigma_y \\ \sigma_z \\ \tau_{xy} \\ \tau_{yz} \\ \tau_{xz} \end{bmatrix} = \frac{E}{(1+\nu)(1-2\nu)} \begin{bmatrix} 1-\nu & \nu & \nu & 0 & 0 & 0 \\ \nu & 1-\nu & \nu & 0 & 0 & 0 \\ \nu & \nu & 1-\nu & 0 & 0 & 0 \\ 0 & 0 & 0 & 1-2\nu & 0 & 0 \\ 0 & 0 & 0 & 0 & 1-2\nu & 0 \\ 0 & 0 & 0 & 0 & 0 & 1-2\nu \end{bmatrix} \begin{bmatrix} \varepsilon_x \\ \varepsilon_y \\ \varepsilon_z \\ \varepsilon_{xy} \\ \varepsilon_{yz} \\ \varepsilon_{xz} \end{bmatrix} \tag{4.2}$$

Thus far, the partial vessel FE analysis has been performed with solely the bending moment adjustment. Next, the analysis is repeated with both the shear force and bending moment adjustment. In Figure 4.11 and Figure 4.12, the normal stress σ_x and von Mises stress σ_{vm}

are shown respectively. Hardly any difference from the foregoing analysis is observed, which proves the shear force adjustment is unnecessary.

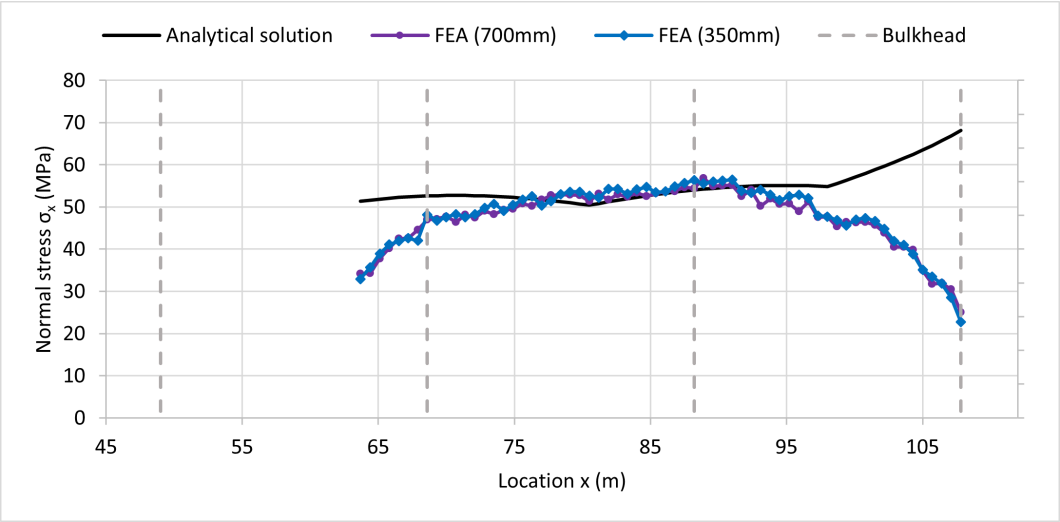

Figure 4.11: CS1a: Comparison of normal stress σ_x between the partial vessel model and analytical solution with both the shear force and bending moment adjustment.

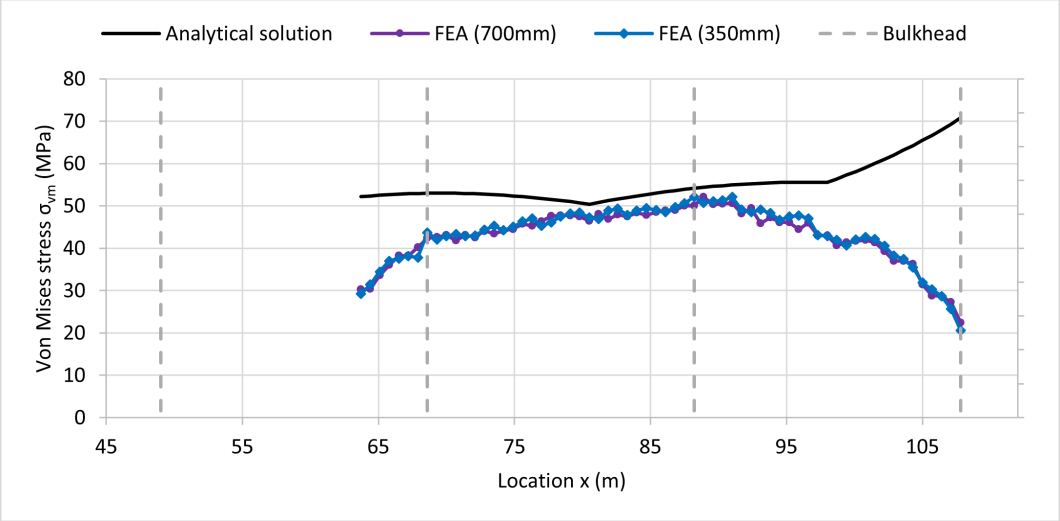

Figure 4.12: CS1a: Comparison of von Mises stress σ_{vm} between the partial vessel model and analytical solution with both the shear force and bending moment adjustment.

4.2 Case study 1b

In case study 1a, it was incorrect to presume the vessel is stable without water ballast. Heavy weights such as the heavy lift crane, crane boom rest, helicopter platform, etc. are positioned away from the centre line and will induce a rolling motion. Case study 1b considers the water ballast and transversal position of weights and as a consequence will also include torsion.

4.2.1 Shear force and bending moment diagrams

Shear force and bending moment diagrams are constructed in reasoning the load adjustments and for the verification of the methodology. In Figure 4.13a and Figure 4.13b the weight w and buoyancy b per unit length at each frame are given respectively. In comparison to case study 1a, the weight per unit length is significantly larger in the midship area indicating the presence of water ballast. On the other hand, the buoyancy per unit length follows a similar trend, although it is now larger.

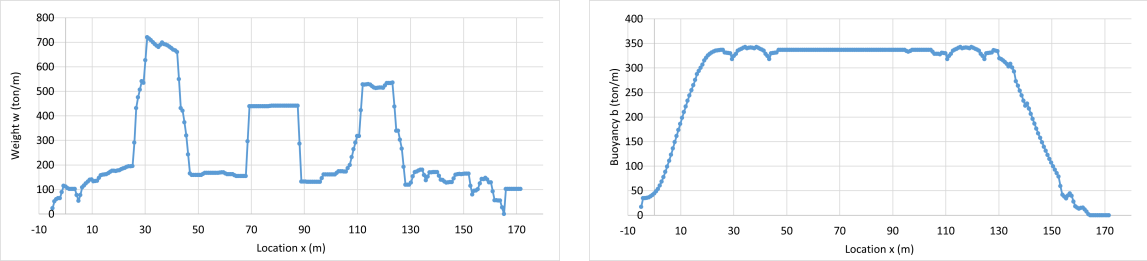

(a) Weight w per unit length.

(b) Buoyancy b per unit length.

Figure 4.13: Case study 1b: Loads per unit length at each frame.

In Figure 4.14, the difference in weight and buoyancy $w - b$ per unit length at each frame is given. The reaction forces at the aft and fore end of the full vessel again indicate that vertical equilibrium exists.

$$R_{aft} = -139.71kN$$

$$R_{fore} = 127.65kN$$

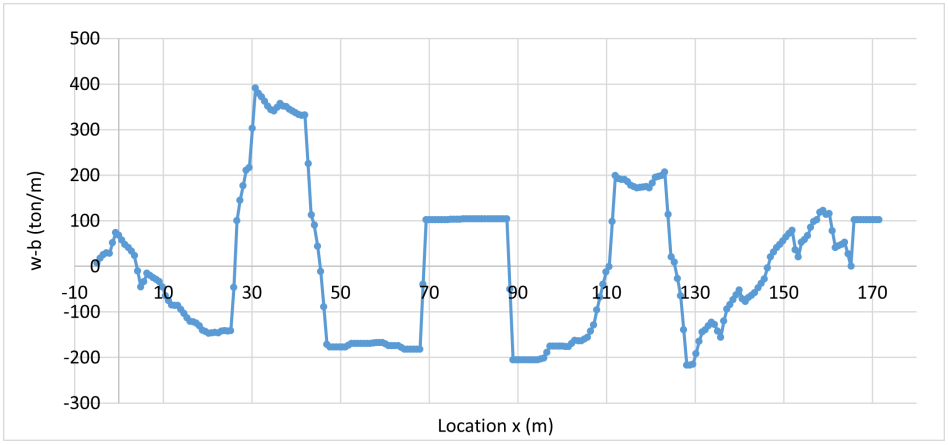

Figure 4.14: Case study 1b: Difference in weight and buoyancy $w - b$ per unit length at each frame.

The shear force and bending moment diagram of the full vessel are given in Figure 4.15 and Figure 4.16 respectively. Despite the presence of water ballast in the midship area, the vessel still experiences hogging in still water, although without any payload. This is expected since heavy weights such as the heavy lift crane, crane boom rest, legs, etc. are located outwards near the stern and bow. Furthermore, the water ballast serves a second purpose besides providing stability. Compared to case study 1a, it is clear that the maximum value of the bending moment has more than halved and that the shear force reduced in magnitude. As a consequence, the stress will become smaller as well.

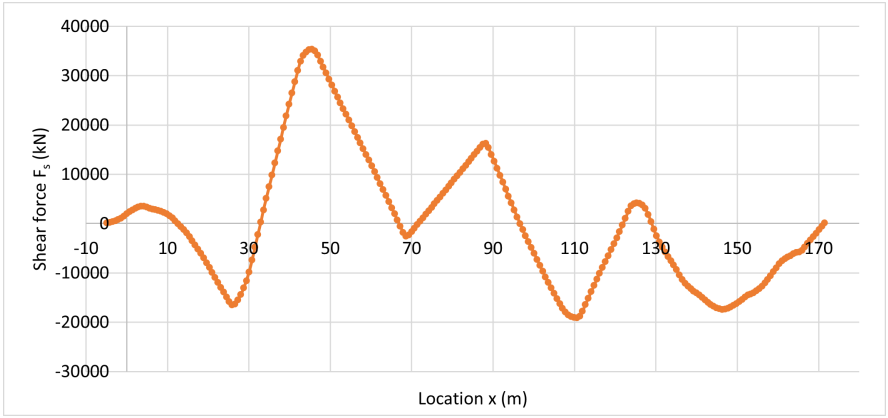

Figure 4.15: Case study 1b: Shear force diagram of the full vessel.

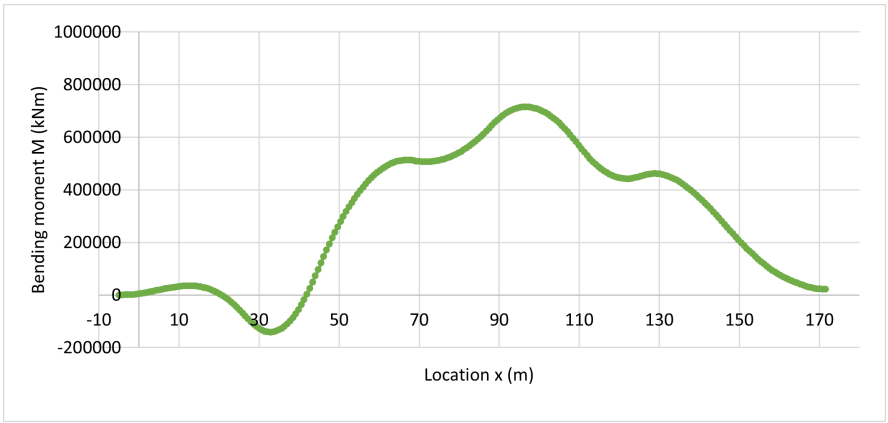

Figure 4.16: Case study 1b: Bending moment diagram of the full vessel.

The shear force and bending moment diagram of the vessel section are also computed. The reaction forces are again both negative, although they are not as small since the water ballast is concentrated in the midship area whereas the buoyancy is spread over the full length of the vessel. Further observe that the reaction forces are no longer similar because more water ballast is positioned near the aft end of the vessel section.

$$R_{aft} = -3313.99kN$$
$$R_{fore} = -20357.35kN$$

The shear force and bending moment diagram of the vessel section, together with those of the full vessel, are given in Figure 4.17 and Figure 4.18 respectively. Since the bending moment of the vessel section is again under-estimated, hull girder load adjustments are needed.

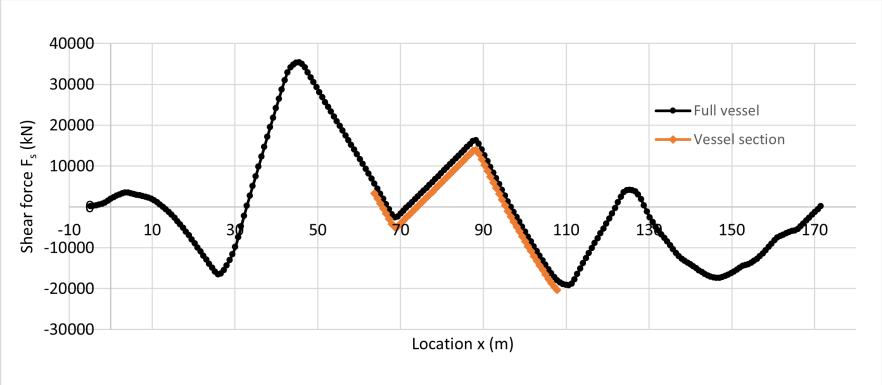

Figure 4.17: Case study 1b: Shear force diagram of the vessel section versus the full vessel.

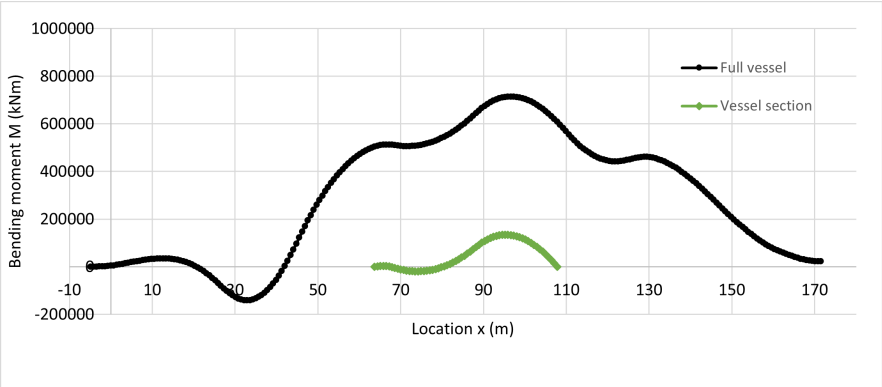

Figure 4.18: Case study 1b: Bending moment diagram of the vessel section versus the full vessel.

4.2.2 Hull girder load adjustments

The hull girder load adjustments are without shear force adjustment since it turned out to be unnecessary. Different to case study 1a, a torsional moment adjustment is now required. As it is desired to evaluate the effect of this adjustment, the partial vessel FE analysis is initially performed without it. Then, the analysis is repeated including the torsional moment adjustment. The procedure in subsection 3.4.1 is followed to calculate the load adjustments, which are given in Table 4.2. Notice that one filled water ballast (WB) tank at port side lies only for 21.9% in the partial vessel model. Therefore, the other 78.1% is considered for the torsional moment adjustment. Moreover, the percentage of the lightship that is used for the adjustment is equal to 38.9%.

Table 4.2: CS1b: Hull girder load adjustments. BM and TM stand for bending moment and torsional moment respectively.

Parameter	BM adjustment	BM and TM adjustment
ΔM	$561775.89kNm$	$561775.89kNm$
ΔT	$0kNm$	$309385.76kNm$

4.2.3 Results and discussion

The results of the partial vessel FE analysis of case study 1b are discussed in this section. The boundary conditions given in section 3.2 are used to constrain the partial vessel model. Besides, the weight, buoyancy and water ballast are applied to the model as described in section 3.5. The adjusted density $\rho_{adj} = 9418.37kg/m^3$, the buoyant force $F_b = 159918.04kN$ and the height $h = 6.01m$. The two heaviest filled WB tanks have the same weight at equal and opposite distance from the centre line. The remaining filled WB tanks are located at port side as the heavy lift crane is at starboard side.

First, the analysis with solely the bending moment adjustment is elaborated upon. Evidently, the water ballast is always modelled since the purpose is to see the effect of the torsional moment adjustment that is required. The directional deformation along z is given in Figure 4.19. The partial vessel model has rotated such that port side lies now lower than starboard side. It is further observed that both sides lie lower compared to the centre line region. Despite that the vessel experiences hogging, the presence of the two heavy WB tanks at the sides reduces this effect there.

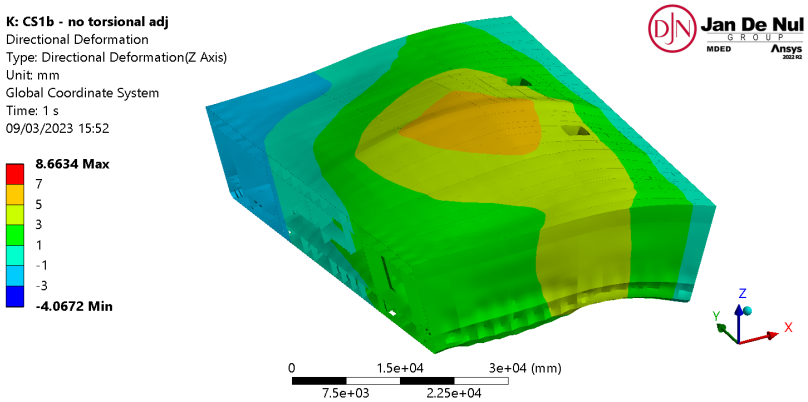

Figure 4.19: CS1b: Directional deformation along z of the partial vessel model with solely the bending moment adjustment. Mesh size = $700mm$ and deformation scale factor = 500.

The normal stress σ_x is given in Figure 4.20. Compared to case study 1a, the stress pattern is not as continuous anymore. The stress is also smaller since the vertical bending moment reduced in magnitude as a result of the added water ballast. It was already observed that the directional deformation in z is smaller at the sides. Similarly, the stress at main deck is smaller at port and starboard side than near the centre line region. This can be attributed to the presence of water ballast at the sides, which relieves the vertical bending moment.

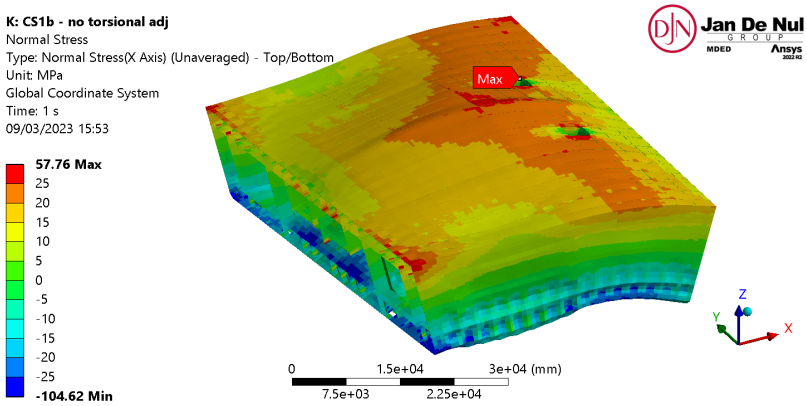

Figure 4.20: CS1a: Normal stress σ_x of the partial vessel model with solely the bending moment adjustment. Mesh size = 700mm and deformation scale factor = 500.

The analytical solution in section 3.6 is used to verify the partial vessel FE analysis. The normal stress σ_x at main deck of the partial vessel model and analytical solution is shown in Figure 4.21. The stress results are retrieved along the centre line, as well as along the lines located a quarter of the vessel's width away from the centre line in y, denoted as $CL_{+1/4}$ and $CL_{-1/4}$, such that the effect of the water ballast at the sides can be evaluated too. The analytical solution assumes a uniform distribution of weight at each frame and so does not take into account the torsion that the water ballast induces. Therefore, it remains difficult to tell how the FEA should compare to the analytical solution. It appears the normal stress of the FEA at $CL_{+1/4}$ and $CL_{-1/4}$ shows a good agreement with the analytical solution. Although, it is rather the case that this normal stress reduces when compared to the normal stress along centre line because the water ballast relieves the vertical bending moment at the sides. It is also observed that the normal stress at $CL_{+1/4}$ is mostly above that at $CL_{-1/4}$, which is expected since more water ballast is located at port side. Besides, the stress is again under-estimated at the aft and fore end.

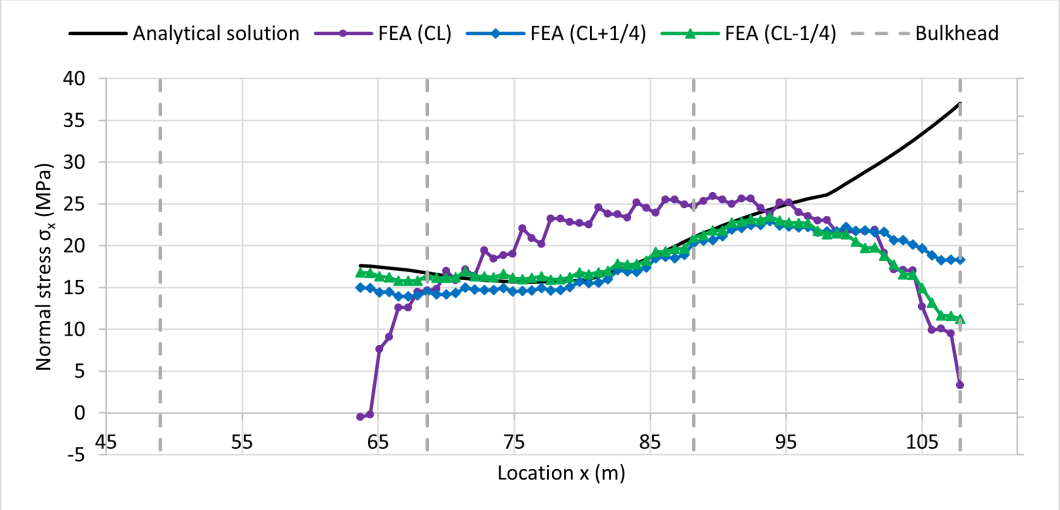

Figure 4.21: CS1b: Comparison of normal stress σ_x between the partial vessel model and analytical solution with solely the bending moment adjustment. CL stands for centre line.

Figure 4.22 shows the von Mises stress σ_{vm} at main deck of the partial vessel model and analytical solution. The von Mises stress follows a similar trend to the normal stress σ_x in both instances, which is expected as it is the largest stress component. Besides, for the FEA, it is observed that the von Mises stress is smaller than the normal stress σ_x. This can be attributed to the fact that the normal stress σ_y is in range of 5-15MPa. The reduction is more pronounced for the von Mises stress along centre line compared to that at $CL_{+1/4}$ and $CL_{-1/4}$. This happens because the normal stress σ_y is larger near the centre line region as the water ballast creates a bending moment about the x-axis.

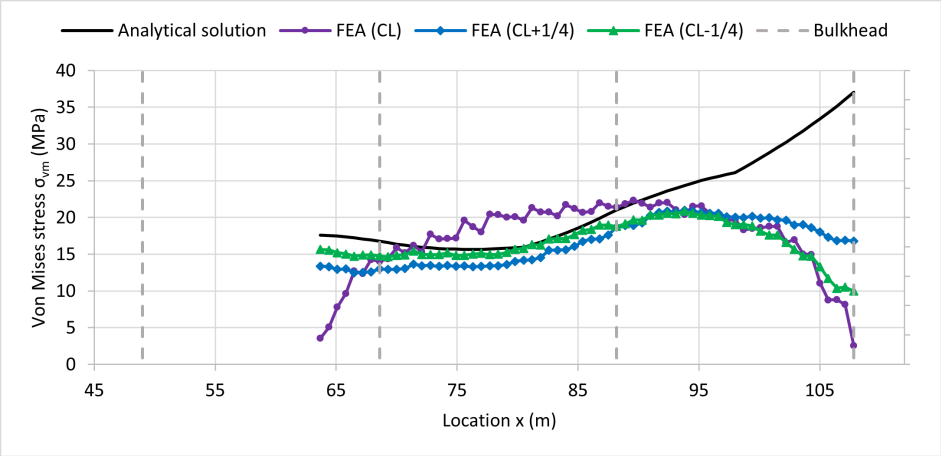

Figure 4.22: CS1b: Comparison of von Mises stress σ_{vm} between the partial vessel model and analytical solution with solely the bending moment adjustment. CL stands for centre line.

Thus far, the partial vessel FE analysis has been performed with solely the bending moment adjustment. This is incorrect since torsion induced by any weight before the aft end of the partial vessel model is neglected. Therefore, the analysis is repeated with both the bending moment and torsional moment adjustment. The directional deformation along z is given in Figure 4.23. Different to the foregoing analysis, port side lies higher than starboard side as the torsional moment adjustment is positive about x.

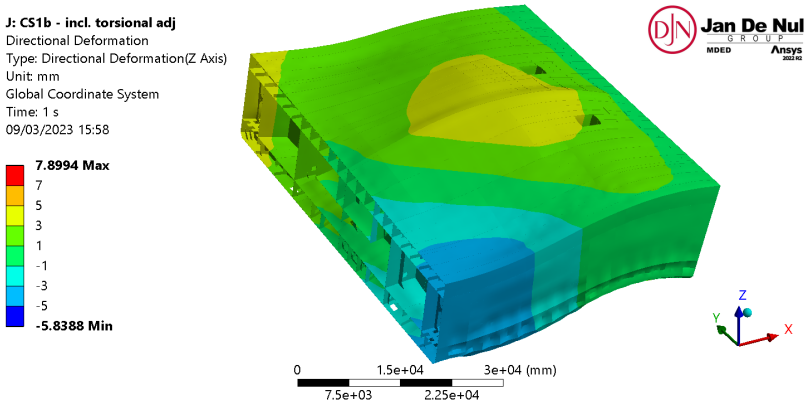

Figure 4.23: CS1b: Directional deformation along z of the partial vessel model with both the bending moment and torsional moment adjustment. Mesh size = 700mm and deformation scale factor = 1000.

The normal stress σ_x is given in Figure 4.24. The stress has reduced compared to the foregoing analysis. This can be attributed to the fact that the torsional moment adjustment is in the same order of magnitude as the torsional moment induced by the water ballast within the partial vessel model. Besides, the stress at main deck is again observed to be smaller at port and starboard side than near the centre line region as a result of the relieve of vertical bending moment from the presence of water ballast at the sides.

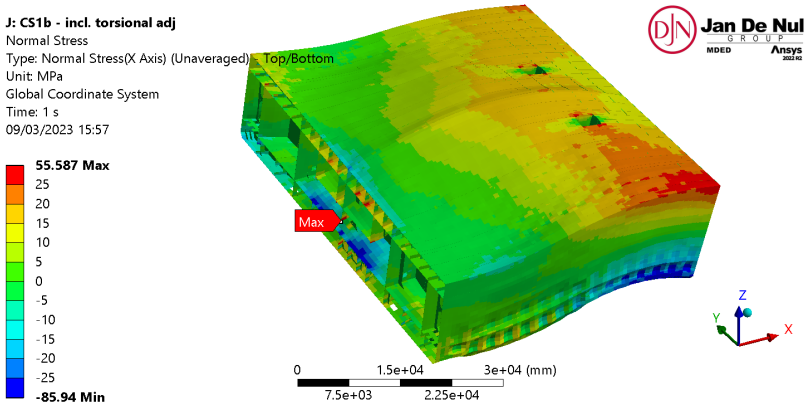

Figure 4.24: CS1b: Normal stress σ_x of the partial vessel model with both the bending moment and torsional moment adjustment. Mesh size $= 700mm$ and deformation scale factor $= 1000$.

Figure 4.25 shows the normal stress σ_x at main deck of the partial vessel model and analytical solution. It is apparent how the normal stress of the FEA is fairly smaller than the analytical solution. This must be due to the torsional moment adjustment, which leads to the normal stress σ_x. However, this is evidently not captured in the analytical solution and thus remains difficult to justify.

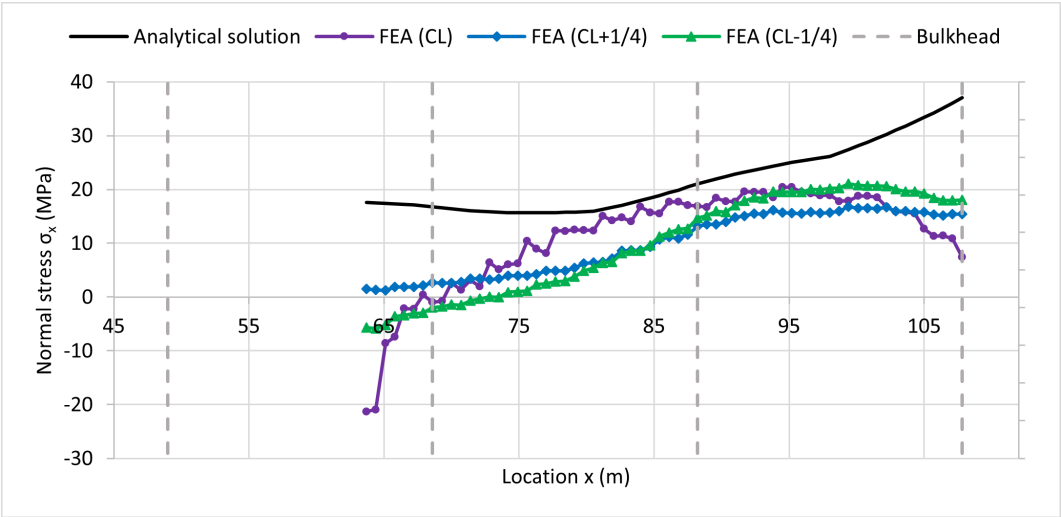

Figure 4.25: CS1b: Comparison of normal stress σ_x between the partial vessel model and analytical solution with both the bending moment and torsional moment adjustment. CL stands for centre line.

The effect of the torsional moment adjustment is isolated in Figure 4.26. The normal stress σ_x of the partial vessel model without torsional moment adjustment is subtracted from the one with adjustment. It was tried to comprehend this plot from analytical equations that consider normal warping stress due to torsion [12, 20]. However, given the complexity of the problem, it remains uncertain if this behaviour is as it should be.

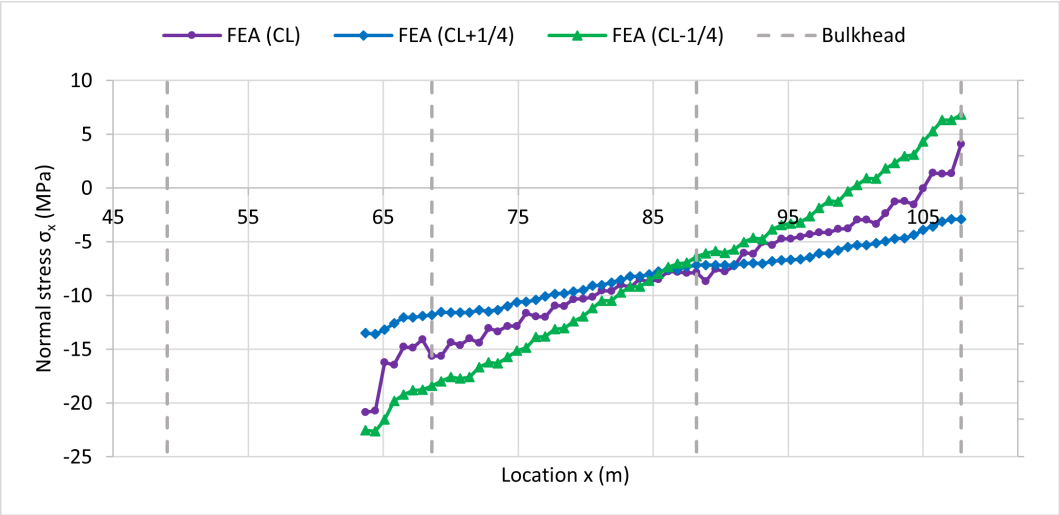

Figure 4.26: CS1b: Subtraction of normal stress σ_x of the partial vessel model without torsional moment adjustment from the one with adjustment. CL stands for centre line.

Lastly, the von Mises stress σ_{vm} at main deck of the partial vessel model and analytical solution is shown in Figure 4.27. It follows the same reasoning as before, which is that it is smaller than the normal stress σ_x, and thus the results are as expected.

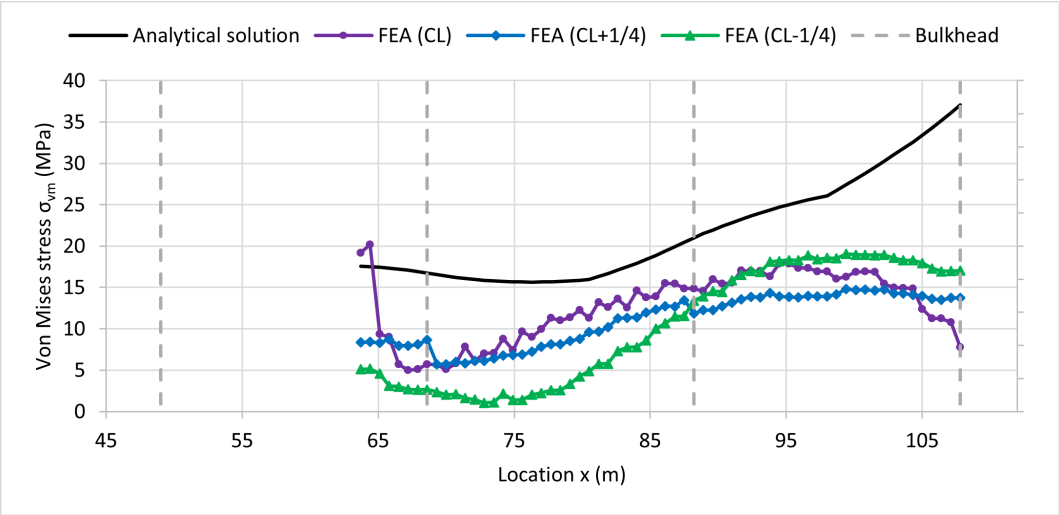

Figure 4.27: CS1b: Comparison of von Mises stress σ_{vm} between the partial vessel model and analytical solution with both the bending moment and torsional moment adjustment. CL stands for centre line.

4.3 Concluding remarks

The partial vessel FE analysis was performed for fictive case study 1a without water ballast. It was observed that the normal stress σ_x of the FEA is in agreement with the analytical solution. Besides, it could be reasoned that the von Mises stress is smaller than the normal stress σ_x due to the existence of the normal stress σ_y. The region that yields accurate results was limited to approximately 50% of the current partial vessel model. It is suggested to use a larger model in case the region that returns trustworthy results must increase. Finally, it was concluded upon that the shear force adjustment is unnecessary.

Subsequently, the partial vessel FE analysis was performed for case study 1b, which takes into account the water ballast and transversal position of weights and as a result also torsion. First, the analysis was performed without torsional moment adjustment to evaluate the effect of it. It was observed that the water ballast relieves the vertical bending moment at port and starboard side and hence locally reduces the normal stress σ_x. Besides, the von Mises stress was again smaller than the normal stress σ_x, which is now more pronounced along centre line. This happens because the normal stress σ_y is larger near the centre line region as the water ballast creates a bending moment about the x-axis. Then, the analysis was repeated including the torsional moment adjustment. It substantially reduced the normal stress σ_x since this adjustment is in the same order of magnitude as the torsional moment induced by the water ballast within the partial vessel model. However, it is evidently not captured in the analytical solution and therefore remains difficult to justify. It is suggested to perform the partial vessel FE analysis for a larger model or, on the other hand, to perform a full vessel FE analysis.

Chapter 5

Offshore installation vessel in waves

This chapter performs the partial vessel FE analysis of the offshore jack-up installation vessel in waves. First, the sea state is described in section 5.1. Then, case study 2 is analysed in section 5.2. Lastly, concluding remarks are made in section 5.3, which includes the results of the still water and wave component combined. While they are separately discussed for obvious reasons, it is relevant to present them together as they occur simultaneously in reality.

5.1 Sea state

A sea state that is common is adopted in this research of which the wave conditions are given in Table 5.1. The significant wave height H_s is equal to $3m$, which is a typical value for a vessel used to install offshore wind turbines. The Joint North Sea Wave Project (JONSWAP) is the wave spectrum with a peak enhancement factor $\gamma = 5$. Multiple peak wave periods that are likely to occur are considered. The return period t is 3 hours, which is a generally accepted value. It should not be, say 100 years, as is the case for permanent offshore platforms. Besides, spreading is not considered for the wave spectrum and notice that the wave directions are not specified here since it is related to the orientation of the vessel with respect to the waves.

Table 5.1: Wave conditions of the sea state.

Property	**Value**
Significant wave height H_s	$3m$
Wave spectrum	JONSWAP
Peak enhancement factor γ	5
Peak wave period T_p	3.092 - 13s for every 0.762s 13 - 16s for every 0.429s 16 - 30s for every 0.875s
Return period t	10800s

5.2 Case study 2

This section analyses the offshore jack-up installation vessel in waves maximising the vertical shear force and bending moment. The latter is typically much larger compared to all other hull girder loads. First, the load response amplitude operators (RAOs) are discussed in subsection 5.2.1. Second, the bending moment diagrams are given in subsection 5.2.2. Based on this, in subsection 5.2.3, the hull girder load adjustment are obtained. Then, the equivalent design waves are defined in subsection 5.2.4. Lastly, the results of the partial vessel FE analysis are examined in subsection 5.2.5.

5.2.1 Load response amplitude operators

The load RAOs are obtained from a diffraction analysis in Ansys AQWA and are used to determine the behaviour of the vessel in response to waves. It gives the magnitude of the load per unit wave amplitude and is expressed as function of the wave direction, wave period and position along the vessel. Maximising the vertical bending moment is more important than the shear force as this load is greater. This is achieved for a stern and head sea when the wavelength is similar to the length of the full vessel. The bending moment (M_y) RAOs of the full vessel for the stern (0°) and head (180°) sea are shown in Figure 5.1a and Figure 5.1b respectively. It is observed that the maximum is almost equal and is found at a wave period around $11s$ in both cases.

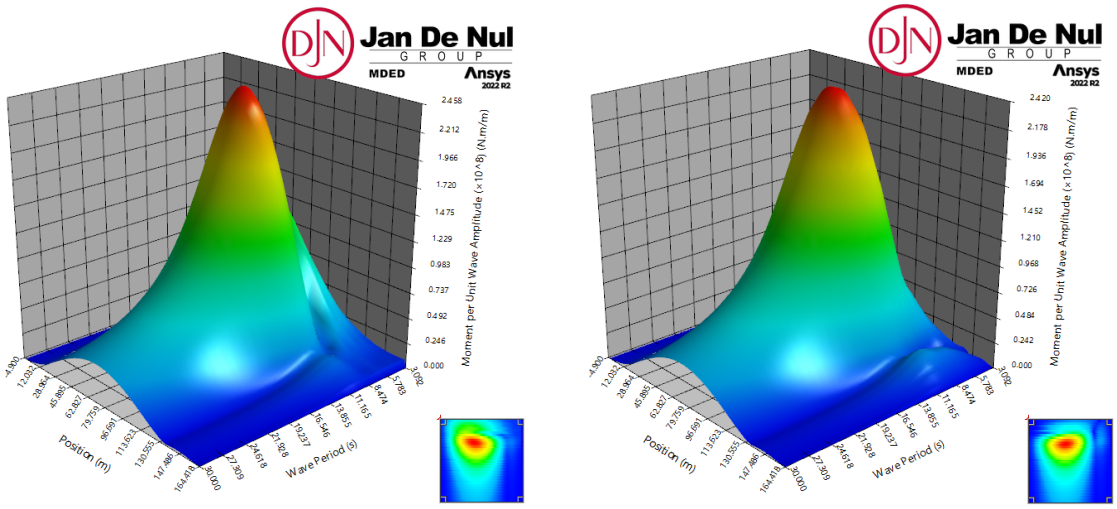

(a) RAO for a stern sea.

(b) RAO for a head sea.

Figure 5.1: Bending moment (M_y) RAOs of the full vessel.

Although it was mentioned that the maximum should occur for a stern or head sea, at higher frequencies, the vertical bending moment can have a maximum when the wave direction is, say 45°. It is expected that the magnitude of such RAO will always be smaller, but it has to be proven. This can be verified from the RAO envelope that combines all wave directions as shown in Figure 5.2 from top view. It is confirmed that the peak value corresponds to that of the RAO of the stern sea in Figure 5.1a at the same wave period.

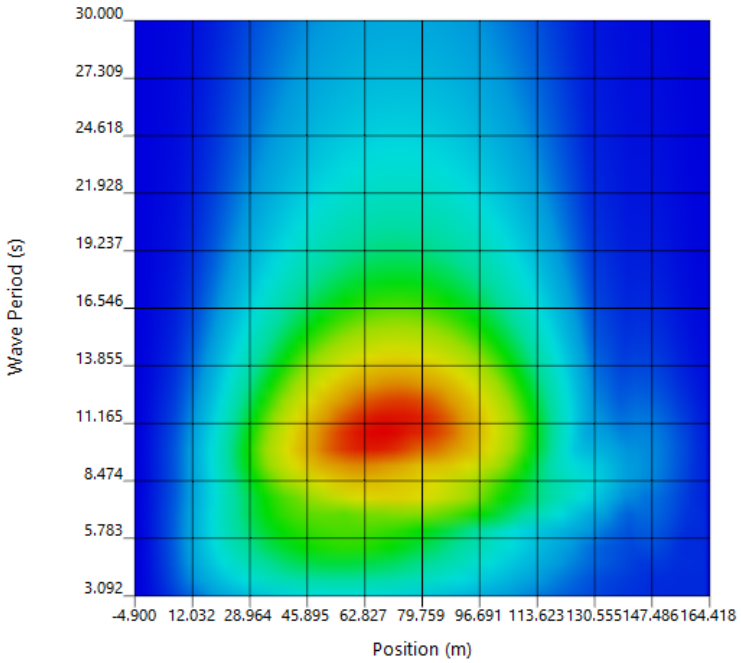

Figure 5.2: Bending moment (M_y) RAO envelope (all wave directions) of the full vessel from top view.

5.2.2 Shear force and bending moment diagrams

Similar to the vessel in still water, there are two reasons to construct shear force and bending moment diagrams. First, it is used to determine the hull girder load adjustments and second, it is needed for the analytical solution to verify the methodology. The procedure in subsection 3.4.2 is followed, using the wave conditions as specified in Table 5.1. From the discussion in subsection 5.2.1, it is expected that the highest vertical bending moment occurs in case of a stern and head sea around a (peak) wave period equal to $11s$.

In Figure 5.3 and Figure 5.4, the bending moment (M_y) diagrams of the full vessel in a stern and head sea for peak wave periods $T_p = 9$, 10, 11, 12 and $13s$ are given respectively. Additionally, the envelopes are shown so that the worst value at each position along the vessel is always captured. The peak wave period is varied to ensure that the case in which the energy of the wave is concentrated at the wave period where the RAO is maximum is included. It is observed that the bending moment starts to reduce again for higher periods, which confirms the range selected. Moreover, the bending moment became smaller in magnitude for the wave directions 15° and 165°. It can also be seen that the peak of the bending moment for the head sea is slightly more shifted to the fore end of the vessel than is the case for the stern sea. For this reason, they should both be considered or otherwise the bending moment could be under-estimated at some positions along the vessel. Lastly, notice that the shear force ($F_{s,z}$) diagrams and their envelope are also obtained for the same peak wave periods since they are used in the analytical solution. However, it is not shown as they are irrelevant except for the verification and they are much smaller.

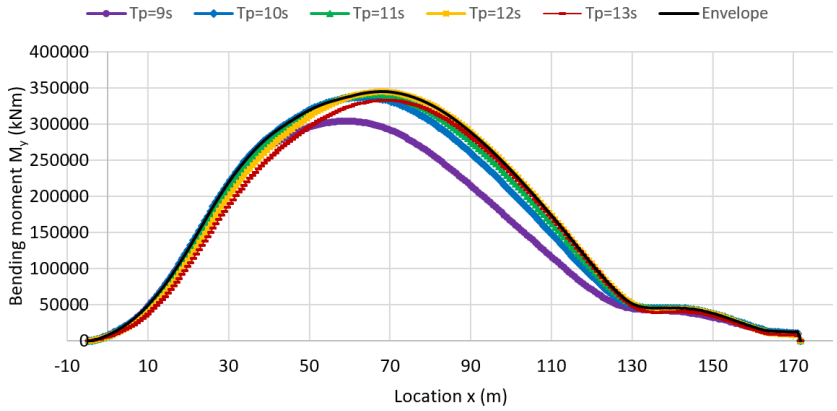

Figure 5.3: Case study 2: Bending moment (M_y) diagram of the full vessel in a stern sea.

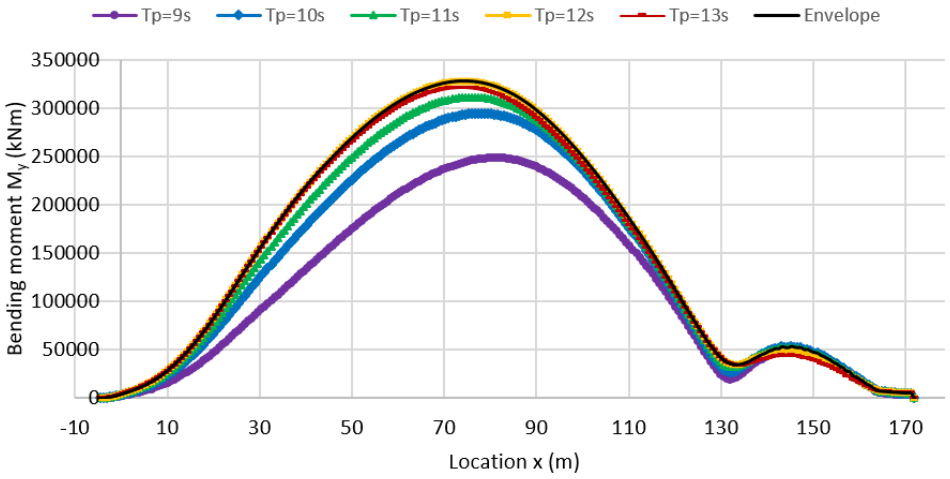

Figure 5.4: Case study 2: Bending moment (M_y) diagram of the full vessel in a head sea.

5.2.3 Hull girder load adjustments

The hull girder load adjustments are needed so that the partial vessel model reflects the full vessel behaviour. The bending moment adjustment is implemented according to the explanation in subsection 3.4.2. The shear force adjustment, on the other hand, is not made because it did not yield different stress results for the vessel in still water. The load adjustments for the stern and head sea are given in Table 5.2.

Table 5.2: CS2: Hull girder load adjustments. BM stands for bending moment.

Parameter	BM adjustment stern sea	BM adjustment head sea
ΔM_{aft}	343250 kNm	316780 kNm
ΔM_{fore}	186410 kNm	199130 kNm

5.2.4 Equivalent design waves

The equivalent design wave (EDW) approach is used to model the waves. It was deliberately not discussed in subsection 3.5.4 since it is best to explain by continuing on the foregoing. The EDW can take on any form, but it is typically decided to adopt a regular travelling wave as this is the easiest to model [65]. The regular wave is uniquely defined by the wave amplitude A, wave period T, wave direction Ω and phase angle φ. Since it is difficult to predict which wave will result in the worst condition, multiple design waves should be analysed. Note that a wave that gives the worst result at some location, does not necessarily do the same at another location. In what follows, the procedure to select appropriate design waves in order to capture the most severe response is explained.

The wave directions 0° and 180° are considered to maximise the vertical bending moment, as explained in subsection 5.2.1. Additionally, wave directions at a 15° and 30° offset from these two will be examined. Furthermore, the wave period is based on where the RAO is maximum. The bending moment (M_y) RAOs are now shown in 2D for the wave directions 0° and 180° in Figure 5.5 and Figure 5.6 respectively. The magnitude per unit wave amplitude is given as function of the wave period for six locations within the vessel section, which goes from 63.7m until 107.8m. It should be clear that wave periods between 9-13s will be selected.

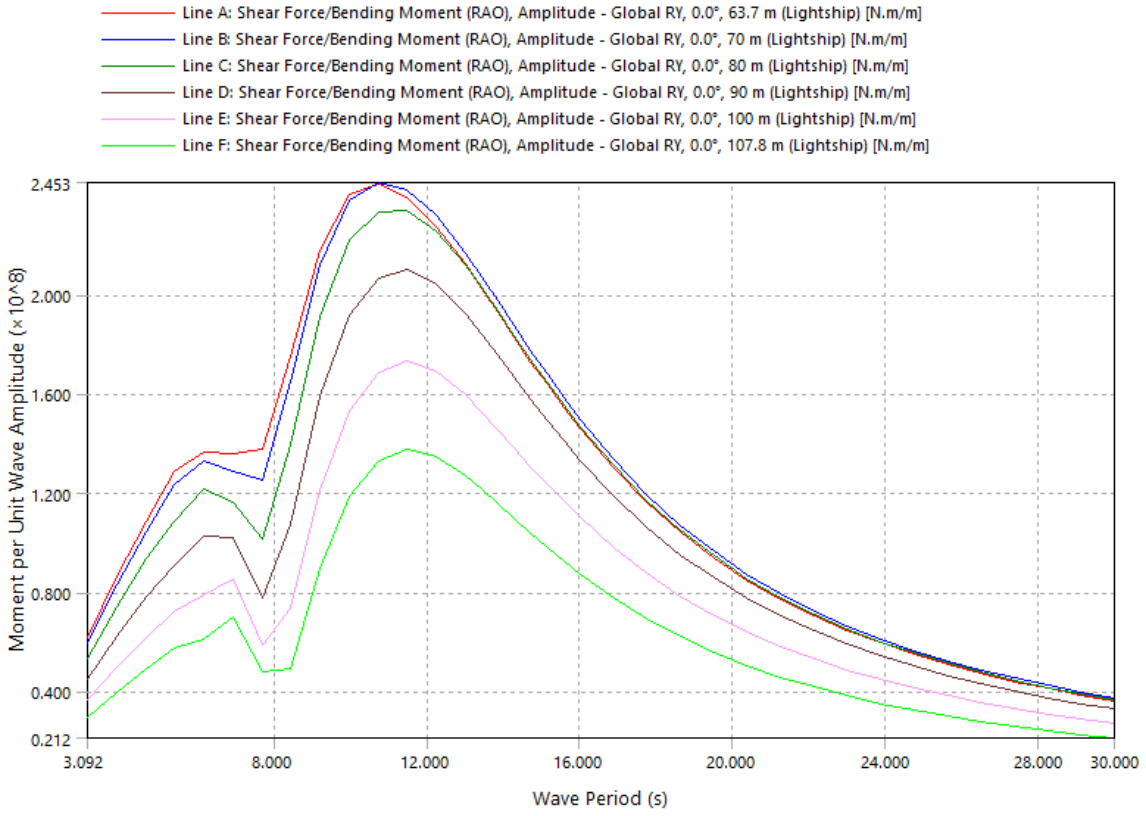

Figure 5.5: Bending moment (M_y) RAO of the full vessel for the wave direction 0°.

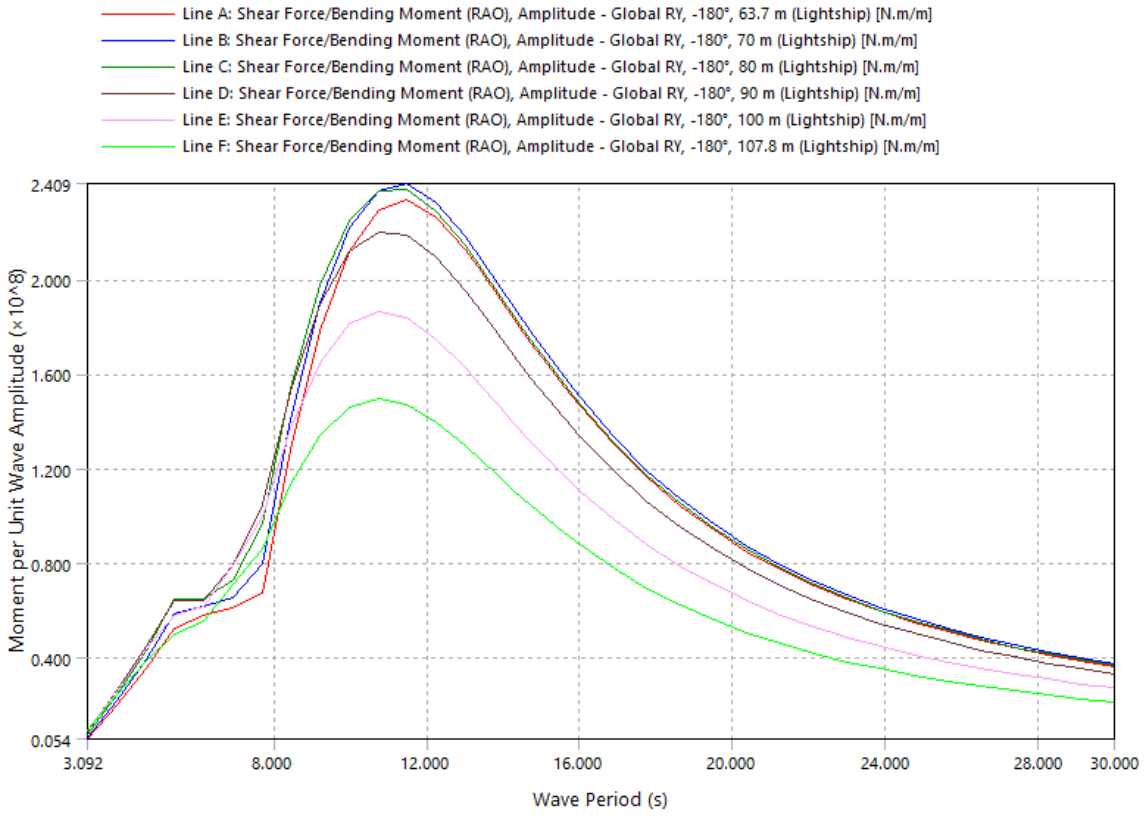

Figure 5.6: Bending moment (M_y) RAO of the full vessel for the wave direction 180°.

The wave amplitude A is based on the expected maximum wave height H_{max} for which the formula from OrcaFlex is used.[1] It is based on the significant wave height H_s, the return period t and the zero crossing wave period T_z. Besides, the constant $k = 1$ as suggested for moderate wave conditions. It is clear that a smaller zero crossing wave period leads to a larger expected maximum wave height.

$$H_{max} = k \cdot H_s \cdot \left(\frac{1}{2}\ln\left(\frac{t}{T_z}\right)\right)^{0.5} \tag{5.1}$$

The zero crossing wave period T_z can be related to the peak wave period T_p. The approximate relation between T_z and T_p for the JONSWAP spectrum is stated in the rules of DNV for environmental conditions and environmental loads [64] and is a function of the peak enhancement factor γ as shown below.

$$\frac{T_p}{T_z} = 0.6673 + 0.5037\gamma - 0.006230\gamma^2 + 0.0003341\gamma^3 \tag{5.2}$$

[1] https://www.orcina.com/webhelp/OrcaFlex/Content/html/Environment,Modellingdesignwaves.htm, Accessed [03-04-2023]

It would be over-conservative to assume the smallest possible peak wave period as the energy of the wave would then not concentrated at the wave period where the RAO is maximum. The smallest wave period within the vessel section where the RAO is maximum is equal to $10.714s$ for both wave directions. It is assumed that the peak wave period of the spectrum is the same as this wave period. Therefore, the expected maximum wave height $H_{max} = 5.665m$ and the wave amplitude $A = 2.833m$.

Lastly, recall that the vessel experiences hogging in still water and thus the vessel in waves is analysed for hogging as well. Therefore, the phase angle should be close to 0° or 360° as the wave crest passes through the centre of gravity of the structure at 0° in Ansys AQWA.

5.2.5 Results and discussion

The results of the partial vessel FE analysis of case study 2 are discussed in this section. The partial vessel model is constrained by the boundary conditions that are given in section 3.2. The wave pressure is applied to the model as explained in subsection 3.5.4. First, the transfer of pressure from the Hydrodynamic Diffraction analysis to the (FE) Static Structural analysis is tested, which is shown for one specific design wave in Figure 5.7 and Figure 5.8 respectively. Comparing the maximum pressure that occurs in both instances, which is almost equal to each other, indicates the pressure transfer has succeeded.

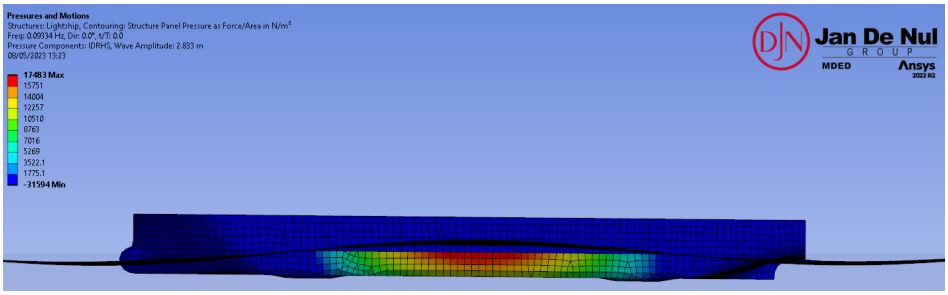

Figure 5.7: Wave pressure for $f = 0.09334Hz$, $\Omega = 0°$, A $= 2.833m$ and $\varphi = 0°$ in Hydrodynamic Diffraction analysis.

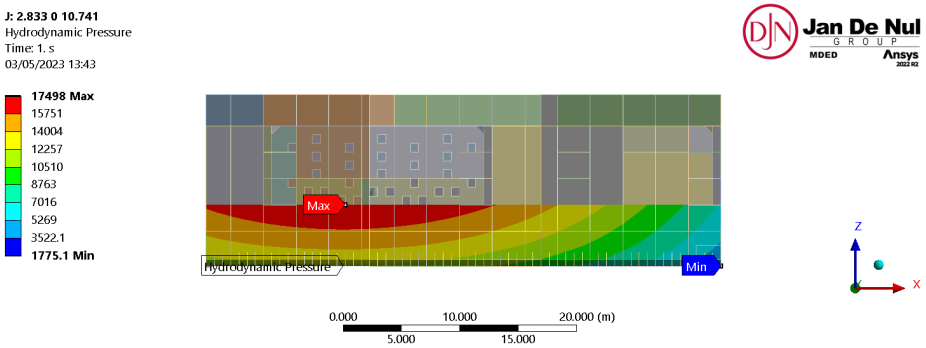

Figure 5.8: Wave pressure for $f = 0.09334Hz$, $\Omega = 0°$, A $= 2.833m$ and $\varphi = 0°$ in (FE) Static Structural analysis.

The analysis is initially performed for the vessel in a stern sea, but yet without the bending moment adjustment. The wave direction is fixed at 0° and the five different wave periods between 9-13s that are specified in Table 5.1 are used. A sequence of 30 time steps is chosen so that the wave is simulated for every 15° in one period. The worst hogging state is captured by selecting the phase angle for the time of maximum. It could also have been decided to use the maximum over time, which retrieves the maximum at each position regardless of the phase angle, but in the end it only matters how accurate the equivalent design wave approach is. Figure 5.9 shows the normal stress σ_x at main deck along centre line of the partial vessel model. The legend gives the wave amplitude A, wave direction Ω and wave period T in this order. It is observed that the maximum stress occurs for the wave period $T = 10.741s$.

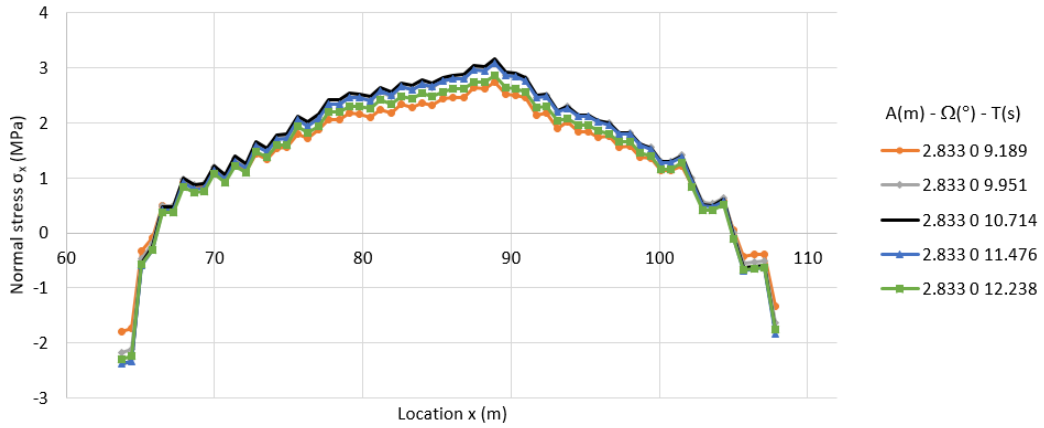

Figure 5.9: CS2: Normal stress σ_x of the partial vessel model in a stern sea for various wave periods.

The analysis is repeated for the wave period $T = 10.741s$ while varying the wave direction. In addition, the period below and above are also tested for the wave direction 15°. The normal stress σ_x at main deck along centre line of the partial vessel model is shown in Figure 5.10. It is observed that the maximum stress occurs for the wave direction 0°, although the head sea must still be analysed as well. Furthermore, it was confirmed that the stress did not increase at main deck away from centre line for wave directions other than 0°.

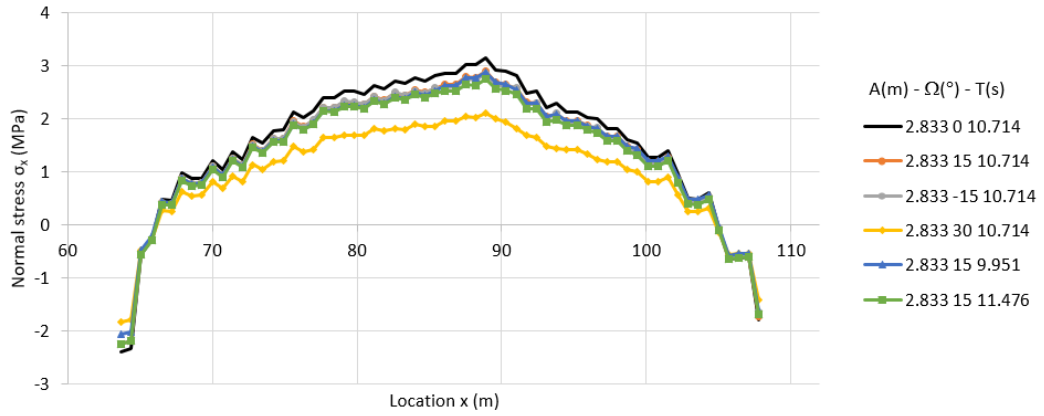

Figure 5.10: CS2: Normal stress σ_x of the partial vessel model in a stern sea for various wave directions and periods.

The same analysis is also performed for the vessel in a head sea, which leads to similar graphs as shown above. They are for this reason not repeated, but the wave parameters of the worst hogging state are the following. The wave amplitude $A = 2.833m$, the wave direction $\Omega = 0°$ and the wave period $T = 9.951s$. Normally, the vessel in both the head and stern sea should be considered. But, since the purpose here is to investigate the accuracy of the equivalent design wave approach, only the stern sea is used. Anyhow, they are very similar to each other. In Figure 5.11, the normal stress σ_x of the partial vessel model for the worst hogging state in a stern sea with bending moment adjustment is shown.

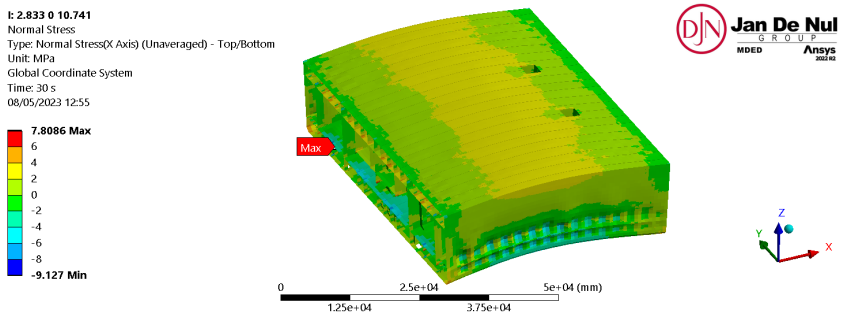

Figure 5.11: CS2: Normal stress σ_x of the partial vessel model for the worst hogging state in a stern sea without bending moment adjustment. Mesh size = $700mm$ and deformation scale factor = 2500.

The analytical solution in section 3.6 is used as verification for the partial vessel FE analysis. The normal stress σ_x at main deck of the partial vessel model and analytical solution is shown in Figure 5.12. The stress results are retrieved along the centre line, as well as along the lines located a quarter of the vessel's width away from the centre line in y, denoted as $CL_{+1/4}$ and $CL_{-1/4}$. While it is expected that the three results are very similar, this is done on purpose as it will be combined with the results of the still water component. It is observed that the normal stress of the FEA is somewhat larger than the analytical solution due to the conservative assumptions in the equivalent design wave approach.

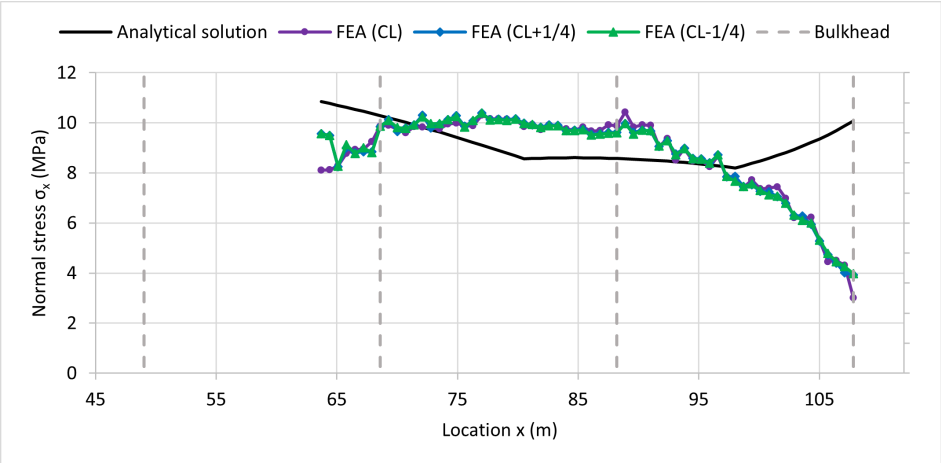

Figure 5.12: CS2: Comparison of normal stress σ_x between the partial vessel model and analytical solution with the bending moment adjustment. CL stands for centre line.

Lastly, the von Mises stress σ_{vm} of the partial vessel model and analytical solution is shown in Figure 5.13. Similar to the vessel in still water, the von Mises stress is smaller than the normal stress σ_x of the FEA due to the existence of the normal stress σ_y. Finally, the region that shows a good agreement with the analytical solution is limited to just over $20m$, or in other words to 50% of the current partial vessel model. Besides, the stress is under-estimated at the aft and fore end.

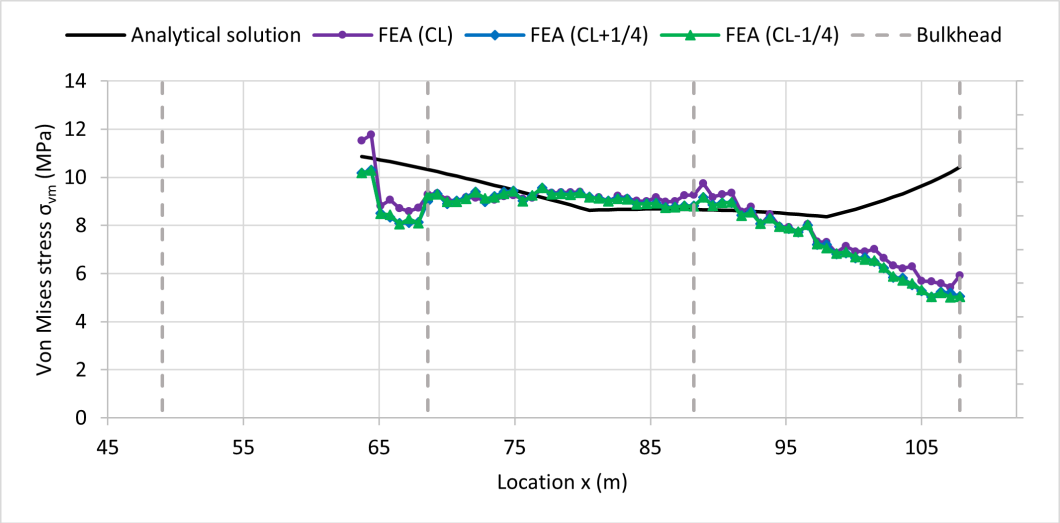

Figure 5.13: CS2: Comparison of von Mises stress σ_{vm} between the partial vessel model and analytical solution with the bending moment adjustment. CL stands for centre line.

5.3 Concluding remarks

The partial vessel FE analysis was performed for case study 2, which studies the vessel in waves trying to maximise the vertical shear force and bending moment. The equivalent design wave approach was used to model the waves. A regular travelling wave was assumed with an amplitude based on the expected maximum wave height. It was observed that the normal stress σ_x of the FEA is slightly larger than the analytical solution due to the conservative assumptions of this approach. The von Mises stress of the FEA, on the other hand, is in agreement with the analytical solution. Lastly, similar to the vessel in still water, 50% of the current partial vessel model yields accurate results.

Finally, the results of the still water and wave component are combined. For an offshore jack-up installation vessel, the still water component is larger due to the intrinsic high variation in weight and because the significant wave height cannot be too high either when wind turbines are installed. The normal stress σ_x at main deck of the partial vessel model and analytical solution is given in Figure 5.14 and the von Mises stress σ_{vm} in Figure 5.15. Whereas the von Mises stress of the FEA compared to the analytical solution for the wave component did not yield better results, the still water component substantially improved.

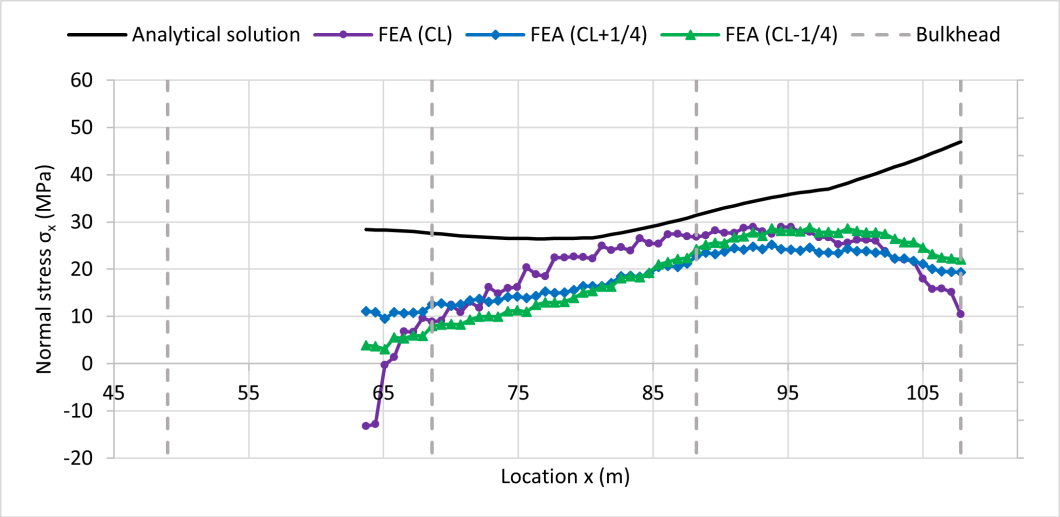

Figure 5.14: CS2: Comparison of normal stress σ_x between the partial vessel model and analytical solution for still water and wave component combined.

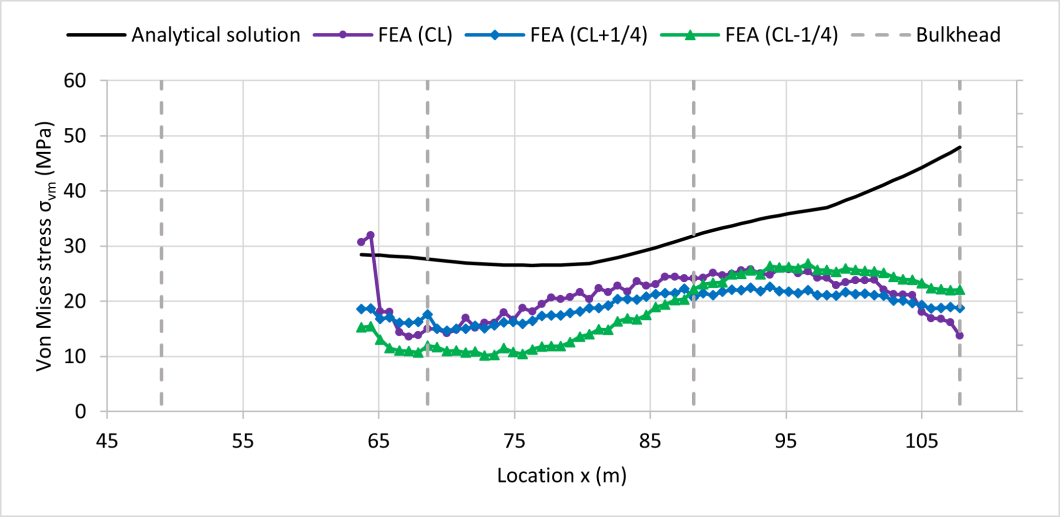

Figure 5.15: CS2: Comparison of von Mises stress σ_{vm} between the partial vessel model and analytical solution for still water and wave component combined.

Chapter 6

Offshore installation vessel carrying heavy payload

The methodology of the partial vessel FE analysis was developed in chapter 3. Subsequently, it was tested for an offshore jack-up installation vessel in still water and waves in chapter 4 and chapter 5 respectively. Ultimately, the goal is to perform this analysis with heavy payload. This chapter studies a wind turbine tower sea fastened on deck of the vessel. First, the tower specifications are described in section 6.1. Then, the partial vessel FE analysis is performed in section 6.2.

6.1 Wind turbine tower

The choice behind the wind turbine tower is because it is located on deck of the studied vessel section. The required data of the tower is specified in Table 6.1. It is secured by a seafastening grillage, which forms the interface between payload and vessel. Three functions can be distinguished, first it is used to level the payload since the deck is not perfectly straight. Second, it sea fastens the payload (usually bolted in case of the tower) and third, it transfers the high load into the vessel.

Table 6.1: Wind turbine tower data. COG stands for centre of gravity.

Parameter	**Value**
Weight	1000ton
x_{COG}	85.40m
y_{COG}	14.00m
z_{COG}	65.16m

6.2 Partial vessel FE analysis

This section covers the partial vessel FE analysis of the offshore jack-up installation vessel with a wind turbine tower sea fastened on deck. First, the model setup is defined in subsection 6.2.1. Then, the effect of the payload is independently studied in subsection 6.2.2. Lastly, the results of the partial vessel FE analysis are discussed in subsection 6.2.3.

6.2.1 Model setup

The partial vessel model is built conforming the guidelines in section 3.1. The grillage is also modelled as it transfers the wind turbine tower load into the vessel. Evidently, the grillage stands on strongpoints that are underneath deck, namely bulkheads, longitudinals, girders and transverses. Batch connections are used for the grillage like for the partial vessel model. The connection between these two structures is made by a bonded contact. The tower is modelled as a point mass and is scoped to the grillage. Normally, as well a limited part of the tower would be modelled to check the connection with the grillage. However, this is not necessary since the vessel response will only be examined.

The mesh size of the partial vessel model is equal to the frame spacing ($700mm$). On the other hand, the grillage was given a more refined mesh ($350mm$). In Figure 6.1, the setup of the partial vessel model and grillage with visible mesh can be seen.

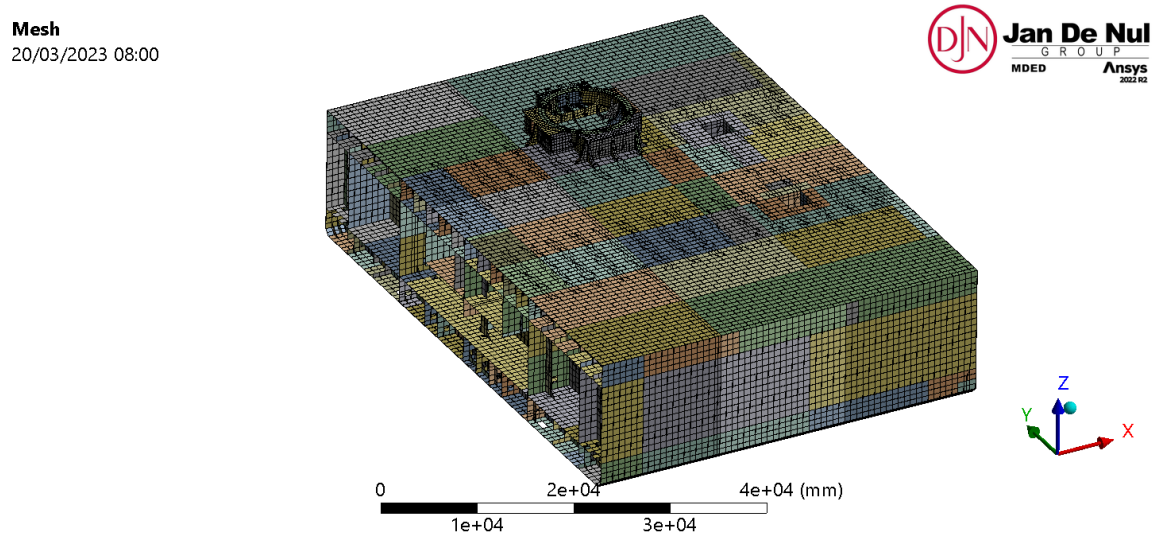

Figure 6.1: Setup of the partial vessel model and grillage with visible mesh.

6.2.2 Local analysis of payload

It is relevant to see how the stress develops in the vessel due to the wind turbine tower load. Therefore, the effect of the tower is independently studied, which is realised when only its weight is activated. Loads on the tower other than its weight (e.g. wind) are not considered. The grillage weight can be neglected since it is far smaller than the tower load. Besides,

the partial vessel model remains constrained according to the boundary conditions given in section 3.2. The following APDL command in Ansys is used to apply the gravity acceleration to the tower only, where 'pmTower' stands for the identifier of its point mass.

```
NSEL,S,,,pmTower
ESLN,S
ESEL,R,ENAME,,21
CM,pmTower,ELEM
CMACEL,pmTower,0,0,9806.65
ALLSEL,ALL
```

The directional deformation along z is given in Figure 6.2. It is observed that the deformation stays small with an absolute minimum at the grillage. Next, in what follows, the stress field will be investigated by looking at the individual stress components. Besides, the required mesh size will be discussed.

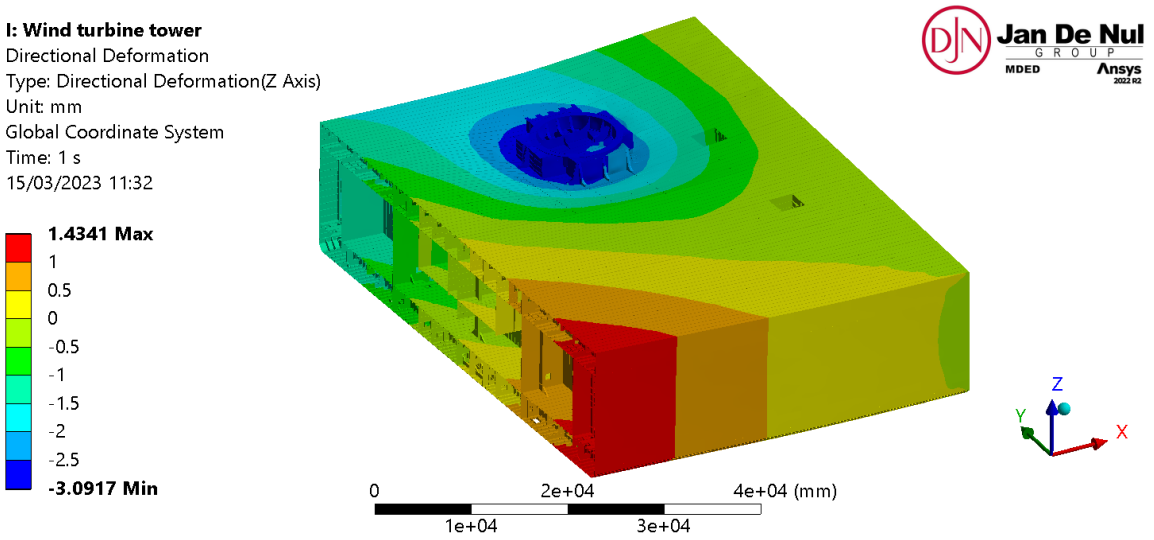

Figure 6.2: Directional deformation along z of the partial vessel model and grillage. Mesh size $= 700mm$ and deformation scale factor $= 1000$.

Stress field

The normal stress σ_x is given in Figure 6.3. The stress remains small while higher values are only seen in the vicinity of the grillage. This can be attributed to local bending due to the tower load. Similarly, the normal stress σ_y does not fully develop except near the grillage as shown in Figure 6.4. Recall that these two stress components were more pronounced in the partial vessel FE analysis.

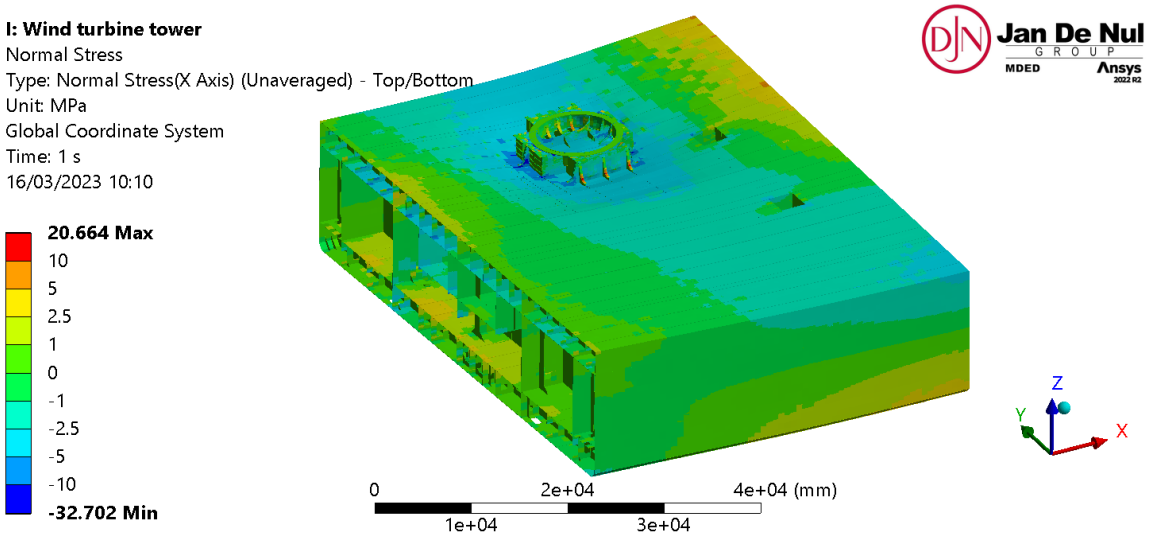

Figure 6.3: Normal stress σ_x of the partial vessel model and grillage. Mesh size = 700mm and deformation scale factor = 1000.

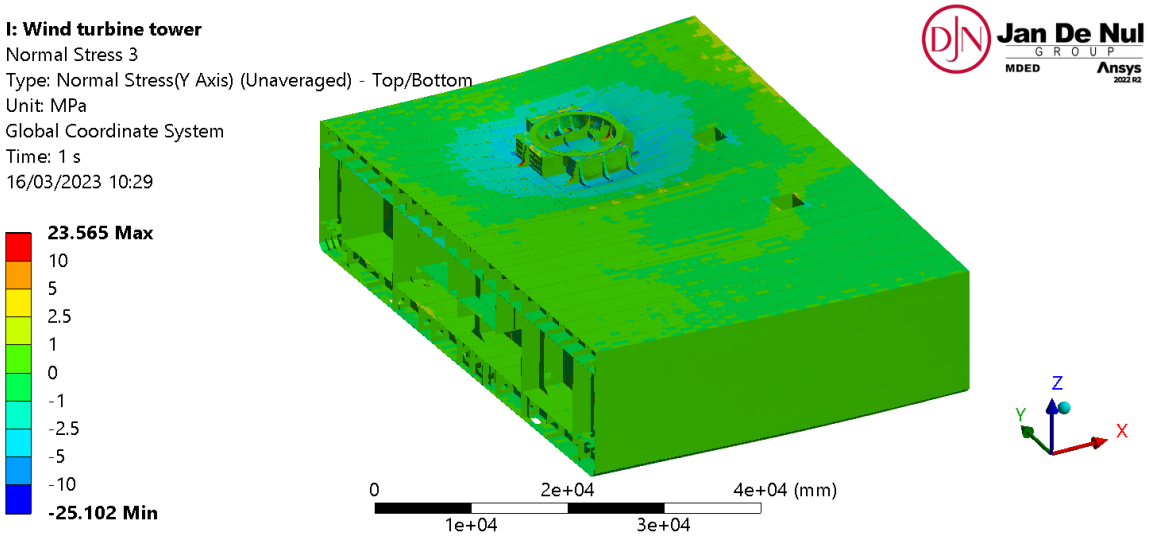

Figure 6.4: Normal stress σ_y of the partial vessel model and grillage. Mesh size = 700mm and deformation scale factor = 1000.

Figure 6.5 shows the normal stress σ_z, looking at the longitudinal underneath the grillage. Compared to the normal stresses σ_x and σ_y, the absolute minimum is greater. The stress is large where the tower load is introduced, but then quickly reduces as it spreads out. Although not shown, the same behaviour is observed when viewed from the yz-plane. Recall the decision in section 3.1 to keep the (man)holes between the cofferdam and main deck at their original location, even if this resulted in a less structured mesh. This was done on purpose to obtain the most realistic vessel response. Besides, it remains conservative to represent a hole as rectangular cutout.

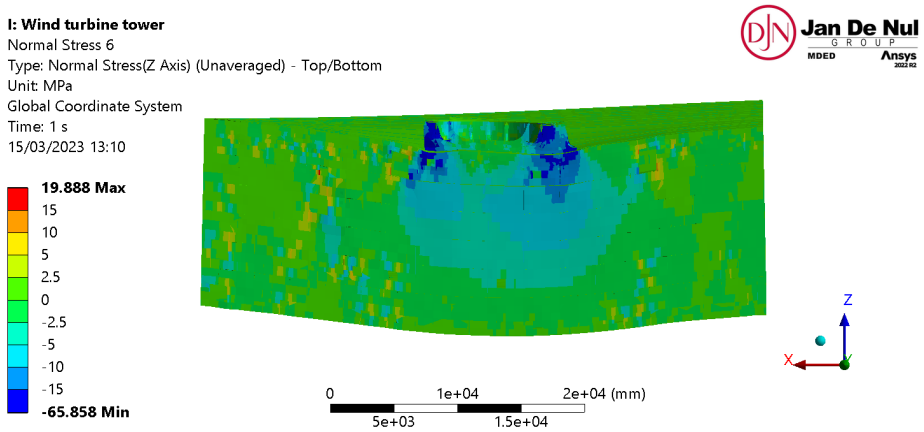

Figure 6.5: Normal stress σ_z of the partial vessel model and grillage, looking at the longitudinal underneath the grillage. Mesh size = 700mm and deformation scale factor = 1000.

In Figure 6.6, the shear stress τ_{xz} is given, looking at the longitudinal underneath the grillage. It is observed that the shear stress extends further than the normal stress. The stress pattern can be compared to a beam with a point load applied to it. Irrespective of the beam's boundary conditions, the shear force changes sign at this load as shown in Figure 6.7.

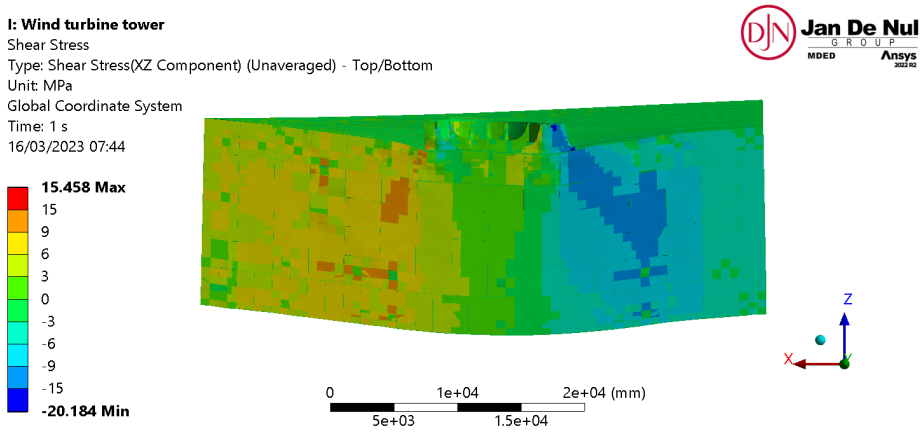

Figure 6.6: Shear stress τ_{xz} of the partial vessel model and grillage, looking at the longitudinal underneath the grillage. Mesh size = 700mm and deformation scale factor = 1000.

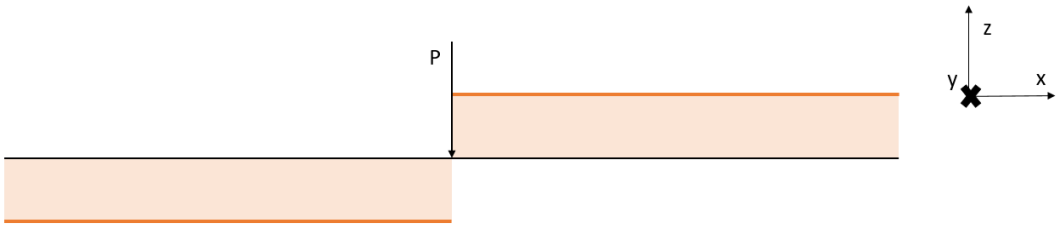

Figure 6.7: Shear force diagram of a beam with a point load P applied to it. The shear force changes sign at this load.

The shear stress τ_{yz} is shown in Figure 6.8, looking at the bulkhead underneath the grillage. The same stress pattern as in the case of the shear stress τ_{xz} is observed. Lastly, the shear stress τ_{xy} is, as expected, near zero everywhere.

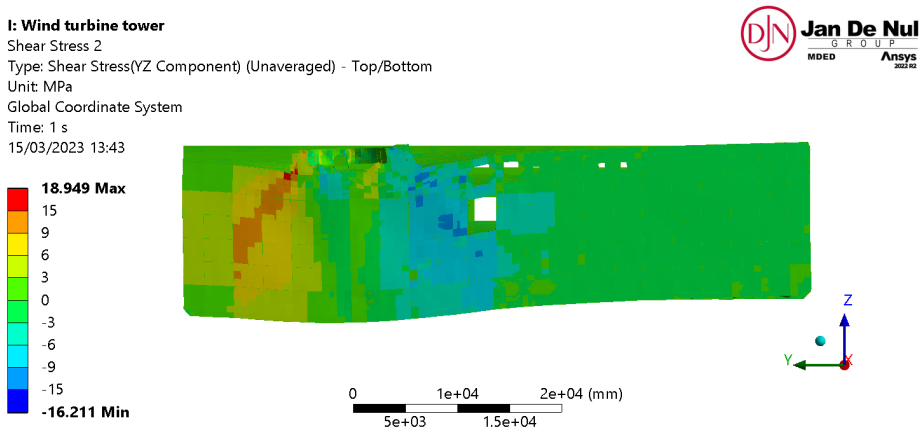

Figure 6.8: Shear stress τ_{yz} of the partial vessel model and grillage, looking at the bulkhead underneath the grillage. Mesh size = 700mm and deformation scale factor = 1000.

Mesh size

A mesh convergence study of the partial vessel FE analysis had previously shown that a mesh size equal to the frame spacing (700mm) is satisfactory. Thus far, this size was adopted in the current analysis of the vessel with a wind turbine tower sea fastened on deck. However, it is possible that it is too rough in the vicinity of the tower. For this reason, the analysis is first repeated for an overall mesh size of 350mm, further refined to 175mm near the grillage. Then, for an overall mesh size of 233.33mm and refined to 100mm. The comparison with the foregoing results is limited to the normal stress σ_z as this component was most pronounced. Figure 6.9 shows the normal stress like in Figure 6.5, but for the finer mesh size. It can be seen that the stress patterns are as good as identical.

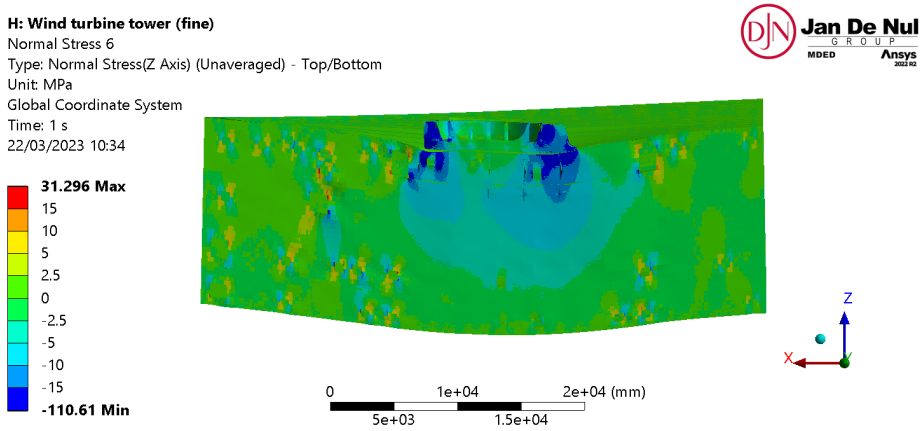

Figure 6.9: Normal stress σ_z of the partial vessel model and grillage, looking at the longitudinal underneath the grillage. Mesh size = 350 / 175mm and deformation scale factor = 1000.

In Figure 6.10, the normal stress for the finest mesh size is shown. The stress pattern is again nearly identical, implying an adequate mesh size at first sight. However, the absolute minimum is also observed to have increased as a result of refining the mesh size. This minimum, which always occurred at the same vertex of the grillage, is most likely a singularity as it grows exponentially. But this does not hold for every other point and so it is further investigated.

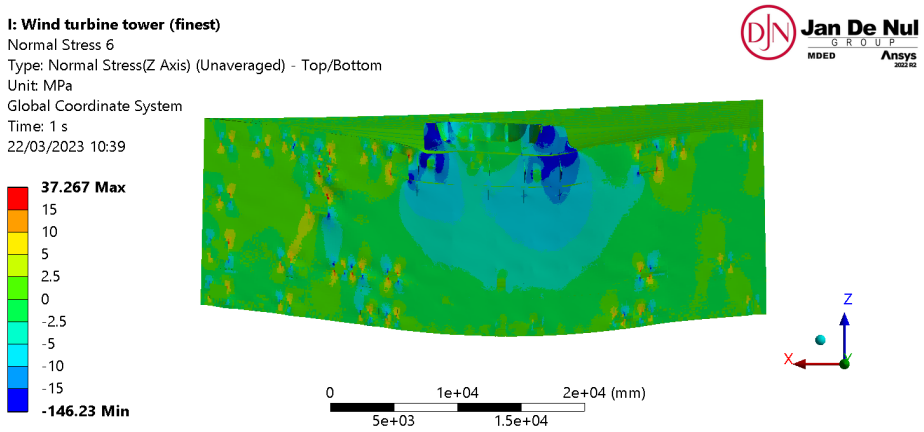

Figure 6.10: Normal stress σ_z of the partial vessel model and grillage, looking at the longitudinal underneath the grillage. Mesh size = 233.33 / 100mm and deformation scale factor = 1000.

The following comparison between the different mesh sizes retrieves the normal stress σ_z at four locations of which the coordinates are given in Table 6.2. Location 1 is at the corner of a rectangular cutout, location 2 and 3 are at a high stressed region but away from any boundary, and location 4 is right underneath the main deck.

Table 6.2: Coordinates of four locations used to compare the normal stress σ_z there for different mesh sizes.

Location	x (mm)	y (mm)	z (mm)
1	90300	14008.5	13925
2	89600	14008.5	12575
3	80500	14007.5	13925
4	79100	14007.5	14650

In Table 6.3, the values of the stress at the four locations are given for the original, fine and finest mesh size. Additionally, it includes the relative error Δ in percent between each consecutive mesh refinement. It tells that the fine mesh size gives satisfactory results, except for location 1, which was deliberately added to prove that convergence is not achieved everywhere. Since this location is at the corner of a rectangular cutout, a high stress is expected there. Moreover, it will have difficulty to converge as the stress cannot flow smoothly around this cutout. However, in reality, it is not the case that the holes are rectangular.

Table 6.3: Values of the normal stress σ_z for each mesh size and their respective relative error at the four locations.

Mesh size	Location 1	Location 2	Location 3	Location 4
Original	-21.054MPa	-12.337MPa	-15.254MPa	-17.062MPa
Fine	-33.525MPa	-11.983MPa	-16.433MPa	-17.554MPa
Finest	-39.476MPa	-11.861MPa	-16.572MPa	-17.583MPa
$\Delta_{original/fine}$	-59.233%	2.869%	-7.729%	-2.884%
$\Delta_{fine/finest}$	-17.751%	-1.018%	-0.846%	0.165%

While it is advised from the above discussion to refine the mesh size near the payload, it is not needed to unnecessarily increase the element count. Rules exist such as those of DNV [17] that define acceptance criteria based on the mesh size used. For instance, it includes that a mesh size equal to the frame spacing will reduce the allowable stress to a percentage of its original value. In this way, the fact that the stress may not have fully converged is taken into account. These rules are particularly useful in the maritime industry because a fine mesh is not always possible due to long simulation times.

6.2.3 Results and discussion

Following the discussion of the local analysis of payload in the previous section, the partial vessel FE analysis is performed. For simplicity, the wind turbine tower and grillage are moved to the centre line such that the water ballast is the same as in case study 1b (see section 4.2). Besides, still water loads are considered in the analysis, but not the wave loads. The tower load is clearly visible from the weight w per unit length, as shown in Figure 6.11. Together with the buoyancy b per unit length, the shear force and bending moment diagram can be constructed, which neither are shown for the reason that they are very similar to those of case study 1b.

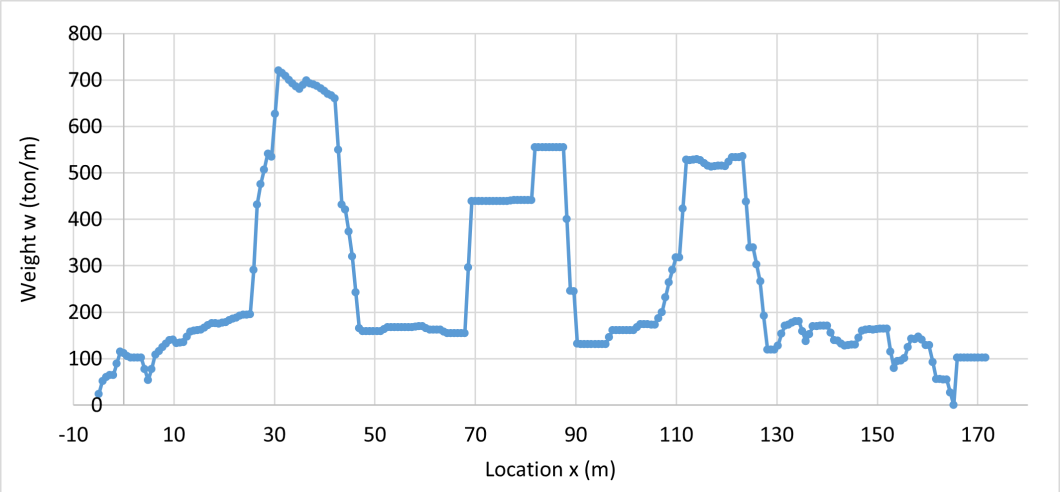

Figure 6.11: Weight w per unit length at each frame.

The hull girder load adjustments are given in Table 6.4, except for the shear force adjustment as it barely made any difference in the FEA results. In addition, the following data for the weight and buoyancy is calculated. The adjusted density $\rho_{adj} = 9418.37 kg/m^3$, the buoyant force $F_b = 162995.81 kN$ and the height $h = 6.13 m$.

Table 6.4: Hull girder load adjustments. BM and TM stand for bending moment and torsional moment respectively.

Parameter	BM and TM adjustment
ΔM	468300.04 kNm
ΔT	309385.76 kNm

The results of the FEA should no longer be compared to the analytical solution in section 3.6, since it is unable to fully capture the tower load. Instead, the analysis is repeated for the same adjustments and loads, but without tower and grillage. This is a non-existing case that should provide a better understanding of the global behaviour versus the local response of the vessel. The von Mises stress σ_{vm} is compared in both cases as it encompasses every stress component, and is given in Figure 6.12 and Figure 6.13 for the case with and without payload respectively. It is observed that the global behaviour is very alike, which indicates that the tower load mainly causes a local change in stress field. It can also be seen that the plate area in the xz- (and xy-) plane has regions of high stress since the vessel is subjected to torsion, which causes shear stress. This was previously not discussed in chapter 4 because this stress component was not compared to the analytical solution.

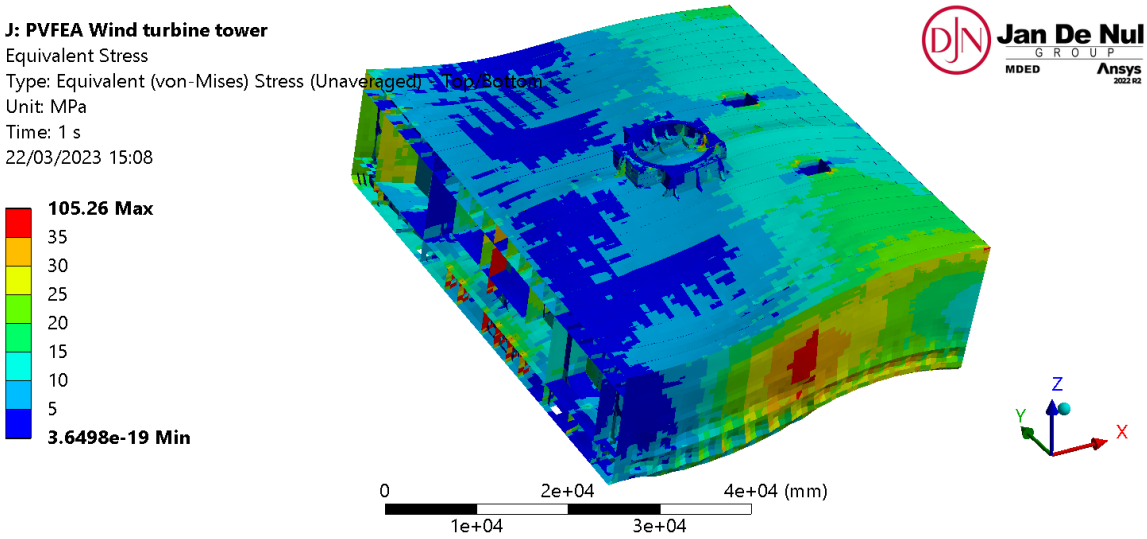

Figure 6.12: Von Mises stress σ_{vm} of the partial vessel model and grillage with wind turbine tower. Mesh size = $700mm$ and deformation scale factor = 1000.

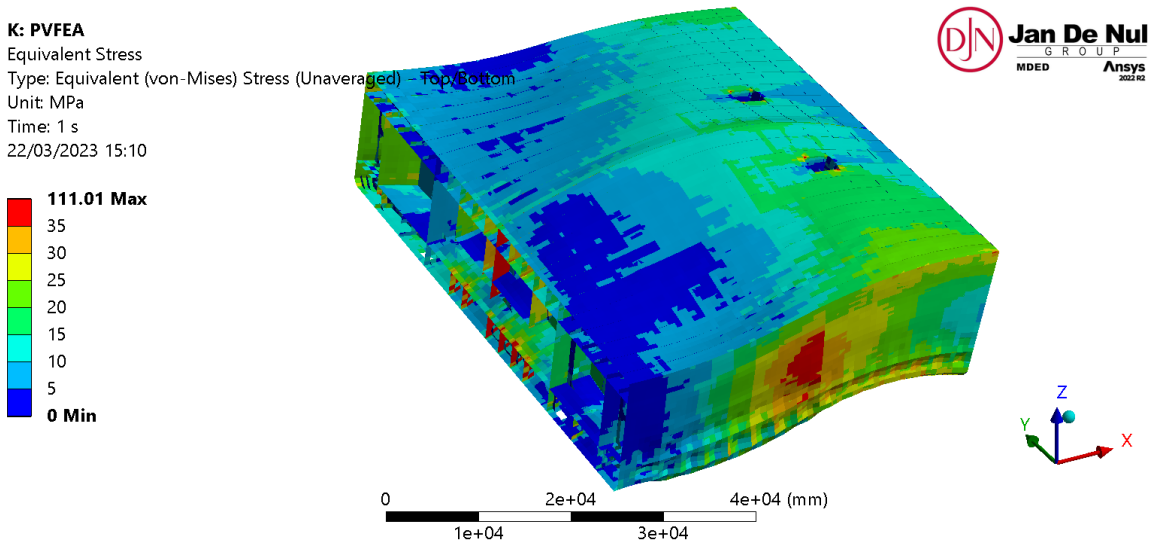

Figure 6.13: Von Mises stress σ_{vm} of the partial vessel model. Mesh size = 700mm and deformation scale factor = 1000.

The von Mises stress σ_{vm}, looking at the centre longitudinal, is given in Figure 6.14 and Figure 6.15 for the case with and without payload respectively. Two observations are made, which were already mentioned in the discussion about the local analysis of payload in subsection 6.2.2. First, the von Mises stress is high underneath the grillage at the location where it introduces the tower load into the vessel. This can be attributed to the normal stress σ_z, as was shown in Figure 6.5. Second, the von Mises stress became smaller left from the grillage and larger to its right. This can be associated with the shear stress τ_{xz} and was shown in Figure 6.6.

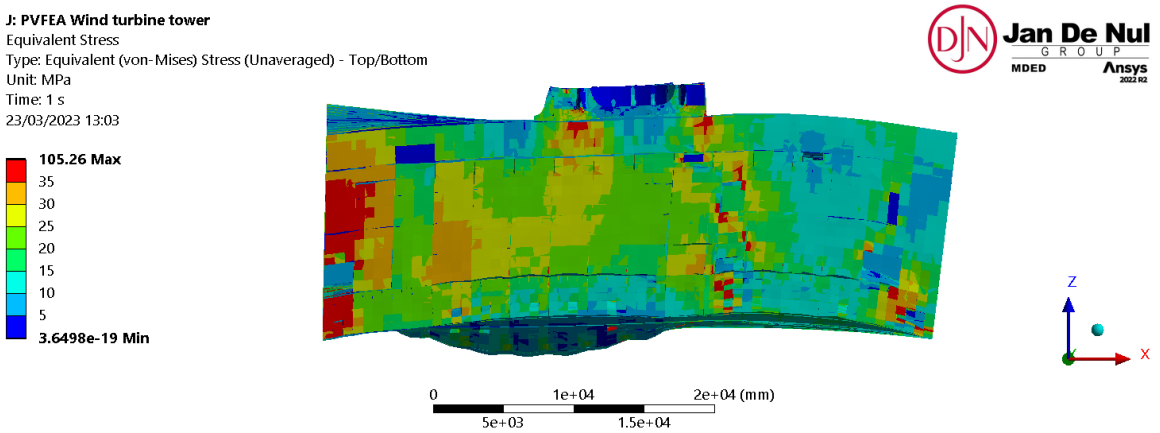

Figure 6.14: Von Mises stress σ_{vm} of the partial vessel model and grillage with wind turbine tower, looking at the centre longitudinal. Mesh size = 700mm and deformation scale factor = 500.

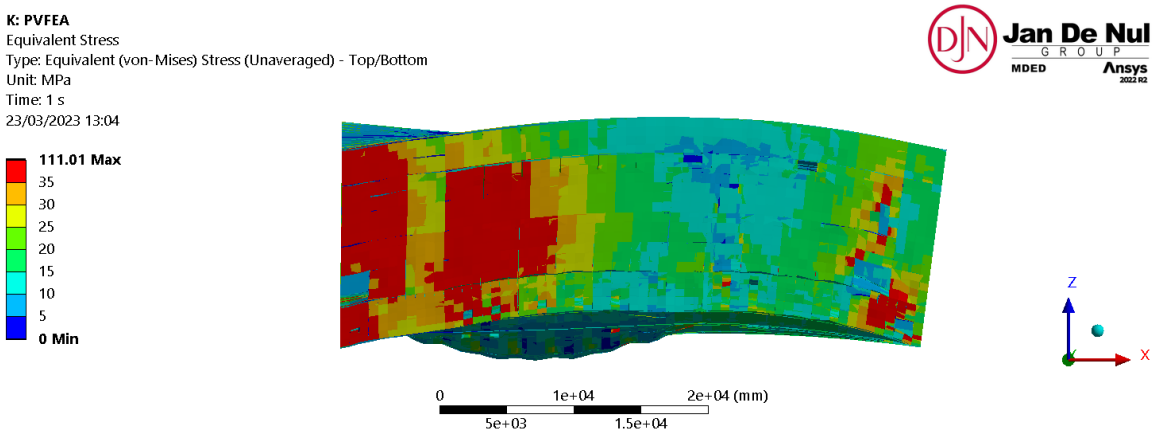

Figure 6.15: Von Mises stress σ_{vm} of the partial vessel model, looking at the centre longitudinal. Mesh size = 700mm and deformation scale factor = 500.

While the above serves as a good comparison, it is not entirely realistic. During operation of the offshore jack-up installation vessel, the grillage will always be there. Therefore, the analysis is repeated with grillage, but without wind turbine tower. Notice that the bending moment adjustment will slightly differ due to the absence of the tower. In order to see the change in results from the case with wind turbine tower (see Figure 6.12), the difference in stress of the partial vessel model is calculated. In Figure 6.16, the region is shown where a difference higher than 5MPa is noted. It is observed that this occurs for the bulkhead and longitudinal underneath the grillage, which is due to the shear stress. Furthermore, the maximum does not exceed 20MPa. On the other hand, in Figure 6.17, the region is shown where a difference lower than -5MPa is noted. This occurs only locally underneath the grillage, as expected, due to the normal stress σ_z. In this case, the stress does differ by up to -70MPa.

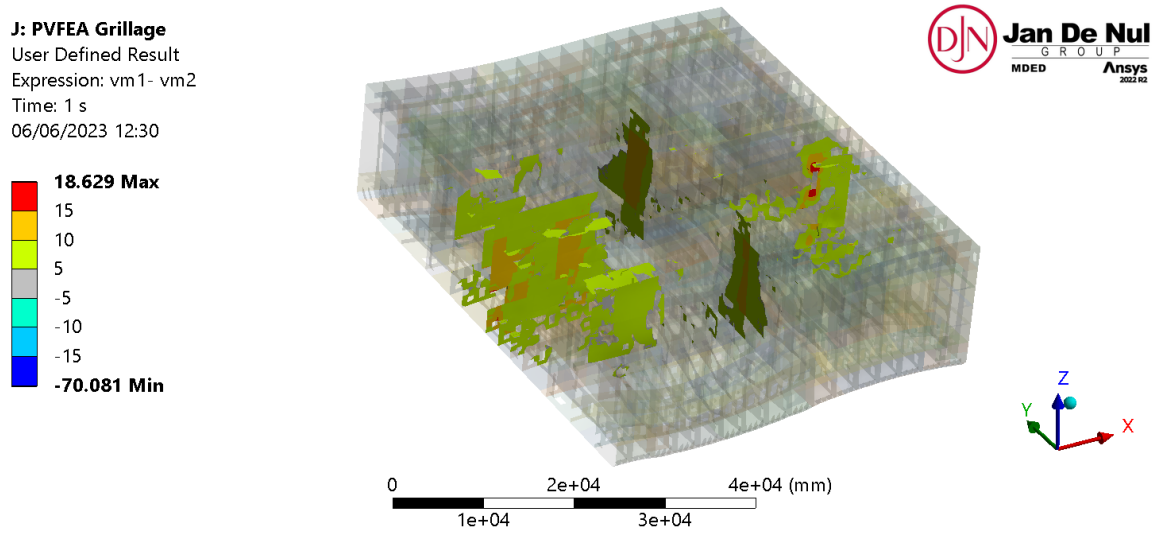

Figure 6.16: Difference in von Mises stress σ_{vm} of the partial vessel model with and without wind turbine tower. Results show region with a magnitude higher than 5MPa.

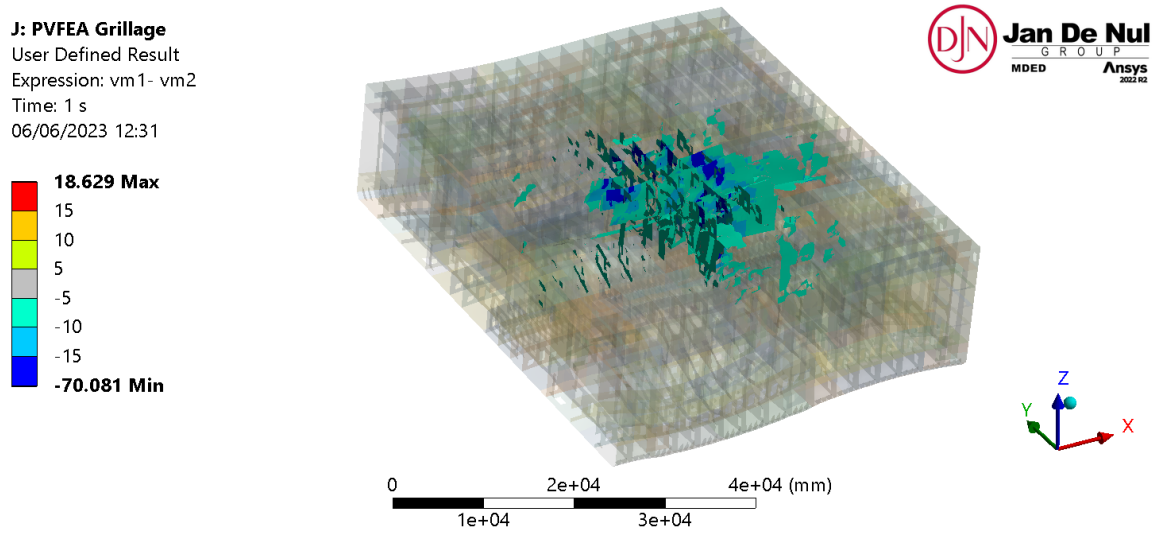

Figure 6.17: Difference in von Mises stress σ_{vm} of the partial vessel model with and without wind turbine tower. Results show region with a magnitude smaller than -5MPa.

6.3 Concluding remarks

The partial vessel FE analysis of the offshore jack-up installation vessel with payload was performed. A wind turbine tower with corresponding grillage on deck of the vessel was studied. First, the local analysis of payload was made, where only the weight of the tower was activated to examine how as a result the stress develops in the vessel. The tower load is locally introduced into the vessel and predominantly leads to the normal stress σ_z and shear stresses τ_{xz} and τ_{yz}. While the normal stress is confined to the region right underneath the grillage, the shear stress extends further. Besides, it is advised to refine the mesh size only near the payload and to follow the rules about acceptance criteria as defined by ship classification societies.

Next, the partial vessel FE analysis was performed. The case with payload was compared to the case without by means of the von Mises stress σ_{vm}. The global behaviour was very alike and the tower load only resulted in local changes in the stress field. The von Mises stress was high underneath the grillage, which is caused by the normal stress σ_z. Moreover, the von Mises stress altered left and right from the grillage due to the shear stress τ_{xz} and τ_{yz}.

Chapter 7

Conclusions and recommendations

The aim of this thesis was to develop a methodology for the partial vessel finite element (FE) analysis of an offshore jack-up installation vessel. The purpose was to analyse a section of the vessel that reflects the structural behaviour of the full vessel. This has the two main advantages over the full vessel FE analysis that it avoids the time-consuming task to model the entire vessel and a finer mesh can be adopted as well. The conclusions from the research and recommendations for future work are elaborated upon here.

7.1 Conclusions

The studied section of the offshore jack-up installation vessel nearly consists of the entire region between the four legs, which is where the highest bending moment is expected and the wind turbine towers are located on deck. The partial vessel model in the finite element analysis (FEA) was built from shell and beam elements. Several simplifications to the model were made. They were based on the frame spacing ($700mm$) to attain a possible (maximum) mesh size equal to it. The new feature batch connections of Ansys was used to connect the parts, which replaces the contact tool shared topology.

The part of the vessel that is not modelled was represented by appropriate boundary conditions at each end of the partial vessel model. A simply supported constraint was formed so that the vessel is allowed to bend and experience hogging or sagging. The most important constraint is therefore the free rotation about the two axes perpendicular to the longitudinal axis of the vessel. For the reason that the vessel is a 3D structure, a remote displacement constraint was needed, which scopes a selected geometry to an independent point. This point was constrained to translate, but allowed the selected geometry (i.e. the ends of the model) to rotate.

Loads acting on the part of the vessel that is not modelled are not seen by the partial vessel model. For this reason, hull girder load adjustments were applied on the ends of the model, namely the shear force, bending moment and torsional moment adjustment. The first two adjustments are based on the vertical shear force and bending moment diagrams of the vessel

section and full vessel. The main assumption is that the weight and buoyancy are uniformly distributed across the width of the vessel. It was observed from the finite element analyses that the shear force adjustment is not needed, but the bending moment adjustment is necessary. Besides, the torsional moment adjustment is required as it is incorrect to assume a uniform distribution of the weight across the width of the vessel.

The four loads acting on the vessel are the weight, buoyancy, water ballast and wave pressure. The weight and water ballast are related in the following manner. The weight of the model in the FEA is always smaller than the actual weight of the vessel section due to the simplifications made and components that were not modelled. Therefore, the density of the model was adjusted by assuming the deficit in weight is uniformly distributed. However, first, the water ballast was subtracted from the vessel section weight as it is a heavy weight that must be separately applied on the partial vessel model. It was decided to model the water ballast as a point mass instead of a hydrostatic pressure since this amount of detail was adequate for the purpose of this research.

First, the vessel was analysed in still water where it experiences hogging. The first case study (1a) did not consider the water ballast by assuming any weight is positioned along the centre line. The stress results were compared to a simple analytical solution of the vessel based on Euler-Bernoulli beam theory. The normal stress σ_x (along the longitudinal axis of the vessel) of the FEA was in agreement with the analytical solution and thus verified the correct setup of the methodology. Besides, the von Mises stress σ_{vm} of the FEA was smaller than the analytical solution due to the presence of σ_y (along the transverse axis of the vessel), which is not considered in this analytical solution. The results were accurate in the middle region for approximately 50% of the partial vessel model and the stress was under-estimated at the aft and fore end. It was also confirmed that a mesh size equal to the frame spacing is sufficient as the mesh size = $350mm$ returned the same stress results. The second case study (1b) took into account the water ballast and transversal position of weights and hence torsion as well. The added water ballast reduced the bending moment and thus the stresses in the vessel became smaller. Additionally, the water ballast at port and starboard side made the stress smaller there. The normal stress σ_x is now smaller than the analytical solution, which was observed to be caused by the torsional moment adjustment. However, it could not be fully justified for the reason that the analytical solution does not consider torsion. This adjustment was in the same order of magnitude as the torsional moment that the water ballast within the partial vessel model creates.

Second, the vessel was analysed in waves trying to maximise the vertical bending moment. The response amplitude operator (RAO) indicated this occurs for a stern or head sea as expected. The equivalent design wave (EDW) approach was used to select a number of design waves of which the wave pressure was applied on the partial vessel model. The simplest wave type was assumed, which is the regular travelling wave. The expected maximum wave height was used to determine the wave amplitude and the wave periods were based on the maximum of the RAOs within the vessel section. The normal stress σ_x of the FEA was somewhat larger than the analytical solution due to the conservative assumptions of the EDW approach. Besides, the von Mises stress σ_{vm} of the FEA showed a good agreement with the analytical solution. Similar to the vessel in still water, the results were accurate in the middle region for approximately 50% of the partial vessel model and the stress was under-estimated at the aft and fore end.

The stress results of the still water component were larger than those of the wave component due to the intrinsic high variation in weight of an offshore jack-up installation vessel and because the significant wave height may not be too high for the installation of wind turbines. The still water and wave component combined yielded better results compared to the simple analytical solution of the vessel. This could be attributed to the torsional moment adjustment, which reduced the normal stress σ_x considerably.

Lastly, the partial vessel FE analysis was performed with a wind turbine tower on deck, which is secured by a seafastening grillage. The tower was modelled as a point mass since it was only needed to examine the vessel response. The tower load was locally introduced into the vessel and led to the normal stress σ_z (along the vertical axis of the vessel) and shear stresses τ_{xz} and τ_{yz}. The presence of payload only leads to local changes in the stress field, but not in the global behaviour of the vessel.

7.2 Recommendations

Reflecting on the methodology of the partial vessel FE analysis, some uncertainties remained due to the limitations of the simple analytical solution of the vessel. In order that the methodology can be approved for future use, the following recommendations are made.

- The torsional moment adjustment reduced the normal stress σ_x considerably, but this could not be captured in the analytical solution. It is advised to perform the partial vessel FE analysis for a larger model or, to perform a full vessel FE analysis and compare the results. A barge could perhaps be used as this takes less time to model.
- The water ballast should be modelled as a hydrostatic pressure for future use. It was only decided to model it as a point mass since the stress in the vicinity of the water ballast tanks was irrelevant in this research.
- The equivalent design wave approach could be further investigated. The procedure to select design waves can be combined with the accelerations of a wind turbine tower. It is more accurate as the wave heading will be related to the payload accelerations. This research only considered the weight of the tower.
- It was assumed that the presence of the legs does not affect the rigidity of the surrounding structure. It is recommended to model the legs as well, which will not be straightforward, and compare the results.
- The methodology should be validated by experimental testing.

Bibliography

[1] E. P. Soares-Ramos, L. de Oliveira-Assis, R. Sarrias-Mena, and L. M. Fernández-Ramírez, "Current status and future trends of offshore wind power in Europe," *Energy*, vol. 202, p. 117 787, Jul. 2020. DOI: https://doi.org/10.1016/j.energy.2020.117787.

[2] L. Sartori, F. Bellini, A. Croce, and C. Bottasso, "Preliminary design and optimization of a 20MW reference wind turbine," *Journal of Physics: Conference Series*, vol. 1037, no. 4, p. 042 003, Jun. 2018. DOI: 10.1088/1742-6596/1037/4/042003.

[3] Y. Bai and W.-L. Jin, "Chapter 9 - Ship Hull Scantling Design by Analysis," in *Marine Structural Design*, Y. Bai and W.-L. Jin, Eds., Second Edition, Oxford: Butterworth-Heinemann, 2016, pp. 171–180. DOI: https://doi.org/10.1016/B978-0-08-099997-5.00009-5.

[4] M. Shama, "Hull Girder Loading," in *Buckling of Ship Structures*. Berlin, Heidelberg: Springer Berlin Heidelberg, 2013, ch. 5, pp. 117–140. DOI: 10.1007/978-3-642-17961-7_5.

[5] K. van Dokkum, *Ship knowledge, a modern encyclopedia*. Enkhuizen, The Netherlands: Dokmar, 2003.

[6] Y. Gu, A. Day, E. Boulougouris, and S. Dai, "Experimental investigation on stability of intact and damaged combatant ship in a beam sea," *Ships and Offshore Structures*, vol. 13, no. sup1, pp. 322–338, Jun. 2018. DOI: 10.1080/17445302.2018.1465012.

[7] E. C. Tupper, "Chapter 13 - Structures," in *Introduction to Naval Architecture*, E. C. Tupper, Ed., Fifth Edition, Oxford: Butterworth-Heinemann, 2013, ch. 13, pp. 299–341. DOI: https://doi.org/10.1016/B978-0-08-098237-3.00013-8.

[8] R. Bhattacharyya, *Dynamics of marine vehicles*. New York: John Wiley & Sons, Inc., 1978.

[9] H. Yudo, S. Yulianti, O. Pratiwi, and T. Tuswan, "The conversion strategy from landing craft tank into livestock carrier: An overview of technical evaluation and economical benefit," *Brodogradnja*, vol. 72, no. 3, pp. 29–44, Sep. 2021. DOI: 10.21278/brod72303.

[10] Y. Bai and W.-L. Jin, "Chapter 8 - Scantling of Ship's Hulls by Rules," in *Marine Structural Design*, Y. Bai and W.-L. Jin, Eds., Second Edition, Oxford: Butterworth-Heinemann, 2016, pp. 153–170. DOI: https://doi.org/10.1016/B978-0-08-099997-5.00008-3.

[11] L. Fagerberg, "Wrinkling in sandwich panels for marine applications," Ph.D. dissertation, Royal Institute of Technology, 2003.

[12] M. Shama, "Torsion of Container Ships," in *Torsion and Shear Stresses in Ships*. Berlin, Heidelberg: Springer Berlin Heidelberg, 2011, ch. 4, pp. 65–90. DOI: 10.1007/978-3-642-14633-6_4.

[13] D. Eyres and G. Bruce, "8 - Stresses to which a ship is subject," in *Ship Construction*, D. Eyres and G. Bruce, Eds., Seventh Edition, Oxford: Butterworth-Heinemann, 2012, pp. 67–78. DOI: https://doi.org/10.1016/B978-0-08-097239-8.00008-8.

[14] International Association of Classification Societies, *Classification Societies - Key Role*, Accessed on 12/10/22, 2022. [Online]. Available: https://iacs.org.uk/about/.

[15] D. Eyres and G. Bruce, "4 - Classification societies," in *Ship Construction*, D. Eyres and G. Bruce, Eds., Seventh Edition, Oxford: Butterworth-Heinemann, 2012, pp. 37–43. DOI: https://doi.org/10.1016/B978-0-08-097239-8.00004-0.

[16] Bureau Veritas, *Rules for the classification of steel ships: Part B - Hull and Stability - NR467 B DT R14*, Accessed on 03/10/22, Jul. 2022. [Online]. Available: https://marine-offshore.bureauveritas.com/nr467-rules-classification-steel-ships.

[17] Det Norske Veritas, *Finite element analysis - DNV-CG-0127*, Accessed on 06/10/22, Aug. 2021. [Online]. Available: https://rules.dnv.com/docs/pdf/DNV/CG/2021-08/DNV-CG-0127.pdf.

[18] A. H. Ertas, V. Alkan, and A. F. Yilmaz, "Finite Element Simulation of a Mercantile Vessel Shipboard under Working Conditions," *Procedia Engineering*, vol. 69, pp. 1001–1007, 2014, 24th DAAAM International Symposium on Intelligent Manufacturing and Automation, 2013. DOI: https://doi.org/10.1016/j.proeng.2014.03.082.

[19] J. Rörup, I. Darie, and B. Maciolowski, "Strength analysis of ship structures with open decks," *Ships and Offshore Structures*, vol. 12, S189–S199, Mar. 2017. DOI: 10.1080/17445302.2016.1264257.

[20] M. Shama, "Torsion Warping Deformations and Stresses," in *Torsion and Shear Stresses in Ships*. Berlin, Heidelberg: Springer Berlin Heidelberg, 2011, ch. 3, pp. 41–64. DOI: 10.1007/978-3-642-14633-6_3.

[21] Det Norske Veritas, *Allowable thickness diminution for hull structure - DNV-CG-0182*, Accessed on 26/10/22, Jul. 2022. [Online]. Available: https://rules.dnv.com/docs/pdf/DNV/CG/2022-07/DNV-CG-0182.pdf.

[22] Bureau Veritas, *MARS 2000 2D ship structural assessment software*, Accessed on 05/10/22, Jun. 2022. [Online]. Available: https://marine-offshore.bureauveritas.com/mars-2000-2d-ship-structural-assessment-software.

[23] Det Norske Veritas, *Ship structural analysis and design - Nauticus Hull*, Accessed on 05/10/22, 2022. [Online]. Available: https://www.dnv.com/services/ship-structural-analysis-and-design-nauticus-hull-1061.

[24] Det Norske Veritas, *Strength assessment of hull structures – POSEIDON*, Accessed on 05/10/22, 2022. [Online]. Available: https://www.dnv.com/services/strength-assessment-of-hull-structures-poseidon-18518.

[25] M. Shama, "Configurations and Characteristics of Ship Structural Assemblies," in *Buckling of Ship Structures*. Berlin, Heidelberg: Springer Berlin Heidelberg, 2013, ch. 2, pp. 25–43. DOI: 10.1007/978-3-642-17961-7_2.

[26] M. Shama, "Ship Structure Configurations and Main Characteristics," in *Buckling of Ship Structures*. Berlin, Heidelberg: Springer Berlin Heidelberg, 2013, ch. 1, pp. 3–23. DOI: 10.1007/978-3-642-17961-7_1.

[27] M. M. Rahman, R. S. Kamol, and R. Islam, "Structural analysis of a ship on global aspect using ANSYS," *AIP Conference Proceedings*, vol. 1919, no. 1, p. 020 008, Dec. 2017. DOI: 10.1063/1.5018526.

[28] J. Rörup and C. Cabos, "Advanced Whole Ship Analysis – A New Generation of FE Based Strength Analysis for Container Vessels," International Conference on Computer Applications in Shipbuilding, Bremen, Germany, Sep. 2015. DOI: 10.3940/rina.iccas.2015.09.

[29] J. Rörup, B. Maciolowski, and I. Darie, "FE-based strength analysis of ship structures for a more advanced class approval," PRADS2016, Copenhagen, Denmark, Aug. 2016.

[30] A. M. Elhewy, A. M. Hassan, and M. A. Ibrahim, "Weight optimization of offshore supply vessel based on structural analysis using finite element method," *Alexandria Engineering Journal*, vol. 55, no. 2, pp. 1005–1015, Jun. 2016. DOI: https://doi.org/10.1016/j.aej.2016.02.032.

[31] Det Norske Veritas, *Wave loads - DNV-CG-0130*, Accessed on 19/10/22, Oct. 2021. [Online]. Available: https://rules.dnv.com/docs/pdf/DNV/CG/2021-10/DNV-CG-0130.pdf.

[32] J. Rörup, T. Schellin, and H. Rathje, "Load Generation for Structural Strength Analysis of Large Containerships," *Proceedings of the International Conference on Offshore Mechanics and Arctic Engineering - OMAE*, vol. 2, pp. 89–98, Jun. 2008. DOI: 10.1115/OMAE2008-57121.

[33] C. Cabos, M. Krömer, and H. Eisen, "GL.ShipLoad: An Integrated Load Generation Tool for FE Analysis," *Proceeding of the International Conference on Computer Applications and Information Technology in the Maritime Industries - COMPIT*, pp. 199–210, May 2006.

[34] N. Dementyev, "Quasi-dynamic global strength analysis of a passenger ship in regular waves," Oct. 2019.

[35] Ansys, Inc., *ANSYS Aqwa in Workbench*, Accessed on 19/10/22, Nov. 2012. [Online]. Available: https://storage.ansys.com/corp/2012/November/aqwa/wb_update.pdf.

[36] Bureau Veritas, *Rules for the classification of steel ships: Part B - Hull and Stability - NR467 B DT R14*, Accessed on 03/10/22, 2021. [Online]. Available: https://marine-offshore.bureauveritas.com/nr467-rules-classification-steel-ships.

[37] C. M. Salazar-Domínguez, J. Hernández-Hernández, E. D. Rosas-Huerta, G. E. Iturbe-Rosas, and A. L. Herrera-May, "Structural Analysis of a Barge Midship Section Considering the Still Water and Wave Load Effects," *Journal of Marine Science and Engineering*, vol. 9, no. 1, p. 99, Jan. 2021. DOI: 10.3390/jmse9010099.

[38] Det Norske Veritas, *Finite element analysis - DNV-CG-0127*, Accessed on 06/10/22, Oct. 2015. [Online]. Available: https://rules.dnv.com/docs/pdf/DNV/CG/2016-02/DNVGL-CG-0127.pdf.

[39] T. T. Tanny, N. Akter, and O. Md. Amin, "Finite element analysis of container ship's cargo hold using ANSYS and POSEIDON software," *AIP Conference Proceedings*, vol. 1919, no. 1, p. 020 012, Dec. 2017. DOI: 10.1063/1.5018530.

[40] Ansys, Inc., *ANSYS Mechanical User's Guide*, Canonsburg, Pennsylvania, U.S., 2022.

[41] E. Narvydas and N. Puodziuniene, "Applications of Sub-modeling in Structural Mechanics," Proceedings of 19th International Conference Mechanika, Kaunas, Lithuania, Apr. 2014, pp. 172–176.

[42] R. C. Hibbeler, *Mechanics of Materials*. London, United Kingdom: Pearson Education, Inc., 2018.

[43] L. Boni and D. Fanteria, "Development of analytical methods for fuselage design: Validation by means of finite element analyses," *Proceedings of The Institution of Mechanical Engineers Part G-journal of Aerospace Engineering*, vol. 218, pp. 315–327, Oct. 2004. DOI: 10.1243/0954410042467022.

[44] L. Boni and D. Fanteria, "Finite-element-based assessment of analytical methods for the design of fuselage frames," *Proceedings of the Institution of Mechanical Engineers, Part G: Journal of Aerospace Engineering*, vol. 220, no. 5, pp. 387–398, Apr. 2006. DOI: 10.1243/09544100JAERO74.

[45] A. Adams and H. M. Lankarani, "A modern aerospace modeling approach for evaluation of aircraft fuselage crashworthiness," *International Journal of Crashworthiness*, vol. 8, no. 4, pp. 401–413, Jan. 2003. DOI: 10.1533/ijcr.2003.0234.

[46] B. Shetty, S. Reddy, and R. Mishra, "Finite Element Analysis of an Aircraft Wing Leading Edge Made of GLARE Material for Structural Integrity," *Journal of Failure Analysis and Prevention*, vol. 17, pp. 948–954, Aug. 2017. DOI: 10.1007/s11668-017-0331-2.

[47] A. Aabid, M. Zakuan, S. Khan, and Y. Ibrahim, "Structural analysis of three-dimensional wings using finite element method," *Aerospace Systems*, vol. 5, pp. 47–63, Mar. 2022. DOI: 10.1007/s42401-021-00114-w.

[48] A. Nath, R. Anand, J. Desai, M. Sultan, and A. Sakthivel, "Modelling and Finite Element Analysis of an Aircraft Wing using Composite Laminates," *IOP Conference Series: Materials Science and Engineering*, vol. 1183, p. 012 006, Sep. 2021. DOI: 10.1088/1757-899X/1183/1/012006.

[49] J. H. Jang and S. Ahn, "FE Modeling Methodology for Load Analysis and Preliminary Sizing of Aircraft Wing Structure," *International Journal of Aviation, Aeronautics, and Aerospace*, vol. 6, no. 2, pp. 1–32, Jan. 2019. DOI: 10.15394/ijaaa.2019.1301.

[50] K. E. Jackson, J. D. Littell, M. S. Annett, and I. M. Haskin, "Finite Element Simulations of Two Vertical Drop Tests of F-28 Fuselage Sections," Langley Research Center, Hampton, Virginia, Feb. 2018.

[51] V. Negro, J.-S. López-Gutiérrez, M. D. Esteban, P. Alberdi, M. Imaz, and J.-M. Serraclara, "Monopiles in offshore wind: Preliminary estimate of main dimensions," *Ocean Engineering*, vol. 133, pp. 253–261, Mar. 2017. DOI: https://doi.org/10.1016/j.oceaneng.2017.02.011.

[52] E. C. Tupper, "Chapter 10 - Seakeeping," in *Introduction to Naval Architecture*, E. C. Tupper, Ed., Fifth Edition, Oxford: Butterworth-Heinemann, 2013, ch. 10, pp. 243–263. DOI: https://doi.org/10.1016/B978-0-08-098237-3.00010-2.

[53] B. Barrass *et al.*, "Chapter 4 - ship structures," in *The Maritime Engineering Reference Book*, A. F. Molland, Ed., First Edition, Oxford: Butterworth-Heinemann, 2008, ch. 4, pp. 116–180. DOI: https://doi.org/10.1016/B978-0-7506-8987-8.00004-4.

[54] J. Jiao, H. Ren, S. Sun, N. Liu, H. Li, and C. A. Adenya, "A state-of-the-art large scale model testing technique for ship hydrodynamics at sea," *Ocean Engineering*, vol. 123, pp. 174–190, Sep. 2016. DOI: https://doi.org/10.1016/j.oceaneng.2016.06.028.

[55] J. Jiao, C. Chen, and H. Ren, "A comprehensive study on ship motion and load responses in short-crested irregular waves," *International Journal of Naval Architecture and Ocean Engineering*, vol. 11, no. 1, pp. 364–379, 2019. DOI: https://doi.org/10.1016/j.ijnaoe.2018.07.003.

[56] Z. Zhu, J. Lee, Y. Kim, J.-H. Lee, and T.-H. Park, "Experimental measurement and numerical validation of sloshing effects on resistance increase in head waves," *Ocean Engineering*, vol. 234, p. 109 321, Aug. 2021. DOI: https://doi.org/10.1016/j.oceaneng.2021.109321.

[57] S. K. Chakrabarti, "Chapter 13 - Physical Modelling of Offshore Structures," in *Handbook of Offshore Engineering*, S. K. Chakrabarti, Ed., London: Elsevier, 2005, pp. 1001–1054. DOI: https://doi.org/10.1016/B978-0-08-044381-2.50020-5.

[58] C. P. Coutinho, A. J. Baptista, and J. Dias Rodrigues, "Reduced scale models based on similitude theory: A review up to 2015," *Engineering Structures*, vol. 119, pp. 81–94, Jul. 2016. DOI: https://doi.org/10.1016/j.engstruct.2016.04.016.

[59] M. Shama, "Hull Girder Bending Stresses," in *Buckling of Ship Structures*. Berlin, Heidelberg: Springer Berlin Heidelberg, 2013, ch. 6, pp. 141–152. DOI: 10.1007/978-3-642-17961-7_6.

[60] S. Misra, *Design Principles of Ships and Marine Structures*. Boca Raton: Taylor & Francis Group, Dec. 2015, pp. 1–461. DOI: 10.1201/b19041.

[61] Y. Bai and W.-L. Jin, "Chapter 5 - Wave Loads for Ship Design and Classification," in *Marine Structural Design*, Y. Bai and W.-L. Jin, Eds., Second Edition, Oxford: Butterworth-Heinemann, 2016, pp. 73–93. DOI: https://doi.org/10.1016/B978-0-08-099997-5.00005-8.

[62] American Bureau of Shipping, *Selecting design wave by long term stochastic method*, Accessed on 05/06/23, Oct. 2016. [Online]. Available: https://ww2.eagle.org/content/dam/eagle/rules-and-guides/current/offshore/238_Guidance_Notes_on_Selecting_Design_Wave_by_Long_Term_Stochastic_Method/Long_Term_Design_Wave_GN_e.pdf.

[63] S.-V. Kontomaris and A. Malamou, "A simple explanation of the classic hydrostatic paradox," *Physics Education*, vol. 51, no. 4, p. 045 010, May 2016. DOI: 10.1088/0031-9120/51/4/045010.

[64] Det Norske Veritas, *Environmental conditions and environmental loads - DNV-RP-C205*, Accessed on 05/04/23, Sep. 2019. [Online]. Available: https://rules.dnv.com/docs/pdf/DNV/RP/2019-09/DNV-RP-C205.pdf.

[65] G. de Hauteclocque, Q. Derbanne, and A. El-Gharbaoui, "Comparison of Different Equivalent Design Waves With Spectral Analysis," vol. 1: Offshore Technology, Jul. 2012, pp. 353–361. DOI: 10.1115/OMAE2012-83405.